

MASTER THESIS

**Development and Establishment of
Performance Evaluation System
for Light Concentrators of
the Large-Sized Telescopes
in the Cherenkov Telescope Array**

**(CTA大口径望遠鏡用ライトガイドの開発
および性能評価システムの確立)**

Fiscal 2016

(Fiscal Heisei 28)

**Department of Astrophysics, Major of Science
Graduate School of Science and Engineering, Ibaraki University**

15NM171A

DANG VIET TAN

Abstract

Master Thesis

by DANG VIET TAN

The Cherenkov Telescope Array (CTA) project is an very-high-energy gamma-ray ground-based observatory using three sizes of Imaging Atmospheric Cherenkov Telescopes (IACT) with different diameters. By placing about 100 IACTs in the Southern and Northern hemisphere, CTA can observe the whole sky, achieve ten times the sensitivity of current gamma-ray telescopes and expand the observable energy band from 20 GeV to 300 TeV. There are more than 1200 researchers in 32 countries around the world participating in CTA now. The CTA-Japan team is mainly conducting research on Large-Sized Telescopes (LSTs).

When a high energy primary particle such as gamma ray or high-energy cosmic ray enters the Earth's atmosphere, it will interact with nuclei in the atmosphere and generate a series of reactions called air shower. The generated charged particles travel through dielectric atmosphere and cause the Cherenkov light. The CTA then observes this Cherenkov light and detects the high energy primary particle as gamma ray or cosmic ray. Among the IACTs of CTA project, the LSTs play an important role in observing gamma rays in the lowest energy range from 20 GeV to 1 TeV. Because the total number of generated Cherenkov photons is almost directly proportional to the gamma-ray energy, the amount of Cherenkov light at low energy levels are quite low. So various factors of LST are being studied in order to improve the light collection performance and detect more Cherenkov light as much as possible.

In this research, we are developing the light concentrator, an important optical part which collects the Cherenkov light reflected from LST main mirror to camera. The LST camera consists of 1855 photomultiplier tubes (PMT) as light detector. Each PMT has a spherical entrance surface, which creates a gap with the adjacent PMT and loses a lot of photons. By mounting a light concentrator in front of each PMT, this gap can be reduced well and more Cherenkov photons can be detected. Moreover, light concentrator also plays an important role in eliminating terrestrial background light from outside the field of view (FOV).

The LST light concentrator has a particular structure. It is hand-made by combining an ESR (Enhanced Specular Reflector) as reflecting material with a hexagonal cylindrical cone. In current design, the thin ESR protrudes from the entrance of cone in order to maximize the light detection surface. However, because the ESR protruding part is warped,

the reflective surface is distorted and the measurement results showed that the performance dropped. In addition, the warped part is structurally weak. When attaching to the interface plate, it is pushed by other adjacent light concentrators, deforms the surface or forms a gap. In order to correct this warpage, the reinforcements by two-side tapes, polyethylene terephthalate (PET) films and Stainless special Used Steel (SUS) films were studied and executed. As result, the warpage was eliminated best by SUS film reinforcement, and the performance of the light concentrator was improved.

On the other hand, light concentrators are also measured the light collection efficiency carefully one by one to evaluate clearly its performance. One light concentrator can be evaluated by 2 measurements: on-axis measurement and rotation measurement, with three light-emitting diodes (LEDs) of 310 nm, 365 nm and 465 nm in peak wavelength, respectively. The on-axis case is a fast measurement at 0° , while the rotation case is a time-consuming measurement checking angle by angle from -40° to 40° . In current experimental system, there was a problem that about 1.6% difference in the light collection efficiency always occurs between the measurement results of on-axis case and rotation case at 0° . Besides, a lot of systematic errors sometimes occur during the rotation measurement. In order to solve these problems, the experimental system was established entirely, namely the rearrangement, rewriting the measuring scripts, change in replacement steps and more. As result, the 1.6% difference disappeared and the systematic errors reduced well. These factors are very important and significant to evaluate correctly the collection efficiency of light concentrator.

Acknowledgements

I would never been able to finish this research without the guidance of my professors, help from my friends and support from my family.

Firstly, I would like to thank Professor Tatsuo Yoshida, my research supervisor, because of the infinite helps and advices he has given me. Without his support, I would not have been able to complete this research. Secondly, my deep gratitude goes to Associate Professor Hideaki Katagiri and Assistant Professor Akira Okumura, who gave me a lot of useful suggestions to my research.

My sincere thanks also goes to my seniors, Doctor Mika Kagaya, Kazuhito Yoshida, Norihito Cho, Sakiya Ono, and my friends in my laboratory for all their support.

Special thanks goes to my Vietnamese friend, Joni Pham. She is very nice helping me to check the grammar mistakes of this thesis carefully.

Finally, thank you to all of my friends, teachers, and family for everything you have done for me over these past six years at Ibaraki University.

Contents

Abstract	iii
Acknowledgements	v
Abbreviations	ix
List of Figures	1
List of Tables	7
1 Introduction	9
1.1 Cosmic ray and the significance of gamma-ray observation	9
1.2 Gamma ray	10
1.2.1 Overview	10
1.2.2 Gamma-ray production mechanisms	11
1.2.2.1 π^0 meson decay	11
1.2.2.2 Electron bremsstrahlung	12
1.2.2.3 Inverse Compton scattering	13
1.3 Gamma-ray detector	14
1.4 Gamma-ray observation by IACTs	15
1.4.1 Electromagnetic cascade	15
1.4.2 Cherenkov radiation	16
1.4.3 The principle of gamma-ray observation by IACTs	17
2 Cherenkov Telescope Array (CTA) project	23
2.1 Overview	23
2.1.1 Telescope types	24
2.1.2 Array location	27
2.2 Large-Sized Telescope (LST)	28
3 Development of light concentrators for LST	33
3.1 Overview	33
3.1.1 LST focal-plane camera	33
3.1.2 Photomultiplier Tube	34
3.1.3 Light concentrator (LC)	35
3.2 Current status	36
3.2.1 Design	36

3.2.1.1	Cone	37
3.2.1.2	Enhanced Specular Reflector (ESR)	38
3.2.2	Production method	39
3.2.3	Mass production	41
3.2.4	Performance evaluation system	43
3.2.4.1	Set-up	43
3.2.4.2	Relative Anode Sensitivity	43
3.2.4.3	On-axis measurement	47
3.2.4.4	Rotation measurement	50
3.2.5	Performance comparison with MST light concentrator	51
3.3	Problems	53
3.4	Solution and discussion	54
3.4.1	Reinforcement of ESR by tape	54
3.4.2	Reinforcement of ESR by PET film	55
3.4.3	Reinforcement of ESR by SUS film	59
3.4.4	Thermostat test	63
3.4.5	Final conclusion	63
4	Establishment of performance evaluation system	67
4.1	Establishment of measurement system	67
4.1.1	Rearrangement and cleaning	67
4.2	Additional set-up of monitor PMT	68
4.3	Establishment of measurement scripts	71
4.4	Establishment of replacement work	73
4.5	Establishment of rotation measurement	76
4.5.1	Problems	76
4.5.2	Solution and discussion	80
5	Future plan	83
5.1	New design	84
6	Summary	85
A	RAS value and standard deviation	87
B	RAS value correction by monitor PMT	91
C	RAS tables of the second and third batch	93
D	On-axis measurement script	97
E	Rotation measurement script	107
	Bibliography	121

Abbreviations

CTA	Cherenkov Telescope Array
LST	Large-Sized Telescope
MST	Medium-Sized Telescope
SCT	Schwarzschild-Couder Telescope
SST	Small-Sized Telescope
SST-1M	Small-Sized Telescope - 1 Mirror
SST-2M	Small-Sized Telescope - 2 Mirrors
ASTRI	Astrofisica con Specchi a Tecnologia Replicante Italiana
GCT	Gamma-ray Compact Telescope
FOV	Field Of View

List of Figures

1.1	Observed energy spectrum of primary cosmic rays [1]. The spectrum is expressed by a power law from 10^{11} to 10^{20} eV with a slight change of slopes around $10^{15.5}$ eV (knee), $10^{17.8}$ eV (second knee), and 10^{19eV} (ankle).	10
1.2	Electromagnetic spectrum showing the gamma-ray part from the full band [2].	11
1.3	Spectrum difference by radiation mechanisms [3].	11
1.4	Schematic diagram of π^0 meson decay.	12
1.5	Schematic diagram of electron bremsstrahlung.	13
1.6	Schematic diagram of inverse Compton scattering.	14
1.7	Fermi Gamma-ray Space Telescope [4].	14
1.8	Top: The H.E.S.S. (High Energy Stereoscopic System) telescope array [5]. Middle: The VERITAS (Very Energetic Radiation Imaging Telescope Array System) telescope array [6]. Bottom: The MAGIC (Major Atmospheric Gamma Imaging Cherenkov) telescope array [7].	15
1.9	Schematic diagram of gamma-ray shower (left) and hadronic shower (right) [8].	16
1.10	The principle of Cherenkov radiation [9].	17
1.11	Left: the light pool observed at the ground level by a γ -ray of 300 GeV [10]. Right: simulation of the Cherenkov light as a function of the impact distance [11]. The solid and dashed lines show showers developing along to the earth magnetic field and 90° perpendicular to it, respectively.	18
1.12	Illustration of an Imaging Atmosphere Cherenkov Telescope (IACT) catching Cherenkov light [10].	18
1.13	Difference in development of air showers by CORSIKA simulation [12]. Left: Gamma-ray shower development. Right: Hadronic shower development.	19
1.14	Left: Camera pixel image when observing γ -ray shower. Right: Camera pixel image when observing hadronic shower [9].	19
1.15	Stereo observation using 4 IACTs [13].	20
1.16	Up: Camera pixel image of each telescope when observing 1 shower using 4 IACTs. Bottom: Principle of the stereo observation using 4 IACTs [14].	21
2.1	CTA structure: a mixed array of different telescopes [1].	23
2.2	CTA sensitivity by Monte Carlo simulation. Both northern and southern site perform a deep sensitivity curve comparing with current arrays [1].	24
2.3	The MST structure [1].	25
2.4	The SCT structure [1].	26
2.5	The structure of 3 SST types [1]. Left: SST-2M GCT. Middle: SST-2M ASTRI. Right: SST-1M.	26

2.6	Two sites of CTA are shown as red point [1].	27
2.7	The current view of northern and southern sites [1]. Up: the northern site at La Palma, Spain, with 2 IACTs of MAGIC in operation now. Down: the southern site at Paranal, Chile.	28
2.8	CTA array layouts in two sites. [1]	28
2.9	The LST in CTA [1].	29
2.10	The LST main parameters [1].	30
3.1	Left: LST camera. Right: PMT module equipped in camera.	33
3.2	One PMT module [15].	34
3.3	Cross-section of photomultiplier tube [16].	34
3.4	Cherenkov light intensity and the QE curve of the R11920-100 PMT as a function of the wavelength [17].	35
3.5	(a): The averaged anode (red dashed) and cathode (black solid) sensitivity of the R11920-100 PMTs versus light source position, provided by Hamamatsu Photonics [18]. Measurements of 90 PMTs were averaged and normalized to the position at $Y = 0$ mm. The insets schematically illustrate a PMT and the definition of the curved Y axis. The value of $\phi = 22$ mm is the exit aperture diameter of the current light concentrator. (b): The result of PMT incident angle dependence analysis (photon detection efficiency versus angle of incidence), measured by S.Ono [16, 18]. The measurement result of each PMT was normalized relative to the vertical (i.e., 0°) as a reference and corrected by cosine. The data points show measured values for eight PMTs. The dashed line shows the average of the eight PMTs. The solid line shows the symmetrical average (and extrapolates to $80^\circ - 90^\circ$).	36
3.6	Seven PMTs of 1 module before (left) and after (right) equipping seven light concentrators [16].	37
3.7	(a): 3D CAD model of the base ABS cone of an LST light concentrator. (b): Same as (a), but six specular ESR films are attached to the cone. (c): A light concentrator cluster comprised of seven copies of (b) and an interface plate at the bottom [19].	37
3.8	(a) 3D CAD model of the base ABS cone of an LST light concentrator. (b) Same as (a), but six specular ESR films are attached to the cone. (c) A light concentrator cluster comprised of seven copies of (b) and an interface plate at the bottom [19].	38
3.9	Left: cone structure. Right: the real one [16].	39
3.10	The coated ERS [16].	40
3.11	(a) The measured reflectance of bare (solid lines) and coated (dashed) ESR films at the angle of incidence such as 20° , 30° , 40° , etc. (b) Same as (a) but only limited wavelength ranges are shown. The systematic uncertainty of these measurements is estimated to be $\sim 1\%$, and thus some data points are higher than 100% [19].	40
3.12	The ERS cutting process [16]. (a): ESR is set into laser cutter. (b): The state of ESR after cutting. (c): ESR warped greatly after removing from glass.	41
3.13	The ESR pasting process [16]. (a): cutting ESR is connected together by Kapton tape and put into a male mold. (b): the state after holding the weight at the top. (c) Applying glue to the backside. (d) Pressing the male mold by producer's weight.	41

3.14	Left: the view of mass-producing place. Right: Mass produced light concentrators.	42
3.15	Left: The RAS value distribution of the second batch (126 pieces - 18 clusters). Right: The state of second batch after boxed.	42
3.16	Left: The RAS value distribution of the third batch (126 pieces - 18 clusters). Right: The state of second batch after boxed.	43
3.17	Schematic diagram of set-up for light concentrator. The distance from the light source to the PMT is 2.4 m, so that the spread of light incident on PMT is within 1°	44
3.18	The performance evaluation system in real. Left: left side of dark room with LED at the leftmost. Right: right side of dark room with PMT and light concentrator at the rightmost.	44
3.19	The performance evaluation system looking from backside.	45
3.20	Left: the hexagonal frame and LC. Right: LC attached into hexagonal frame.	45
3.21	The performance evaluation system. (a): Left side is the state of LED and right side is the setting state of PMT with mask in the case of step 1 (i.e. mask case). (b): Left side is the state of LED and right side is the setting state of PMT with light concentrator in the case of step 2 (i.e. LC case).	46
3.22	Three types of LED: 310 nm, 365 nm and 465 nm.	46
3.23	Schematic diagram of setup in the case of mask measurement.	47
3.24	Top line: In each graph shows 500 signals of mask case at 365 nm. Middle line: In each graph shows the distribution of 500 signals each time. Bottom line: In each graph shows the distribution in numerical order of counts.	48
3.25	Top line: In each graph shows 500 signals of LC case at 365 nm. Middle line: In each graph shows the distribution of 500 signals each time. Bottom line: In each graph shows the distribution in numerical order of counts.	49
3.26	The position of PMT.	51
3.27	The RAS curve ($\varphi = 0^\circ$ case).	51
3.28	Four rotation directions.	51
3.29	The results of 4 rotation directions.	52
3.30	Comparison of LST and MST light concentrator at 310 nm.	52
3.31	Comparison of LST and MST light concentrator at 365 nm.	52
3.32	Comparison of LST and MST light concentrator at 465 nm.	53
3.33	The warpage can be seen near the entrance aperture of light concentrator.	53
3.34	Influence of warpage.	54
3.35	The state after pasting 6 pieces of two-sided tapes on the back of 6 surfaces. Left: 7 mm tape case. Right: 3 mm tape case.	55
3.36	(a-1): The state of warpage. (a-2): The cross section of warpage floating from the ideal surface (dashed line). (b-1): The state after pasting 7 mm tape. (b-2): The cross section of 7 mm tape case. (c-1): The state after pasting 3 mm tape. (c-2): The cross section of 3 mm tape case. (d-1): The state after pasting 1 mm tape. (d-2): The cross section of 1 mm tape case.	56
3.37	Rotation measuring results of LC No.264, in 4 cases of tape.	57
3.38	Rotation measuring results of LC No.29, in only 2 cases: no tape and 3 mm tape.	57
3.39	Comparison of mass-produced light concentrator (left) and 3D printer prototype (right) [16].	58

3.40 (a): Cutting PET film into a rectangular 14 mm x 26 mm. (b): Attaching glue to the back of warpage. (c): Pasting PET film to the back of warpage. (d): The final state after reinforcement.	58
3.41 The results before and after the PET film reinforcement in the case of light concentrator No.29.	59
3.42 The results before and after the PET film reinforcement in the case of light concentrator No.254.	59
3.43 Performance evaluating results of PET film vs 3 mm tape	60
3.44 Left: the state of PET film after pasting. Right: the state of SUS film after pasting.	60
3.45 Left: the state of warpage after PET film reinforcement. Middle: the state of warpage after SUS 0.1 μm film reinforcement. Right: the state of warpage after SUS 0.05 μm film reinforcement.	60
3.46 Performance evaluation results of PET film and 2 cases of SUS film.	61
3.47 Left: The dead space is created by being pressed intentionally in the case that two sides are reinforced by SUS films. Right: A narrow dead space is created by being pressed intentionally in the case that two sides are reinforced by PET films.	62
3.48 Yellow frame: the weak spaces which is not reinforced can be deformed easily and create the dead space.	62
3.49 Thermostat test.	63
3.50 Above: all reinforcement films. From the left side are PET film, SUS 0.05 μm of 13 \times 18 mm film, SUS 0.1 μm of 13 \times 18 mm film, and the rightmost one is the final SUS 0.1 μm film with rectangular shape of 13 \times 26 mm. SUS 0.05 μm of 13 \times 18 mm and SUS 0.1 μm of 13 \times 18 mm films were used in the SUS-film reinforcement test. Bellow: a inclined look from the side.	64
3.51 SUS 0.1 μm film with rectangular shape of 13 \times 26 mm	64
3.52 Cluster with 7 new light concentrators viewed from side.	64
3.53 Cluster with 7 new light concentrators viewed from above.	65
4.1 (a): before rearrangement. (b): after rearrangement.	68
4.2 (a): The monitor PMT. (b): The set-up state of monitor PMT covered by the noise-preventing cloth. (c): The position of both PMTs.	69
4.3 The experimental system after adding monitor PMT.	69
4.4 Left: Measurement PMT signal graph (above) and monitor PMT signal graph (below) of the mask case. Right: Measurement PMT signal graph (above) and monitor PMT signal graph (below) of the LC case.	70
4.5 Left: results of the first confirmation test. Right: results of the second confirmation test.	70
4.6 The results of correction test. (a): The RAS value distribution of traditional way. (b): The corrected RAS value distribution of correcting way.	71

4.7	Screen shot when measuring the rotation case. (a): 500 pulses of each time is displayed immediately after measuring. The above graph shows waveform of 500 pulses detected by measuring PMT. The below graph shows waveform of 500 pulses detected by monitor PMT. Red line shows the time range of noise pedestal (left) and pulse (right). (b): the PMT gain value displayed when measuring so that we can check if some large systematic errors appear. (c): the gain value of pedestal, pulse and their residual were calculated (analysed) immediately after each time and displayed in detail on screen.	72
4.8	Left: location of ceiling light and the experiment system. Right: the mini bulb is turned on for replacement work	73
4.9	LED light pen wrapped in black tape to reduce light.	74
4.10	The measured results of LED light pen confirmation test. Red: PMT gain average value fluctuation before turning off high voltage. Black: PMT gain average value fluctuation after turning off high voltage. Green: error bars of each value.	74
4.11	The measured results of confirmation test in the case turning off voltage. Red: PMT gain average value fluctuation before turning off high voltage. Black: PMT gain average value fluctuation after turning off high voltage. Green: error bars of each value.	75
4.12	The measured results of confirmation test in the case turning off voltage and irradiating by the LED light pen. Red: PMT gain average value fluctuation before turning off high voltage. Black: PMT gain average value fluctuation after turning off high voltage. Green: error bars of each value.	76
4.13	Measurement results of 4 times in the case of light concentrator, after the establishment of replacement work.	77
4.14	Measurement results of 4 times in the case of light concentrator, after waiting 30 minutes.	78
4.15	Rotation measurement results of 4 times in the LC case of detailed test. . .	79
4.16	Left: rotation measurement results of 4 times in the second test of LC case. Right: rotation measurement results of 4 times in the third test of LC case.	80
4.17	Left: old electrical and signal wiring before establishment, hanging a heavy connector in the air. Right: new electrical and signal wiring system.	80
4.18	Left: new electrical and signal wiring viewed from above. Right: closer look.	81
4.19	The measurement results after the establishment of signal cable.	81
4.20	RAS curve comparison for 2 cases of before and after the entire establishment, as black and red line respectively.	82
5.1	CAD view of new design of LST light concentrator.	84
6.1	All light concentrators. From the left side are LC without reinforcement, PET reinforced LC, SUS 0.05 μm LC, SUS 0.1 μm LC, final design LC (1s) and 3D printer LC.	85
A.1	Left: the signal graph of mask case. Right: the signal graph of LC case. . . .	87

List of Tables

1.1	Gamma-ray bands [2].	10
2.1	Main parameters of LST, MST and SCT [1].	25
2.2	Main parameters of 3 SST types [1].	27
4.1	The results of on-axis case and rotation case at $\theta = 0^\circ$	78
C.1	The RAS value table of second batch. The ESR of No.156 was used for test. The LCs of No.167, 178, 187, 194, 237, and 254 were left at Ibaraki University. The rest (126 pieces - 18 clusters) was sent to Spain for attachment test.	93
C.2	The RAS value table of third batch. The LCs of No.349, 350, 351, 352, and 353 were left at Ibaraki University. The rest (126 pieces - 18 clusters) was sent to Spain for attachment test.	95

Chapter 1

Introduction

1.1 Cosmic ray and the significance of gamma-ray observation

Cosmic ray is an indispensable object in the current astronomy. First discovered in 1912 by Victor Hess, cosmic ray is still one of the unresolved important issues until now. Coming from the outside of Solar system, almost 90% of cosmic rays are protons, 9% are helium nuclei and 1% nuclei are heavier elements. Before coming to Earth, cosmic rays pass magnetic fields in space and their directions are bent, so it is difficult to identify where they came from. Due to many experiments over the world, energy spectrum of cosmic rays is shown as Figure 1.1 and extends beyond 10^{20} eV.

However, celestial high-energy sources which generate the cosmic rays also emit high-energy gamma rays. Unlike cosmic rays, high-energy gammas rays are electrically neutral so they can go directly through the space's magnetic fields without any effect. This means that high-energy gamma rays detected on Earth come directly from celestial source where they were emitted. By observing gamma ray sources, we can study the origin of cosmic ray and its acceleration mechanism.

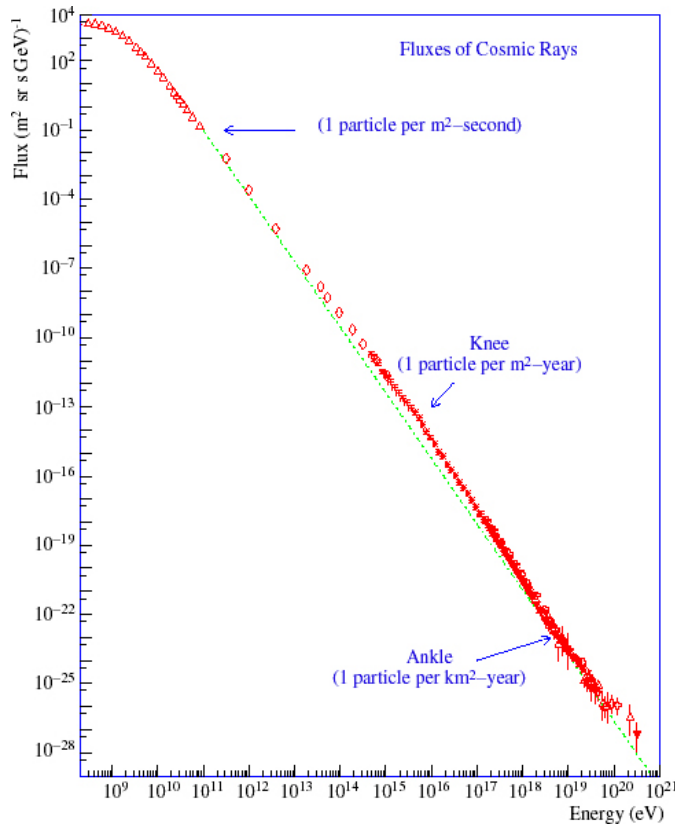


FIGURE 1.1: Observed energy spectrum of primary cosmic rays [1]. The spectrum is expressed by a power law from 10^{11} to 10^{20} eV with a slight change of slopes around $10^{15.5}$ eV (knee), $10^{17.8}$ eV (second knee), and 10^{19} eV (ankle).

1.2 Gamma ray

1.2.1 Overview

Gamma rays own short wavelengths about 0.01 nm and smaller, which are shorter than X-rays in the known electromagnetic spectrum. As shown in Figure 1.2, gamma rays also possess a wide energy range from about 100 keV (10^5 eV) to more than 100 EeV (10^{20} eV). Table 1.1 shows the detail gamma-ray bands in very high energy astronomy. These bands are defined by the interaction phenomena and detecting techniques.

Band	Low/Medium Energy	High Energy	Very High Energy	Ultra High Energy
Shorthand	LE/ME	HE	VHE	UHE
Range	0.1-30 MeV	30 MeV-100 GeV	100 GeV-100 TeV	>100 TeV
Typical energy	keV-MeV	MeV-GeV	TeV	PeV-EeV
Environment	Space	Space	Ground-based	Ground-based

TABLE 1.1: Gamma-ray bands [2].

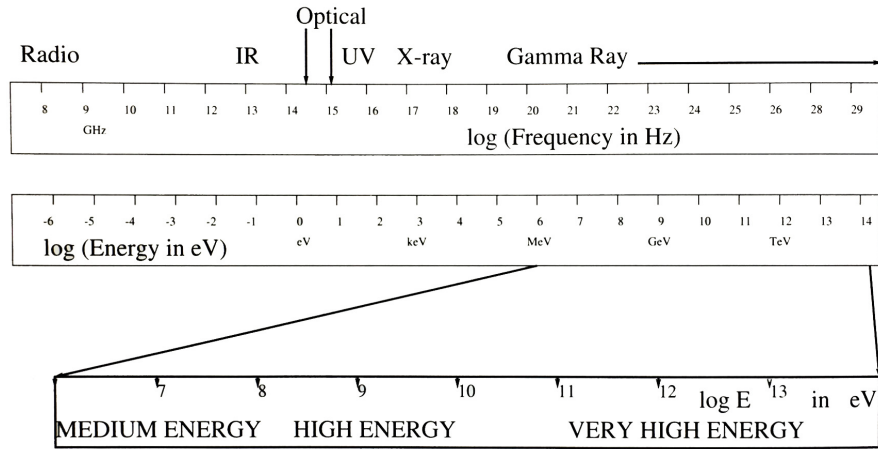


FIGURE 1.2: Electromagnetic spectrum showing the gamma-ray part from the full band [2].

1.2.2 Gamma-ray production mechanisms

Charged particles interact in various ways in the interstellar space and perform electromagnetic radiation. In particular, gamma rays emitted by interaction with interstellar substances indicate directly the presence of high energy particles such as cosmic rays. Figure 1.3 shows the spectrum of radiation mechanisms. The mechanisms of π^0 meson decay, electron bremsstrahlung and inverse Compton scattering are mentioned as below, as the main production mechanisms by which high-energy particles emit gamma rays.

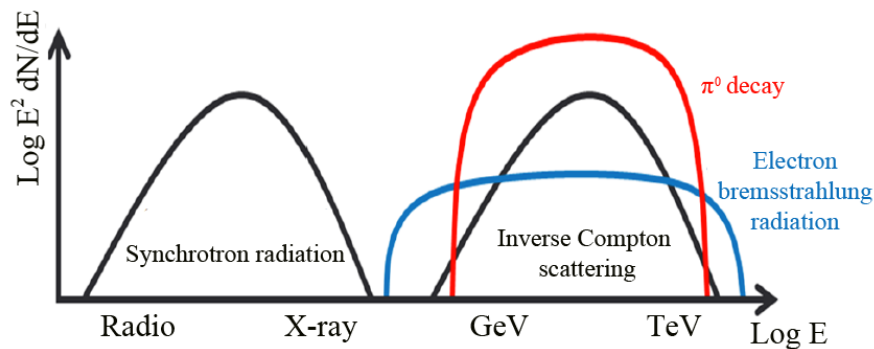
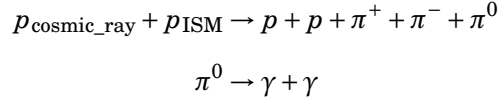


FIGURE 1.3: Spectrum difference by radiation mechanisms [3].

1.2.2.1 π^0 meson decay

The cosmic ray protons collide with interstellar medium (ISM) such as molecular clouds, and generate 3 kinds of π mesons as π^0 meson, π^+ meson and π^- meson. Among them, the π^0 meson decays and emits gamma rays. Because the lifetime of π^0 is very short as

8.4×10^{-17} s, it almost immediately collapses to 2 gamma rays.



The mass of proton m_p , the mass of meson m_π and the kinetic energy E_p of cosmic ray proton must satisfy the following condition [?].

$$E_p - m_p c^2 \leq 2m_\pi c^2 \left(1 + \frac{m_\pi}{4m_p}\right) = 280 \text{ [MeV]}$$

The rest energy of the π^0 meson is $m_\pi c^2 = 135$ MeV. After collapse, 2 generated gamma-ray photons have energy of $m_\pi c^2/2 = 67.5$ MeV in the stationary system of π^0 meson and fly in opposite directions to each other.

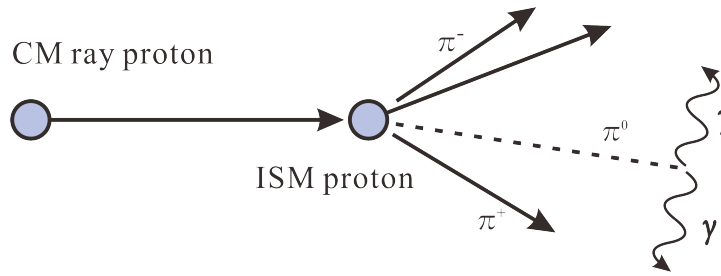


FIGURE 1.4: Schematic diagram of π^0 meson decay.

1.2.2.2 Electron bremsstrahlung

When the cosmic ray electrons approach the nucleus in the ISM, their directions are bent and accelerated by the electric field. At this time, gamma rays are emitted. This phenomenon is called electron bremsstrahlung radiation. The bremsstrahlung radiation spectrum is a continuously distribution in the range of $0 \leq h\nu \leq E$, where E is the energy of the electron, ν is the frequency of the electromagnetic wave radiated and h is Planck's constant. Assuming that the surrounding substances are completely ionized, the energy change rate of relativistic electron is expressed as follows:

$$-\left(\frac{dE}{dt}\right)_{\text{Brems}} = \frac{3}{2\pi} \sigma_{\text{T}} c \alpha Z(Z+1) N [\log \gamma + 0.36] E \quad (1.1)$$

where Z is the atomic number of the nucleus, and N is the number density, σ_T is the Thomson scattering cross section ($0.665 \times 10^{-28} \text{ m}^2$), and α is the fine-structure constant ($1/137$).

Equation 1.1 also represents the emissivity of the electromagnetic wave, which is proportional to the number density N . In the central part of the galaxy where the material density is higher than that surrounding region, an expanded gamma-ray source region has been observed. The observed energy region is from about several tens of MeV to several GeV. Among them, gamma rays in the low energy side (several hundreds MeV or less) are thought to mainly originate from cosmic ray electron bremsstrahlung, while in the higher energy side are thought to be generated by π^0 meson decay.

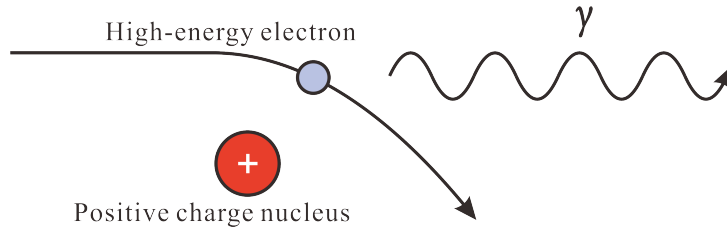


FIGURE 1.5: Schematic diagram of electron bremsstrahlung.

1.2.2.3 Inverse Compton scattering

Inverse Compton (IC) scattering is the phenomenon that relativistic electrons scatter low energy photons and raise the photon energy up to high energy. Like the bremsstrahlung, it is a gamma-ray radiation mechanism originating from electrons. This process is called inverse Compton scattering because it is regarded as an inverse process of Compton scattering (a process in which the high energy photons scatter stationary electrons and turn into low energy photons). The energy change rate of electrons due to inverse Compton scattering is expressed as follows

$$-\left(\frac{dE}{dt}\right)_{\text{IC}} = \frac{4}{3}\sigma_T c \gamma^2 \beta^2 U_{\text{ph}} \quad (1.2)$$

where σ_T , γ , $\beta = v/c$, U_{ph} are the Thomson scattering cross section, the Lorentz factor of electron, the ratio of electron velocity to the speed of light, and the energy density of the radiation field, respectively.

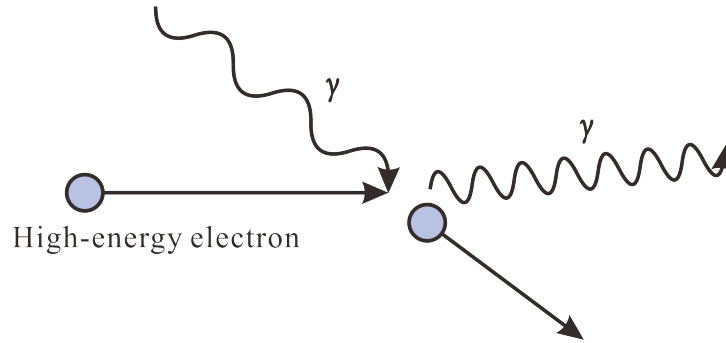


FIGURE 1.6: Schematic diagram of inverse Compton scattering.

1.3 Gamma-ray detector

In different energy regions, gamma rays are detected by various ways. Gamma rays below 30 MeV are detected by Compton telescope, whereas by using artificial satellite in the high energy (HE) range. Since being launched into space in 2008, the Fermi Gamma-ray Space Telescope (see Figure 1.7) has been running until now, detecting more than 3000 high energy objects. On the other hand, the incidence frequency of gamma rays ranging from tens of GeV to TeV is low so a wider effective area is required. Because the effective area of satellites launched into space is limited, it is difficult to observe these gamma rays by satellites. Therefore, there is a method to observe gamma rays indirectly on the ground separately from the observation in space by using artificial satellites. When very high energy (VHE) gamma rays arrive at the Earth, they interact with atomic nuclei in the atmosphere and generate Cherenkov light. By observing this Cherenkov light by using Imaging Atmospheric Cherenkov Telescope (IACT) on the ground, we can reconstruct the directions and the energies of the gamma rays arrived. There are some IACT arrays in operation now like MAGIC, H.E.S.S. and VERITAS as shown in Figure 1.8. The largest IACT arrays will be the Cherenkov Telescope Array (CTA) which is under construction and will be mentioned in more detail in the next chapter.



FIGURE 1.7: Fermi Gamma-ray Space Telescope [4].



FIGURE 1.8: Top: The H.E.S.S. (High Energy Stereoscopic System) telescope array [5]. Middle: The VERITAS (Very Energetic Radiation Imaging Telescope Array System) telescope array [6]. Bottom: The MAGIC (Major Atmospheric Gamma Imaging Cherenkov) telescope array [7].

1.4 Gamma-ray observation by IACTs

This section describes how gamma ray and cosmic ray go through the Earth atmosphere and how to observe gamma rays separately from cosmic-ray background.

1.4.1 Electromagnetic cascade

High energy primary particles entering the Earth's atmosphere will generate secondary particles by interaction with nuclei in the atmosphere. The secondary particles further produce particles by interaction. A series of such reactions repeatedly occurred, and the collection of particles generated is called an air shower. In the case that the primary particle is gamma ray, it is called electromagnetic shower, and in the case that the primary particle is proton, it is called hadron shower.

- Gamma-ray shower (Figure 1.9, left)

In the case the primary particle is high-energy gamma ray, gamma ray interacts with atomic nuclei in the atmosphere and cause electron-positron pair production. The generated electron and positron further emit gamma rays by bremsstrahlung, and emitted gamma rays cause electron-positron pair production again. This loop is repeated until the energy of the emitted gamma ray falls below the energy that electron-positron pair production dominates (about 83 MeV due to the Earth's atmosphere).

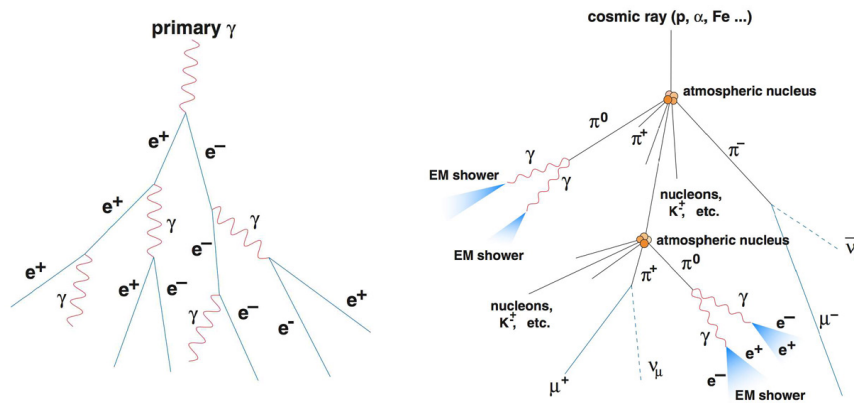


FIGURE 1.9: Schematic diagram of gamma-ray shower (left) and hadronic shower (right) [8].

- Hadronic shower (Figure 1.9, right)

In the case that the primary particle is high energy cosmic ray such as proton and etc, the primary particle interacts with atomic nuclei in the atmosphere and generates π^0 and π^\pm meson. The neutral pion π^0 collapses into two gamma rays, and these gamma rays cause electromagnetic shower.

1.4.2 Cherenkov radiation

When a charged particle travels through a dielectric medium, it causes the Cherenkov radiation in the case that speed of particle exceeds the speed of light in that medium. The electrons and positrons in the air shower generated by gamma rays or protons exceed the speed of light c/n in the atmosphere where c is the velocity of light, n is the refractive index of the atmosphere, and they emit Cherenkov light. Generated Cherenkov light possess wavelengths from the ultraviolet to visible light region. The angle θ formed by

the moving direction of Cherenkov light and particle is given by the following relational expression

$$\theta = \arccos\left(\frac{1}{\beta n}\right), \beta = \frac{v}{c}$$

where v is the speed of electrons and positrons.

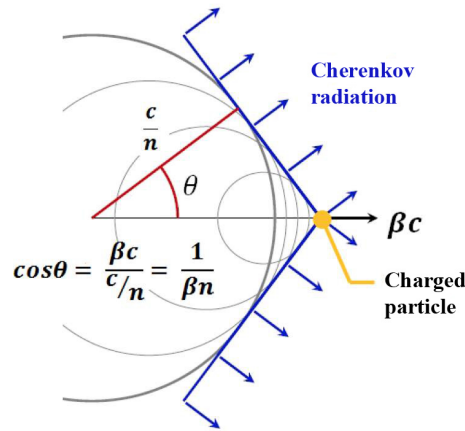


FIGURE 1.10: The principle of Cherenkov radiation [9].

Due to that refractive index of the atmosphere changes according to the altitude, Cherenkov light arriving at the ground level spreads like a circle of about 150 m in radius, regardless of the altitude of air shower occurrence. This area is called a light pool. In the Figure 1.11, the left picture shows the light pool observed at the ground level by a gamma ray of 300 GeV. The total number of Cherenkov photons is almost proportional to the energy of gamma ray. At 1 TeV gamma ray, the photon density on the ground in the light pool is about 50 photons/m².

1.4.3 The principle of gamma-ray observation by IACTs

The IACT is composed of a main mirror as reflector and a focal-plane camera mounting at focal point of the mirror. By placing IACT in the light pool, we can catch and collect the Cherenkov photons reflected from mirror as shown in Figure 1.12. The amount of light and the image of the shower are recorded as digital signals by detectors installed at focal-plane camera.

- **Distinction between gamma ray and cosmic-ray background**

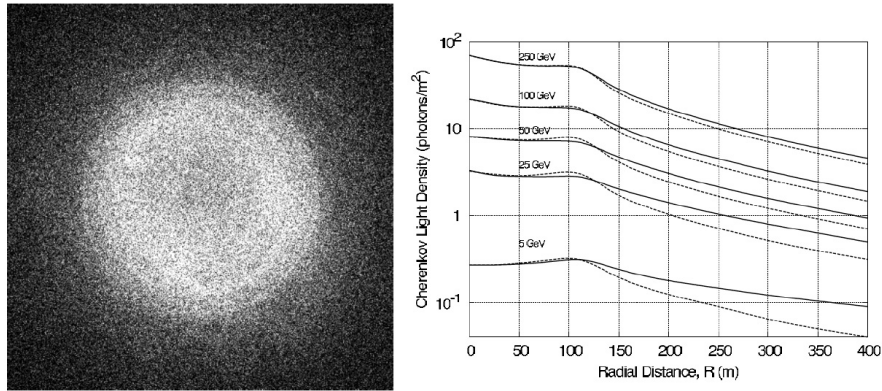


FIGURE 1.11: Left: the light pool observed at the ground level by a γ -ray of 300 GeV [10]. Right: simulation of the Cherenkov light as a function of the impact distance [11]. The solid and dashed lines show showers developing along to the earth magnetic field and 90° perpendicular to it, respectively.

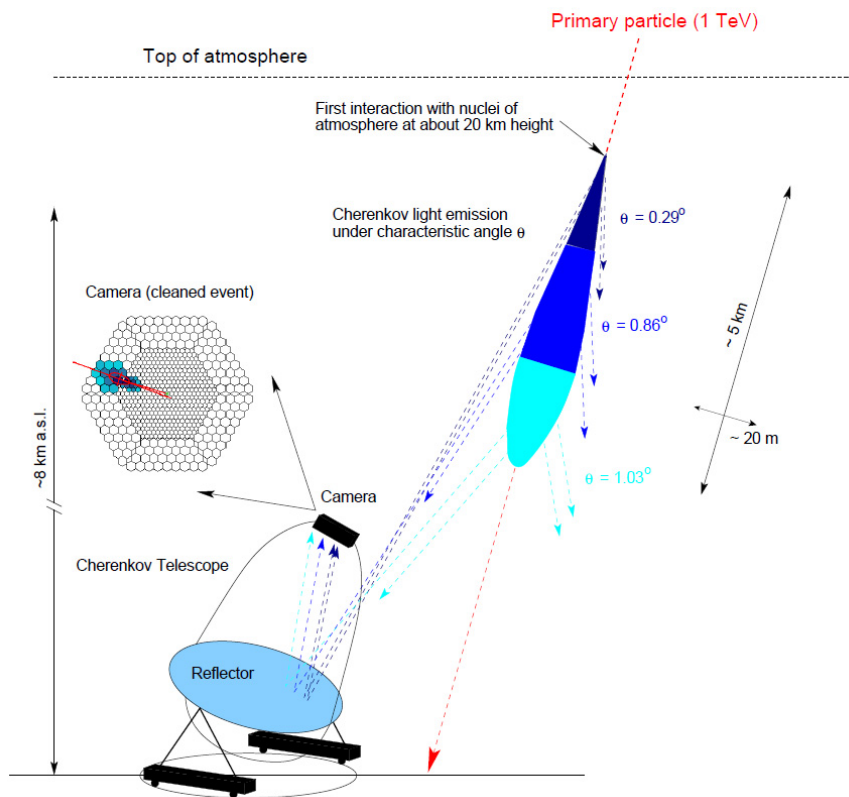


FIGURE 1.12: Illustration of an Imaging Atmosphere Cherenkov Telescope (IACT) catching Cherenkov light [10].

Compared with fewer gamma ray events, the charged cosmic rays are overwhelmingly large (about $10^3 - 10^4$ times) and become almost the background from the universe. However, because the image observed by IACT is different due to shower development, the gamma ray can be distinguished. There are two differences in

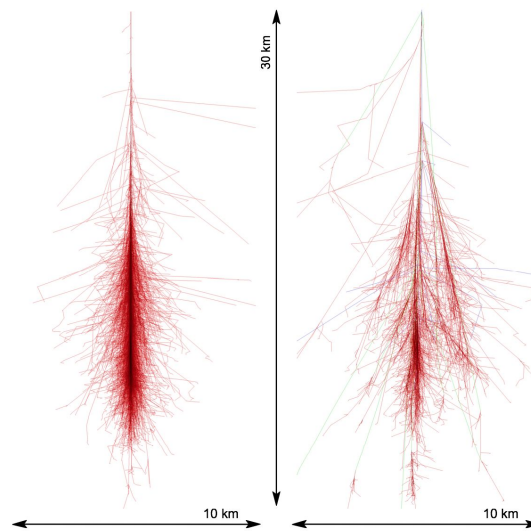


FIGURE 1.13: Difference in development of air showers by CORSIKA simulation [12]. Left: Gamma-ray shower development. Right: Hadronic shower development.

their shower developments. First, as shown in Figure 1.13, the image of gamma-ray shower does not spread and it develops compactly, while the image of hadronic shower spreads anisotropically. Second, if the gamma-ray shower axis and the optical axis of the telescope match together, the image is rounded at the center of the field of view. If it is parallel, the image appears in an ellipse whose long axis intersects the optical axis (see Figure 1.12). This feature does not exist in the case of hadronic shower. Figure 1.14 shows the distribution of photons reaching the focal-plane camera. The method identifying a gamma-ray shower from cosmic rays background based on the differences in the image of Cherenkov light like this way is called Imaging Atmosphere Cherenkov Technique (also called IACT).

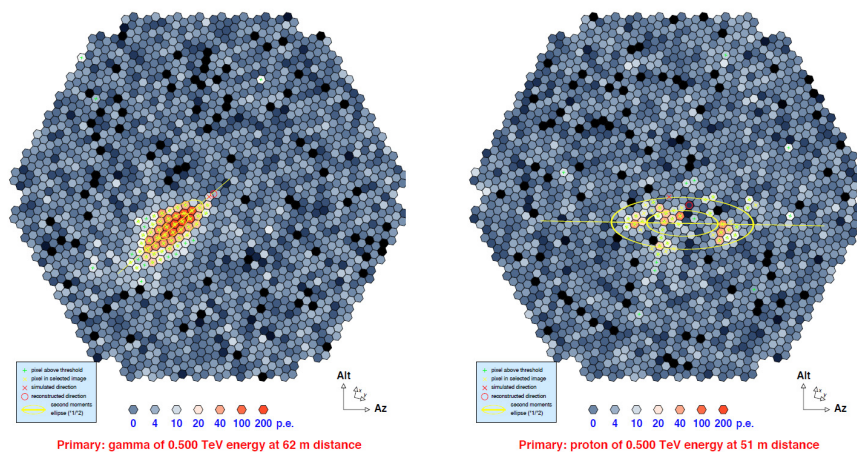


FIGURE 1.14: Left: Camera pixel image when observing γ -ray shower. Right: Camera pixel image when observing hadronic shower [9].

- **The determination of gamma-ray energy and its arrival direction**

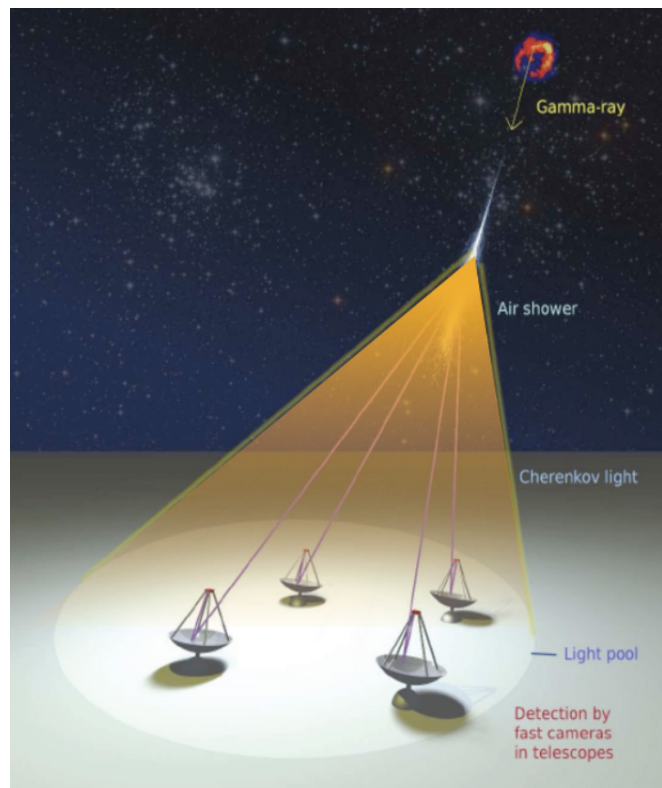


FIGURE 1.15: Stereo observation using 4 IACTs [13].

Because the photon number density in the light pool depends on the magnitude of the gamma ray energy arrived and it is almost constant, irrespective of the distance from the pool center (see Figure 1.11, right). Thus, the energy magnitude of arrival gamma ray can be estimated by only a part of photons detected from the light pool. The minimum energy of gamma rays that can be observed is inversely proportional to the light collecting area of the reflecting mirror. So for 1 TeV gamma ray, about several hundred square meters of effective area are necessary.

Besides, one method called stereo observation allows measuring the arrival direction of gamma ray more effectively. When Cherenkov light is captured at a position distant from the shower axis, parallax occurs between the gamma ray source and the air shower. Therefore, the shower image captured on the ground level is slightly deviated from the direction of the source and the long axis direction of the ellipse crosses the source direction. By observing 1 gamma-ray event by multiple telescopes and superimposing the images, it is possible to determine the arrival direction of the source (see Figure 1.16).

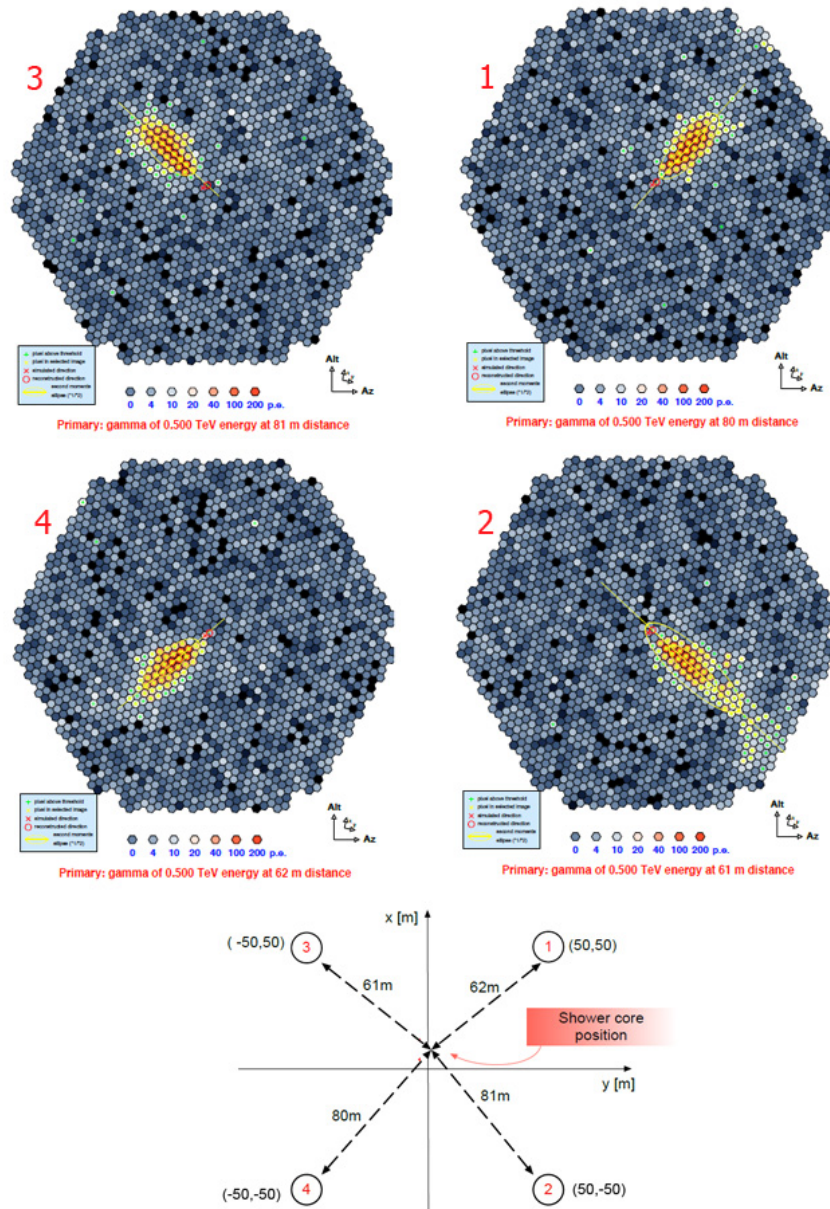


FIGURE 1.16: Up: Camera pixel image of each telescope when observing 1 shower using 4 IACTs. Bottom: Principle of the stereo observation using 4 IACTs [14].

The stereo observation can be performed with at least two telescopes. However, increasing the number of telescopes will increase the number of shower images, so the arrival direction will be predicted with higher accuracy. Moreover, since the stereo method can estimate the altitude of air shower occurrence by using the distance between the telescopes, it is possible to improve the accuracy of determining the energy of gamma rays.

Chapter 2

Cherenkov Telescope Array (CTA) project

2.1 Overview



FIGURE 2.1: CTA structure: a mixed array of different telescopes [1].

Cherenkov Telescope Array (CTA) project is an international plan constructing the largest gamma-ray observatory in human history. By arranging about hundred Cherenkov telescopes with different sizes in the northern and southern hemispheres, CTA can observe the whole universe and achieve sensitivity ten times beyond the current telescopes (see Figure 2.2), with an observable energy range from 20 GeV to 300 TeV. Figure 2.1 shows the imaging structure of CTA project using different types of IACT. With the implementation of CTA, it is expected to reach an observation of over thousand celestial objects, bringing a new deployment to astronomical researches, such as activity of high-energy celestial objects inside and outside our Galaxy, or evolution of galaxy's formation,

and so on. Currently, more than 1300 researchers from about 32 countries around the world are participating in this project.

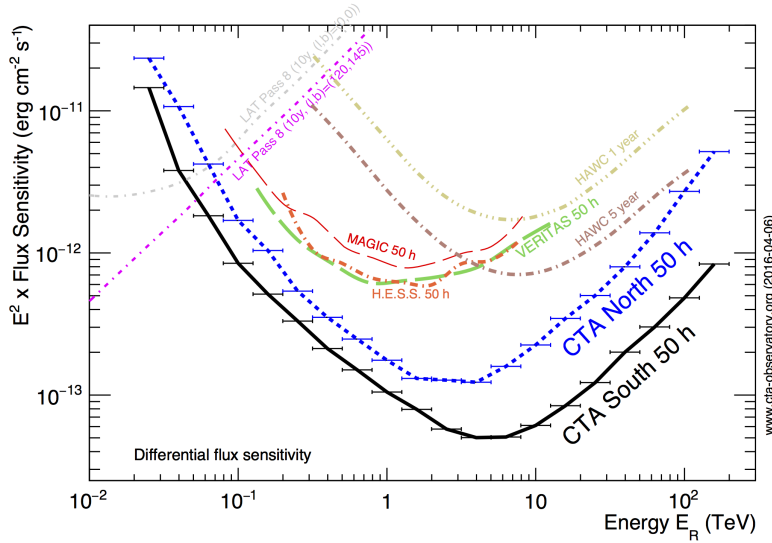


FIGURE 2.2: CTA sensitivity by Monte Carlo simulation. Both northern and southern site perform a deep sensitivity curve comparing with current arrays [1].

2.1.1 Telescope types

There are 4 classes of IACT designed for CTA. They are composed of Large-Sized Telescope (LST), Medium-Sized Telescope (MST), Schwarzschild-Couder Telescope (SCT) and Small-Sized Telescope (SST). Each types of telescope has been developed by an international collaboration.

- **Large-Sized Telescope (LST)**

The LST will be described in more detail in the next section.

- **Medium-Sized Telescope (MST)**

The MST is a modified Davies-Cotton telescope using 90 hexagonal segmented mirrors as one primary mirror as shown in Figure 2.3. This primary mirror possesses a diameter of 12 m and a focal length of 16 m (see Table 2.1). MST is an important part of CTA covering the core energy range from 100 GeV to 10 TeV with a large Field Of View (FOV) of 8° . Two types of camera: NectarCAM and FlashCAM will be used for MST.

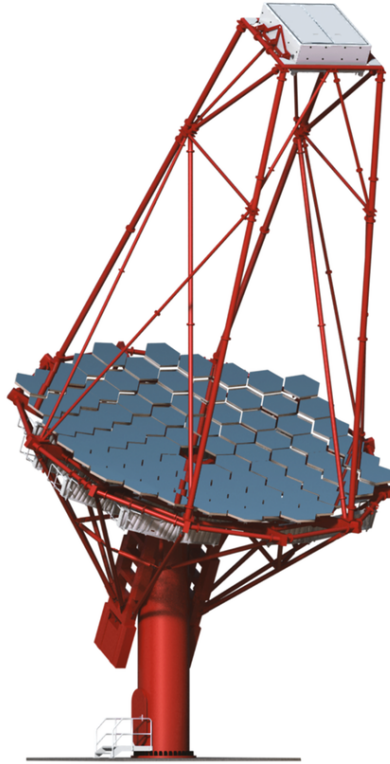


FIGURE 2.3: The MST structure [1].

- **Schwarzschild-Couder Telescope (SCT)**

As shown in Figure 2.4, the SCT is a dual mirror version of MST developed by institutes in the United States since 2006. Figure 2.4 shows the structure of SCT. The 2-mirror optical system is designed to cancel aberrations and de-magnify the image of Cherenkov light. Moreover, SCT is equipped with a compact, high-resolution camera. The SCT cover the same energy range with MST, from 100 GeV to 10 TeV with a wider FOV of 8.3° . Some main parameters of SCT are shown in Table 2.1.

Type	LST	MST	SCT
Reflector type	Parabolic	Davies-Cotton	Schwarzschild-Couder
Focal length	28 m	16 m	5.6 m
Dish diameter (primary)	23 m	12 m	9.7 m
Mirror effective area	368 m ²	>88 m ²	40 m ²
Camera FOV	4.5°	8°	8.3°
Energy range	20 TeV-1 TeV	100 GeV-10 TeV	

TABLE 2.1: Main parameters of LST, MST and SCT [1].

- **Small-Sized Telescope (SST)**

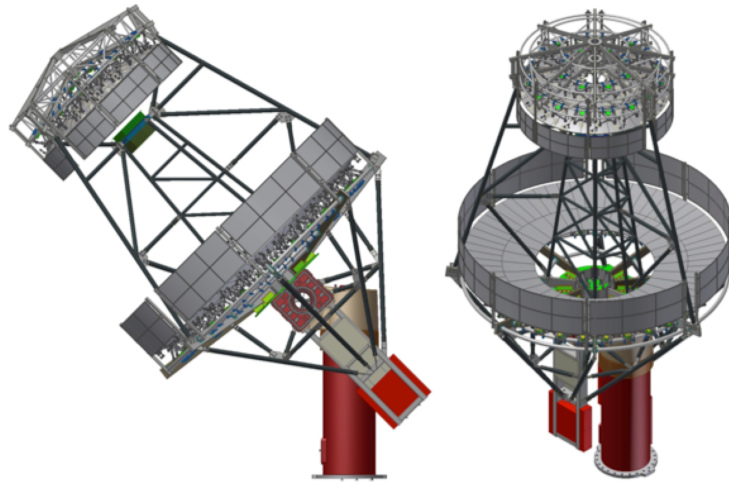


FIGURE 2.4: The SCT structure [1].

There are 3 different types of SST being considered: 1 single-mirror design (SST-1M) and 2 dual-mirror designs (SST-2M ASTRI and SST-2M GCT), as shown in Figure 2.5. A mixture of these types could be expected to be used in CTA, covering the highest energy range from 10 TeV to 300 TeV. Table 2.2 shows more detail about main parameters of these SST types.



FIGURE 2.5: The structure of 3 SST types [1]. Left: SST-2M GCT. Middle: SST-2M ASTRI. Right: SST-1M.

Type	SST		
	SST-2M ASTRI	SST-2M GCT	SST-1M
Reflector type	Schwarzschild-Couder	Schwarzschild-Couder	Davies-Cotton
Focal length	2.15 m	2.28 m	5.6 m
Dish diameter (primary)	4 m	4 m	4 m
Mirror effective area	6 m ²	6 m ²	6.47 m ²
Camera FOV	9.6°	9.2°	9.1°
Energy range	1 TeV-300 TeV		

TABLE 2.2: Main parameters of 3 SST types [1].

2.1.2 Array location

In July 2015, two sites of CTA in southern and northern hemispheres was decided for Paranal in Chile and La Palma in Spain respectively (see Figure 2.6). Figure 2.7 shows the current view of 2 sites. At both places there are other telescopes already in operation.



FIGURE 2.6: Two sites of CTA are shown as red point [1].

The telescope arrangement is optimized by simulation by the Monte Carlo group of CTA. As the baseline arrays, 4 LSTs and 15 MSTs for the north site, 4 LSTs, 25 MSTs and 70 SSTs for the south site will be arranged as shown in Figure 2.8 . Based on basic research so far, we are now advancing the manufacture, assembly and performance evaluation of each part toward the construction of first prototype. The development and



FIGURE 2.7: The current view of northern and southern sites [1]. Up: the northern site at La Palma, Spain, with 2 IACTs of MAGIC in operation now. Down: the southern site at Paranal, Chile.

construction are progressing for the purpose of full observation in 2021, and then observation of whole sky for about 20 years.

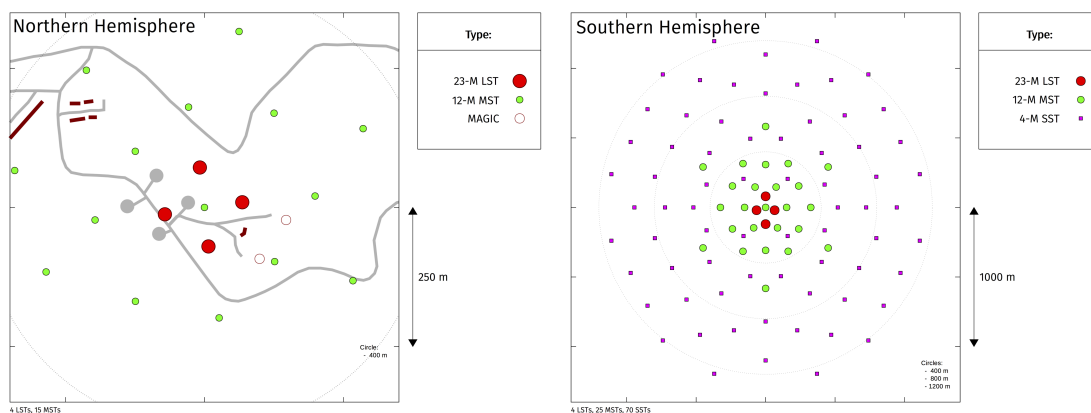


FIGURE 2.8: CTA array layouts in two sites. [1]

2.2 Large-Sized Telescope (LST)

The Large-Sized Telescope is an alt-azimuth telescope possessing a parabolic reflective surface. Figure 2.9 shows the whole structure of LST. The main mirror of LST consist of 198 hexagonal segmented mirrors. The diameter of primary mirror is up to 23 m, giving a large effective area of 400 m^2 , 2 times of MAGIC telescope. Although the LST stands 45

m tall and weighs about 103 tonnes, it can be possible to re-position quickly within only 20 seconds. Figure 2.10 shows all information about LST main parameters.

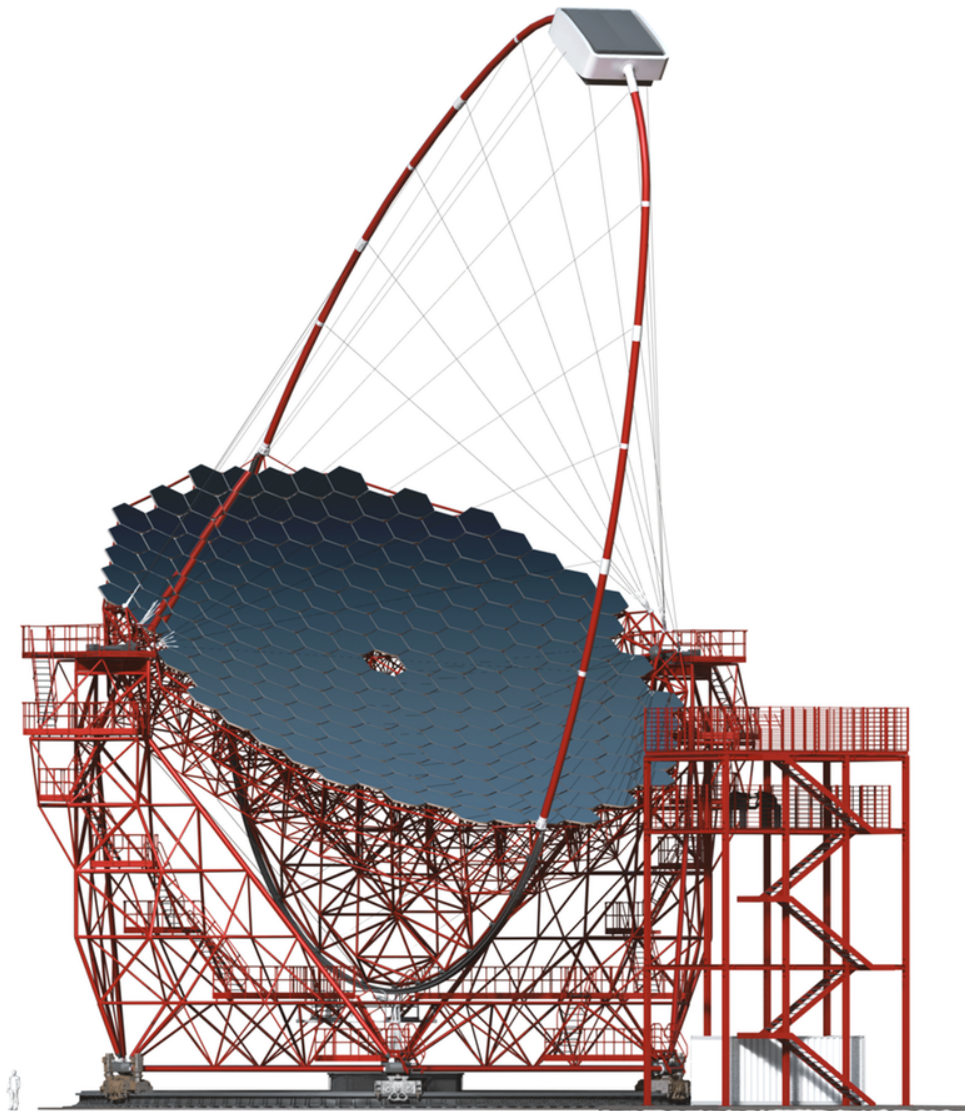


FIGURE 2.9: The LST in CTA [1].

The target energy range of LST is from 20 GeV to 1 TeV, covering the current observation energy range of Fermi. The observation by LSTs will improve the studies of galactic transient, high red-shift active galactic nuclei and gamma ray bursts.

The first LST prototype is now under construction in La Palma, Spain and will be finished until mid-2017. Its operation will verify all the parameters comparing to the simulation results.

- **The role of CTA-Japan group**

LST Main Parameters		
Optical Parameters		
Reflector type	1-mirror, parabolic	
Focal length	28 m	
Dish diameter	23 m	
f/D	1.2	
Mirror area	396 m ²	w/o shadowing
Mirror effective area	368 m ²	Including shadowing
Preliminary on-axis PSF	0.05°	
Preliminary off-axis PSF	0.11°	
Preliminary tracking accuracy	20 arcsec	RMS, online precision
Pointing accuracy	14 arcsec	RMS, post-calibration precision
Camera Parameters		
Camera dimensions (LxHxW)	2.8 m x 2.9 m x 1.15 m	
Weight	< 2000 kg	
Number of pixels	1855	
Pixel linear size	1.5 inch	2 inch including light concentrator
Pixel field of view	0.1°	
Camera field of view	4.5°	
Trigger region field of view	4.5°	
Sampling speed	1 GS/s	
Analogue buffer length	4 μs	for hardware stereo trigger
Readout rate	7.5 kHz (target), 15 kHz (goal)	
Dead time	5% at 7.5 kHz	
Mechanical parameters		
Total weight	103 tons	all moving parts
Repositioning speed	20 s	for 180° in azimuth
Elevation drive range	-70° to 100°	
Azimuth drive range	408°	
Inertia elevation	~6000 tons·m ²	
Inertia azimuth	~12000 tons·m ²	
Park position	zenith angle 95°	locked at the camera tower
Height at Camera Access	13 m above ground	In the parking position

FIGURE 2.10: The LST main parameters [1].

The LST is studied by an international collaboration of institutes and universities from Brazil, France, Germany, India, Italy, Japan, Spain and Sweden. However, CTA-Japan group has been playing an important leadership role, promoting research and development of LST. In particular, Japan group makes a significant contribution in supporting optical system and segmented mirrors, and in developing the focal-plane camera. Concretely, the total number of LST segmented mirrors to be constructed in the north and south sites is about 1600, but almost all of them are produced by CTA-Japan. Moreover, the Japan group also undertakes the development of Active Mirror Control (AMC), which is a mechanism controlling each segmented mirror individually, in order to support the optical system. Along with the development of optical system, the development of a focal-plane camera that detects the focused Cherenkov light and records shower image as electric signals is also an important object of Japan group.

This thesis describes in detail the current status of LST light concentrator, an important optical part of LST camera. The main content includes 2 part: the LST light

concentrator development and the establishment of its performance evaluation system at Ibaraki university.

Chapter 3

Development of light concentrators for LST

3.1 Overview

3.1.1 LST focal-plane camera

The LST camera has a hexagonal shape and weighs less than 2 tons (see Figure 3.1, left). Its focal plane is composed of 1855 Photomultiplier Tubes (PMT) divided into 265 PMT modules (i.e. PMT cluster). One module consists of 1 readout circuit, power supplying part, 7 PMTs, and 7 light concentrators (see Figure 3.2). The calibration test of 2000 PMTs for the first LST prototype has already done and they are being shipped to La Palma by boat at this time. Besides, an efficient cooling system for entire camera is also developed by CTA-Japan group.

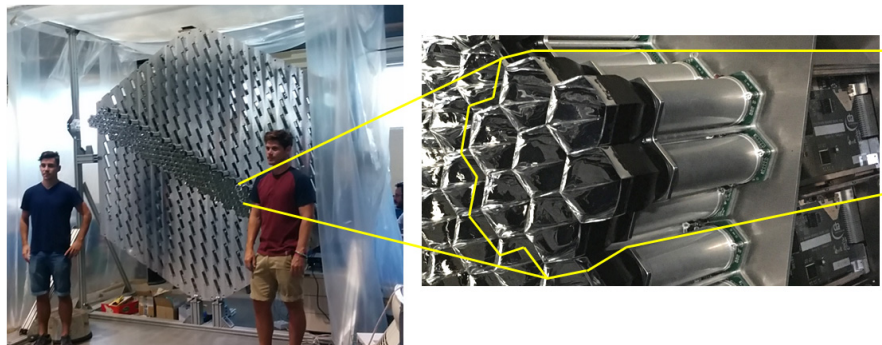


FIGURE 3.1: Left: LST camera. Right: PMT module equipped in camera.

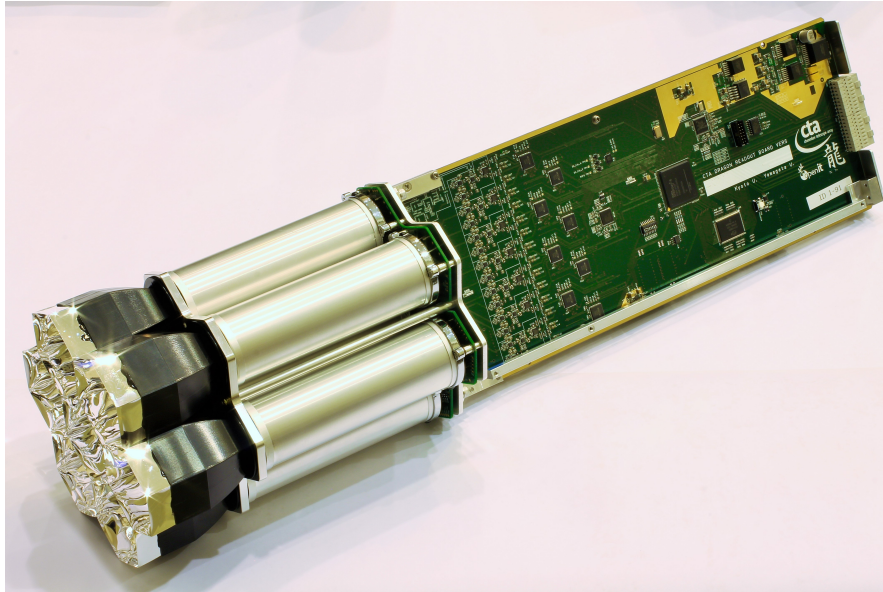


FIGURE 3.2: One PMT module [15].

3.1.2 Photomultiplier Tube

Photomultiplier Tube (PMT) is used in LST camera as a light detector. It is a vacuum tube using photoelectric effect to change incident photon to electric current. Figure 3.3 shows the PMT structure. Basically, it is composed of a light input window, a phototelectron emissive surface (photocathode), an electron multiplier (dynode) and an anode. When a photon comes into the window, a photoelectron will be emitted probabilistically and be multiplied 4×10^4 times overall. This probability is called Quantum Efficiency (QE). Detected photon number depends on the QE of PMT, meaning that if the QE is low, there is a large loss of detected photons.

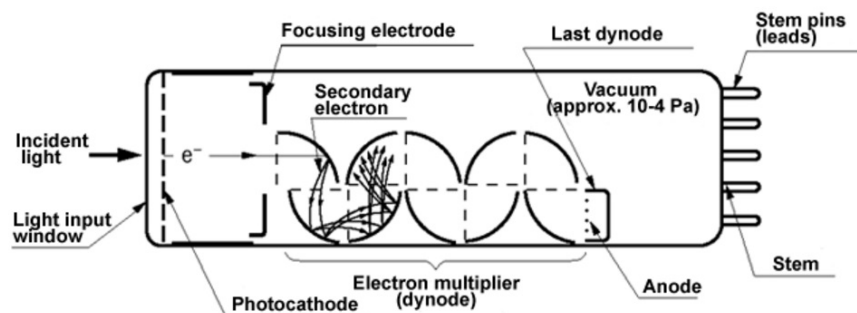


FIGURE 3.3: Cross-section of photomultiplier tube [16].

LST photomultiplier tube is a photosensitive device named R11920-100, which is

developed by both CTA Japan group and Hamamatsu Photonics K.K. This PMT is optimized for detecting the wavelength range from 290 nm to 600 nm, with the best QE at 350 nm wavelength. This wavelength has the strongest intensity that can observe Cherenkov light on the ground. Figure 3.4 shows the Cherenkov light intensity and the QE curve of the R11920-100 PMT as a function of the wavelength. Figure 3.5 shows the averaged anode (red dashed) and cathode (black solid) sensitivity of the R11920-100 PMTs versus light source position (a), and the result of PMT incident angle dependence analysis measured by S.Ono (b). Moreover, the light input window of this PMT series is frosted to increase a few percent of QE. Because the camera's diameter is very large up to 2 m, using totally 1855 PMTs so a few percent up is also important for telescope performance.

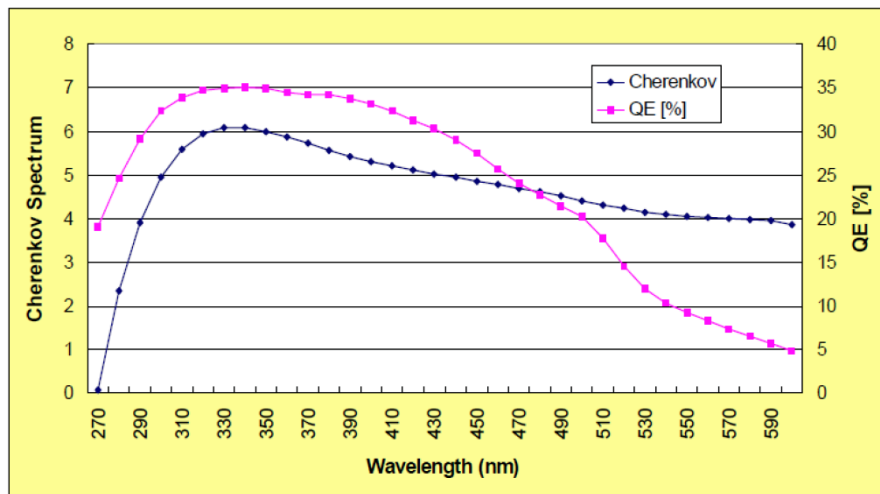


FIGURE 3.4: Cherenkov light intensity and the QE curve of the R11920-100 PMT as a function of the wavelength [17].

3.1.3 Light concentrator (LC)

Light concentrator (LC) is an optical instrument which is usually put in front of the light sensor of focal-plane camera. LST focal-plane camera is made by 1855 PMTs and 1 PMT will be equipped by 1 light concentrator. As shown in Figure 3.6, because the PMT is cylindrical, a gap called “dead space” occurs among PMTs when aligning them side-by-side. This gap will decrease the detected light coming from primary mirror to camera focal plane. Therefore, light concentrator is put in front of the PMT to minimize dead space, increase thoroughly the reflected light into PMT. On the other hand, there is one more use of light concentrator that decreases the stray light from the Earth's background.

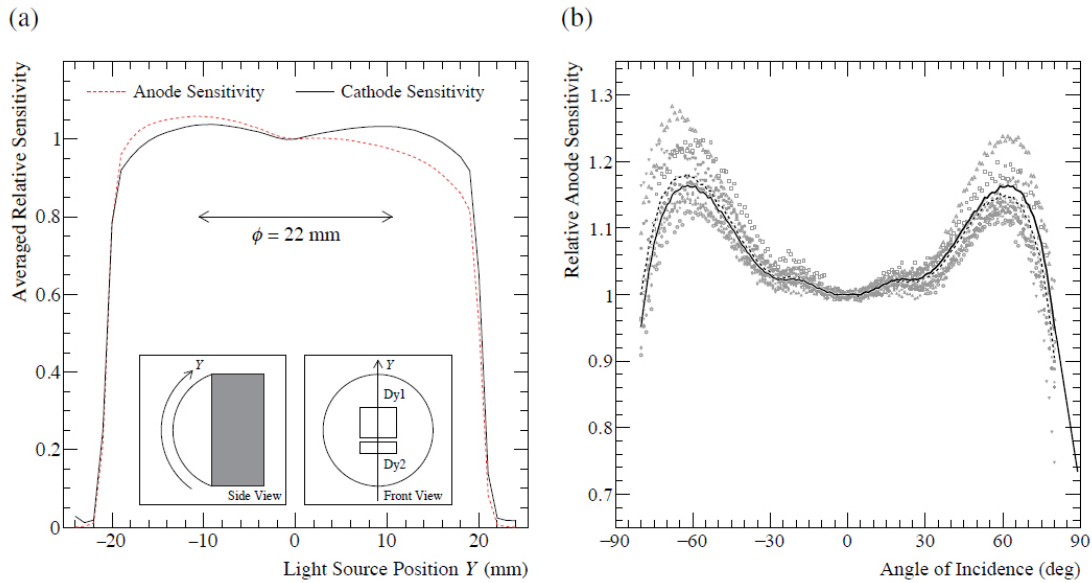


FIGURE 3.5: (a): The averaged anode (red dashed) and cathode (black solid) sensitivity of the R11920-100 PMTs versus light source position, provided by Hamamatsu Photonics [18]. Measurements of 90 PMTs were averaged and normalized to the position at $Y = 0$ mm. The insets schematically illustrate a PMT and the definition of the curved Y axis. The value of $\phi = 22$ mm is the exit aperture diameter of the current light concentrator. (b): The result of PMT incident angle dependence analysis (photon detection efficiency versus angle of incidence), measured by S.Ono [16, 18]. The measurement result of each PMT was normalized relative to the vertical (i.e., 0°) as a reference and corrected by cosine. The data points show measured values for eight PMTs. The dashed line shows the average of the eight PMTs. The solid line shows the symmetrical average (and extrapolates to $80^\circ - 90^\circ$).

3.2 Current status

The light concentrator of LST has been being developed by K.Kuroda, S.Tanaka and S.Ono with the help of Assistant Professor A.Okumura, Associate Professor H.Katagiri, and Professor T.Yoshida from 2009. The last design was approved last year (2015). In this section is described the current status of the LST light concentrator based on Sakiya Ono's previous research [15].

3.2.1 Design

The first design of light concentrator was initiated by Winston, under the name "Winston cone". However, it is not clear that this design of Winston cone is best suited for LST, so the optimization was required. The inner curved surface of light concentrator which based on Winston cone was optimized with quadratic Bézier curve by A.Okumura [19]. The last design was approved last year (2015) with the shape of hexagonal cylinder as shown in

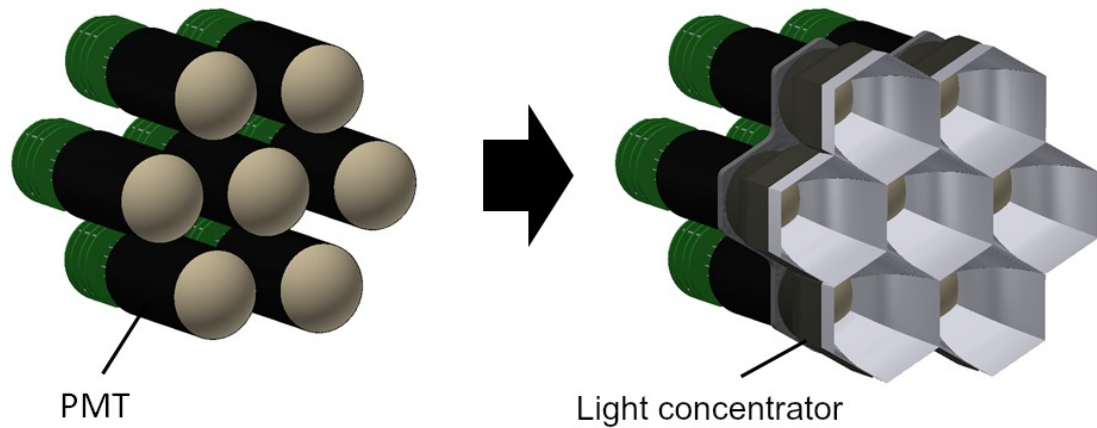


FIGURE 3.6: Seven PMTs of 1 module before (left) and after (right) equipping seven light concentrators [16].

Figure 3.7, consistent with the honeycomb arrangement of PMTs. The final design is a combination of ABS plastic cone and Enhanced Specular Reflector (ESR). Figure 3.8 shows the structure and the real one. The cone and ESR are specifically described as follows.

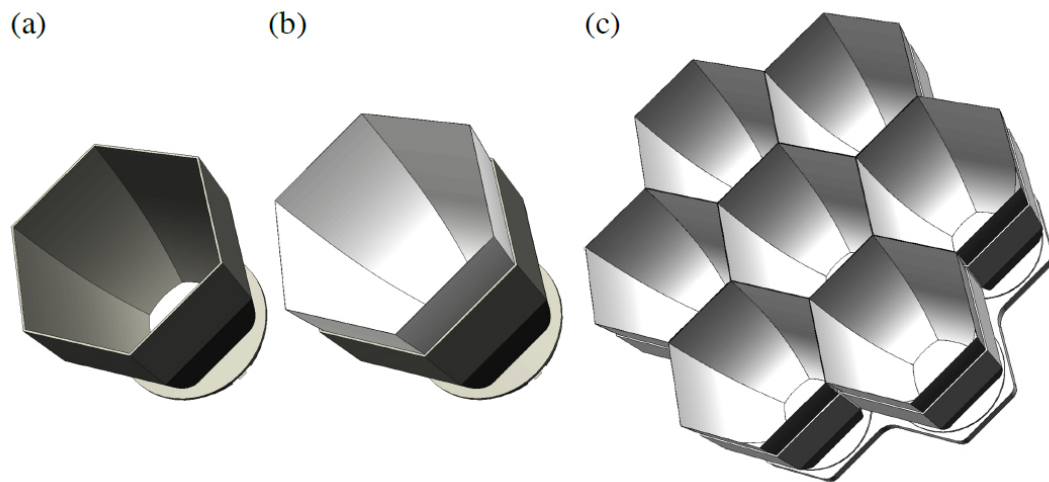


FIGURE 3.7: (a): 3D CAD model of the base ABS cone of an LST light concentrator. (b): Same as (a), but six specular ESR films are attached to the cone. (c): A light concentrator cluster comprised of seven copies of (b) and an interface plate at the bottom [19].

3.2.1.1 Cone

The cone has a shape like a hexagonal cylinder, is made of plastic and manufactured in large quantity by injection molding technology. The model for injection molding was commissioned to Proto Labs G.K. (Japan). The shape of exit aperture is fitted to the spherical



FIGURE 3.8: (a) 3D CAD model of the base ABS cone of an LST light concentrator. (b) Same as (a), but six specular ESR films are attached to the cone. (c) A light concentrator cluster comprised of seven copies of (b) and an interface plate at the bottom [19].

entrance surface of PMT, so that the PMT can "sink into" the concentrator without gap or light leakage. Figure 3.9 shows the cone structure (left) and the real one (right).

3.2.1.2 Enhanced Specular Reflector (ESR)

The Enhanced Specular Reflector (ESR) is originally made to reflect visible light and reflects well in the wavelength range from 400 nm to 800 nm. In order to observe Cherenkov light, it is necessary to coat the ESR to 300 nm in the UV band. This work was commissioned to Bte GmbH German company dealing with the coating processing and optical products. ESR is pasted on glass with Kapton tape and its surface was coated with 54 layers of SiO_2 and Ta_2O_5 alternately by vapor deposition (see Figure 3.10). The performance of bare and coated ESR is shown in Figure 3.11.

The ESR is designed to protrude from the cone at the entrance of light concentrator as shown in Figure 3.7 (b). Since the minimum thickness of the cone is 0.5 mm, so if the cone comes to the tip, the corresponding dead space will be generated. Specifically, the detected area decreases by 4%. This area should be thoroughly reduced, so it was decided that ESR comes to the tip instead of cone, in order to detect the light reflected at the cut-off angle 25.8° as much as possible.

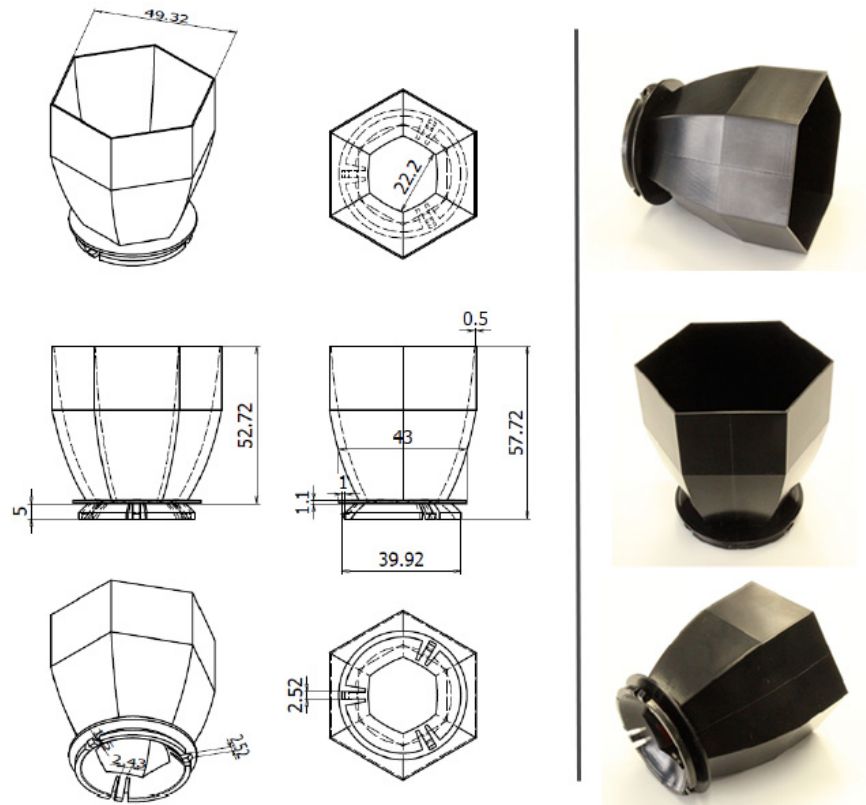


FIGURE 3.9: Left: cone structure. Right: the real one [16].

3.2.2 Production method

The production method of light concentrator was confirmed by S.Ono [16]. It is a hand-made method by 3 steps as follows.

- Cutting ESR:** The ESR coated by Bte GmbH was delivered to Ibaraki university as a state attached on glass by Kapton tape (see Figure 3.10). The ESR is then cut by laser cutter along a ESR cutting drawing. As shown in Figure 3.12 (b), this cutting drawing is consist of 6 pieces for all 6 surfaces of light concentrator, connecting together only by a tip of 2.2 mm. When the ESR was removed from the glass, it warped greatly as shown in Figure 3.12 (c).
- Pasting ESR to cone:** After cut, 2 edges of cutting ESR are connected together by Kapton tape and put into a male mold (see Figure 3.13 (a)). Six surfaces of cutting ESR are hold by a weight at the top of male mold and applied glue to the backside (see Figure 3.13 (b), (c)), and thence covered by plastic cone. The whole setting mold is turned over and pressed by producer's weight.

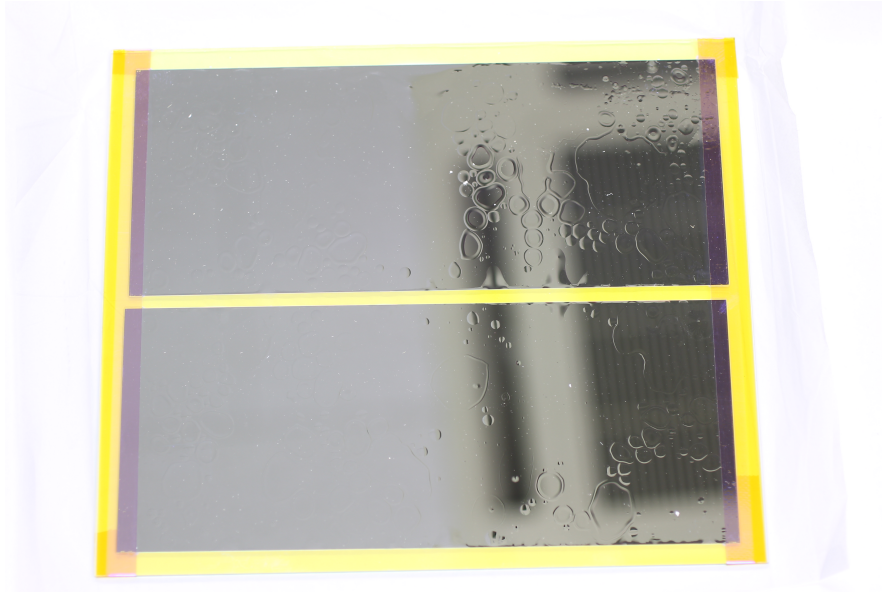


FIGURE 3.10: The coated ERS [16].

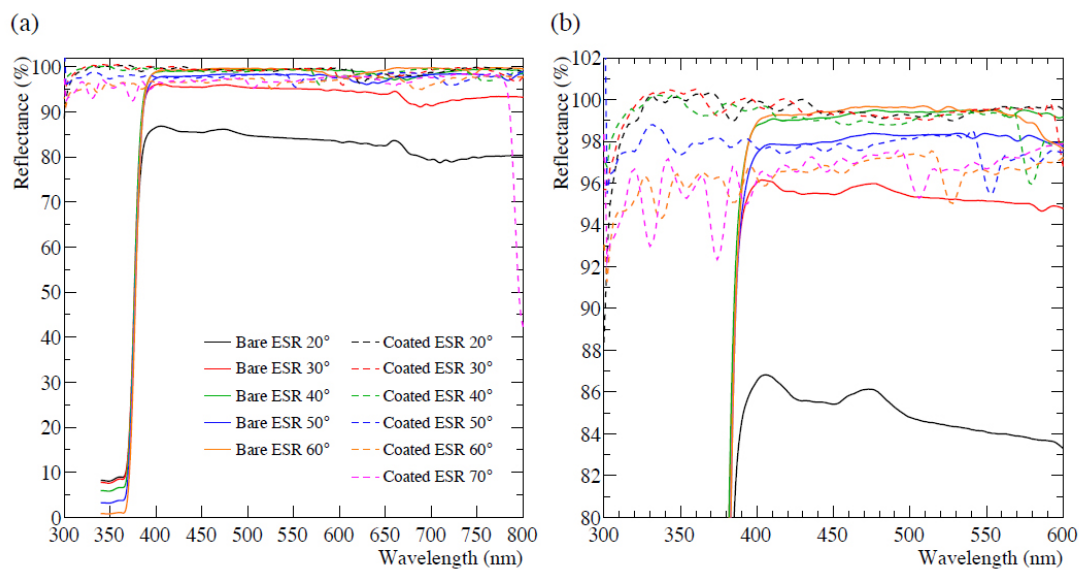


FIGURE 3.11: (a) The measured reflectance of bare (solid lines) and coated (dashed) ERS films at the angle of incidence such as 20° , 30° , 40° , etc. (b) Same as (a) but only limited wavelength ranges are shown. The systematic uncertainty of these measurements is estimated to be $\sim 1\%$, and thus some data points are higher than 100% [19].

- **Checking leaked glue and cleaning:** Leaked glue among 6 ERS surfaces is checked by eyes and wiped with a pointed cotton swab. Thus, the inner surface is wiped carefully with lens cleaning paper and lens cleaning liquid.

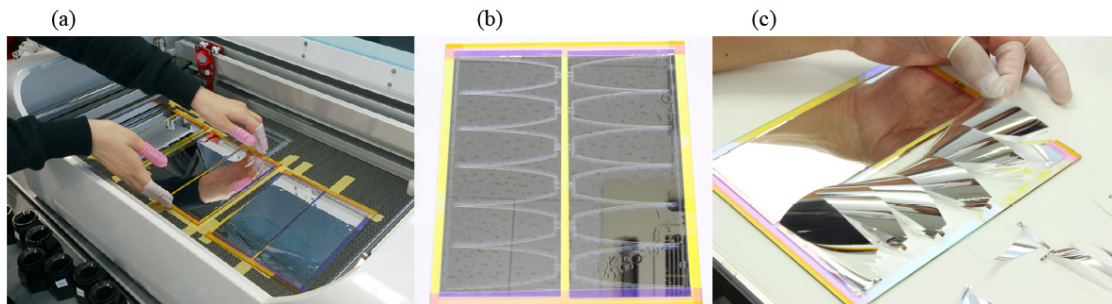


FIGURE 3.12: The ERS cutting process [16]. (a): ESR is set into laser cutter. (b): The state of ESR after cutting. (c): ESR warped greatly after removing from glass.

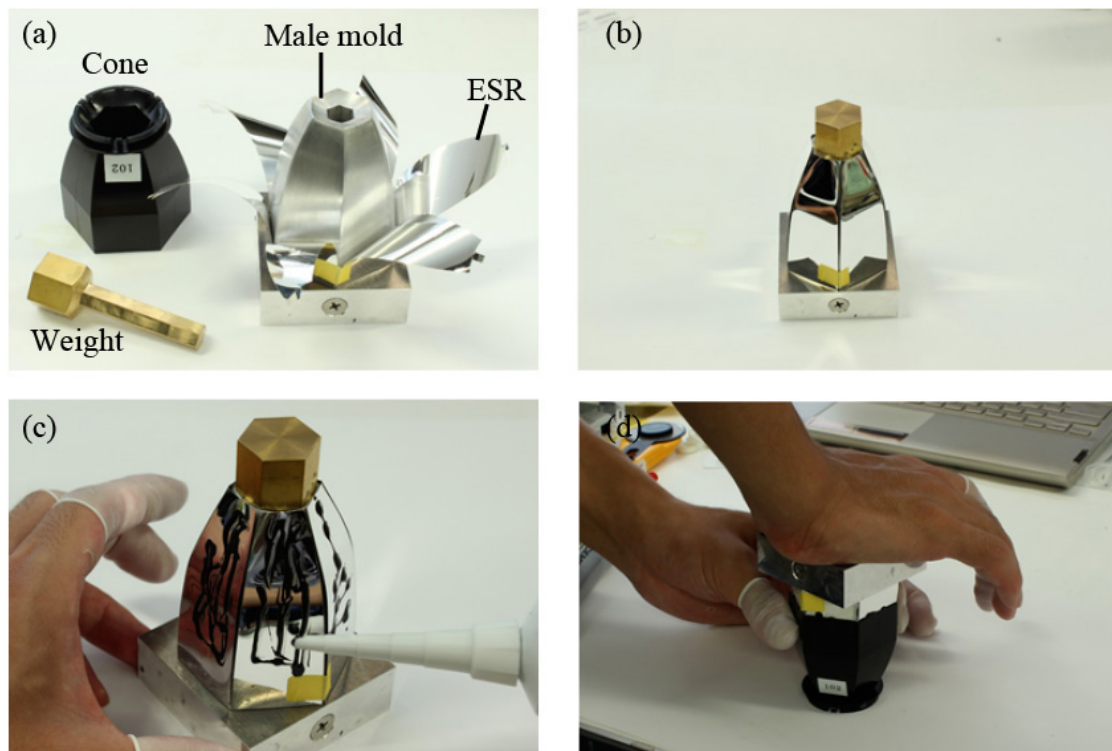


FIGURE 3.13: The ESR pasting process [16]. (a): cutting ESR is connected together by Kapton tape and put into a male mold. (b): the state after holding the weight at the top. (c) Applying glue to the backside. (d) Pressing the male mold by producer's weight.

3.2.3 Mass production

Mass production was started from November 2015. The manufacturing was done by Ibaraki University students, under the direction and management of S.Ono and me. Figure 3.14 left shows the mass-producing place at Ibaraki University. About 900 pieces have been produced here. The completed light concentrators were contained in paper cups one by one, wrapped to preserve from dust (see Figure 3.14, right). Besides, their condition and performance were also checked carefully. Those in bad condition will be fixed or used for testing.



FIGURE 3.14: Left: the view of mass-producing place. Right: Mass produced light concentrators.

About 400 pieces of completed light concentrators has been evaluated and divided into 3 batches. The first batch (150 pieces) was measured by S.Ono and sent to the Institute for Cosmic Ray Research (ICRR), University of Tokyo, for mini camera test. The second and third batches (252 pieces - 36 clusters) were measured by me, then sent to Spain for attachment test. Figure 3.15 and 3.16 show the RAS value distribution of the second and third batch evaluated with LED 365 nm. The average value of RAS of second and third batch was $84.5\% \pm 1.66\%$ and $85.1\% \pm 1.55\%$ respectively. The checked light concentrators are boxed (see Figure 3.15 and 3.16 right), and sent by the shipping company Akabou. The box was also wrapped in blanket in order to avoid shock. The rest of light concentrators has been stored at Ibaraki University.

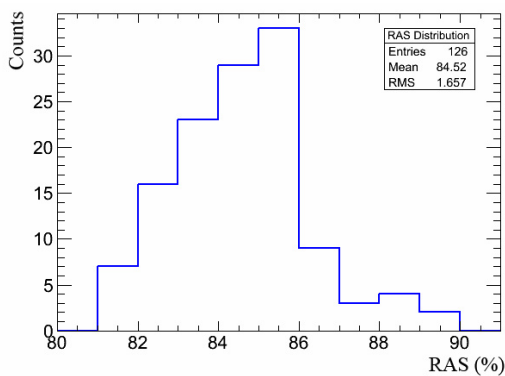


FIGURE 3.15: Left: The RAS value distribution of the second batch (126 pieces - 18 clusters). Right: The state of second batch after boxed.

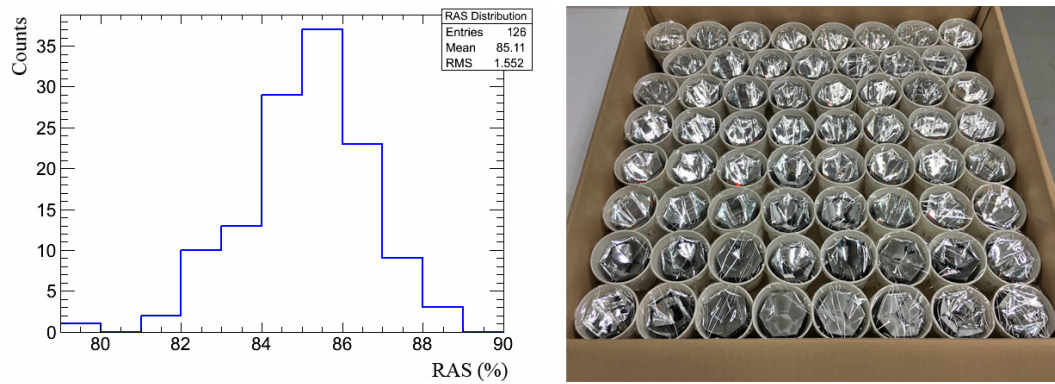


FIGURE 3.16: Left: The RAS value distribution of the third batch (126 pieces - 18 clusters). Right: The state of second batch after boxed.

3.2.4 Performance evaluation system

3.2.4.1 Set-up

The performance of light concentrator is evaluated by an optical measurement system in the darkroom. Figure 3.17 and 3.18 show respectively the schematic diagram and the real status of performance evaluation system for light concentrator. The experimental set-up is mounted on an optical table, attached on rails. The system consists mainly of a rotation machine, PMT, concentrator, LED, DRS4, pulse generator, and voltage supplier. PMT and light concentrator are placed on a rotation stage. Figure 3.19 shows the performance evaluation system looking from backside. When measuring, the light concentrator is attached in a hexagonal frame designed by S.Ono (see Figure 3.20), and pushed by the PMT from behind. The LED is installed 2.4 m away from the position of light concentrator and emits pulse. The spread of light incident on PMT is then within 1° based on the distance of 2.4 m. As shown in Figure 3.22, three types of light-emitting diodes (LEDs) of 310 nm, 365 nm and 465 nm in peak wavelength are used (mainly 365 nm). A black curtain was hung between LG and PMT to prevent light reflected on the ceiling and wall of the darkroom. A rectangular hole of about 17×26 cm is opened in the middle of the curtain, letting light pulses pass through.

3.2.4.2 Relative Anode Sensitivity

Ordinarily, the collection efficiency (CE) is used to evaluate the performance of light concentrator. The CE of 1 concentrator means how much it can collect the light. The CE is a function of the incident angle, calculated by the ratio of the amount of light entering the

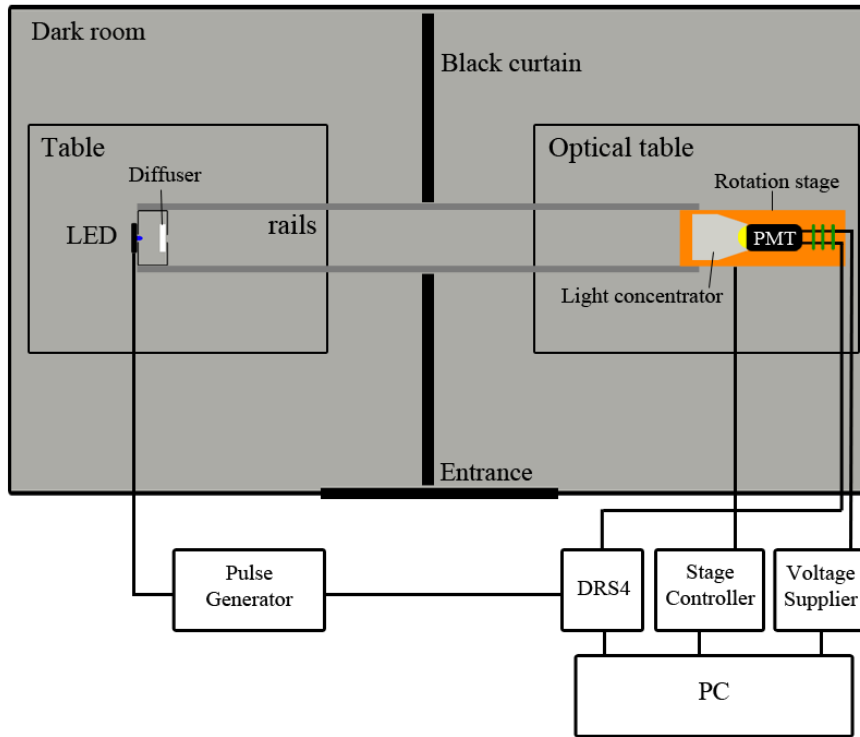


FIGURE 3.17: Schematic diagram of set-up for light concentrator. The distance from the light source to the PMT is 2.4 m, so that the spread of light incident on PMT is within 1° .



FIGURE 3.18: The performance evaluation system in real. Left: left side of dark room with LED at the leftmost. Right: right side of dark room with PMT and light concentrator at the rightmost.

entrance aperture of the concentrator and the amount of light leaving the exit aperture as follows

$$CE(\theta) = \frac{\text{amount_of_light_exiting_the_LC}(\theta)}{\text{amount_of_light_entering_the_LC}(\theta)}. \quad (3.1)$$

However, these two quantities can not be measured simultaneously. Therefore, the formula 3.1 is in fact calculated by measuring at the entrance and at the exit separately. The measurement is executed in two steps as follows.

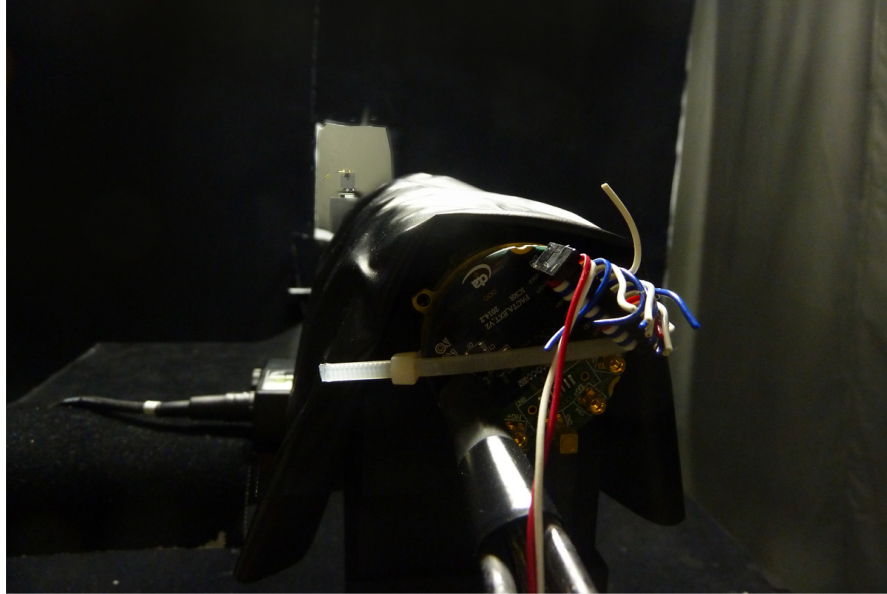


FIGURE 3.19: The performance evaluation system looking from backside.

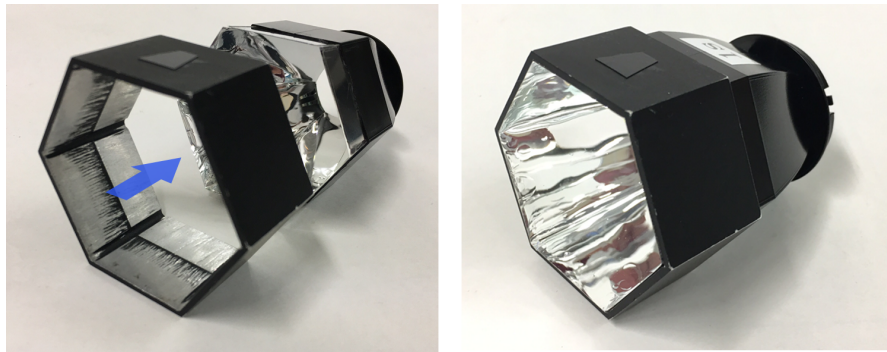


FIGURE 3.20: Left: the hexagonal frame and LC. Right: LC attached into hexagonal frame.

- **Step 1 (mask case):** The PMT is placed on the rotation stage so that the entrance surface is tangent to the position of the LC entrance aperture. Figure 3.21 (a) and 3.23 show respectively the real status and the schematic diagram of mask case. The PMT is then masked with the hexagonal mask whose area is equal to the area of exit aperture. The amount of light recorded by this measurement will be multiplied by the area ratio between the mask hole and the entrance aperture and the cosine of the incident angle θ . The result of this calculation is the amount of light that enters into the concentrator as a function of the incident angle θ :

$$\text{amount_of_light_entering_the_LC}(\theta) = \text{PMT_value_at_entrance}(0^\circ) \times \frac{S_{\text{pixel}}}{S_{\text{mask}}} \times \cos(\theta). \quad (3.2)$$

where $\text{PMT_value_at_entrance}(0)$ is the output value of PMT at incident angle 0°

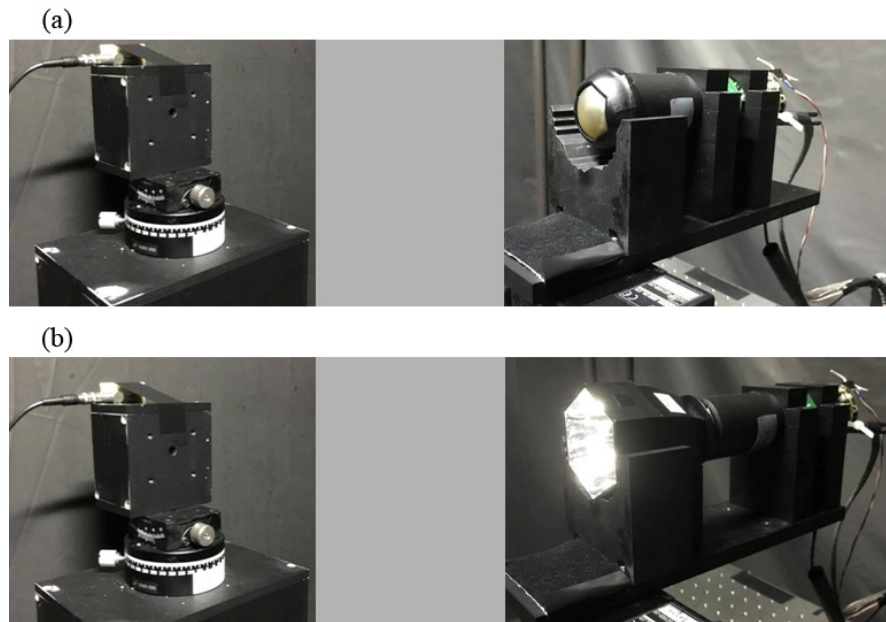


FIGURE 3.21: The performance evaluation system. (a): Left side is the state of LED and right side is the setting state of PMT with mask in the case of step 1 (i.e. mask case). (b): Left side is the state of LED and right side is the setting state of PMT with light concentrator in the case of step 2 (i.e. LC case).

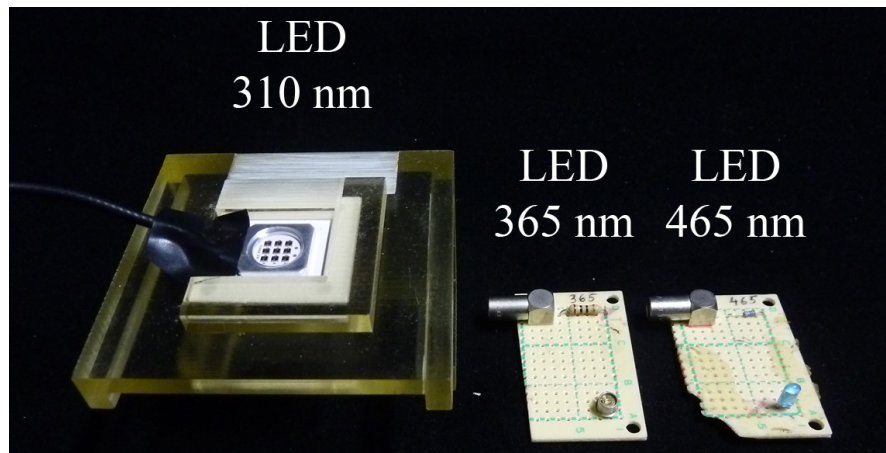


FIGURE 3.22: Three types of LED: 310 nm, 365 nm and 465 nm.

when hexagonal mask is attached, S_{mask} is the area of hexagonal hole of mask, and S_{pixel} is the area of LC entrance aperture, i.e. LST camera pixel. Based on previous research, $\frac{S_{\text{mask}}}{S_{\text{pixel}}}$ is about $\frac{1}{3.7352}$.

- **Step 2 (LC case):** The light concentrator is placed on the rotation stage and the PMT is then attached to the exit aperture of the concentrator (see Figure 3.21 (b)). After that, the rotation stage is rotated to the angle θ and the amount of light exits

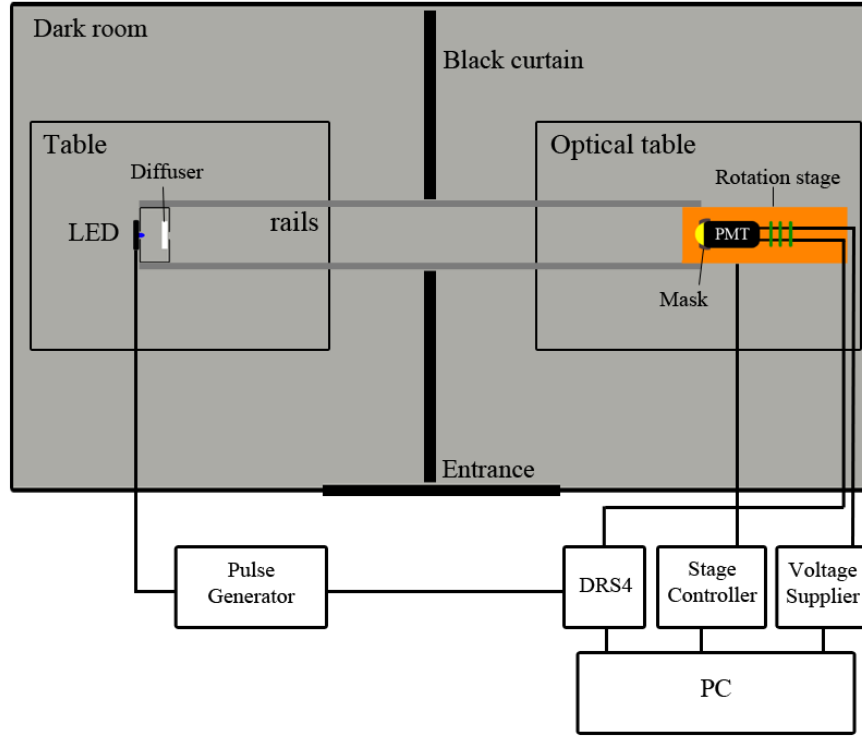


FIGURE 3.23: Schematic diagram of setup in the case of mask measurement.

the concentrator is recorded as:

$$\text{amount_of_light_exiting_the_LC}(\theta) = \text{PMT_value_at_exit}(\theta) \quad (3.3)$$

where $\text{PMT_value_at_exit}(\theta)$ is the output value of PMT at incident angle θ degree when light concentrator is attached.

By substituting Equation 3.2 and 3.3 into Equation 3.1, we define the Relative Anode Sensitivity (RAS) as a new quantity for evaluating performance of light concentrator as follows:

$$\text{RAS}(\theta) = \frac{\text{PMT_value_at_exit}(\theta)}{\text{PMT_value_at_entrance}(0)} \times \frac{S_{\text{mask}}}{S_{\text{pixel}}} \times \frac{1}{\cos \theta} \times 100\%. \quad (3.4)$$

3.2.4.3 On-axis measurement

The on-axis measurement is a procedure measuring only the RAS of each light concentrator at $\theta = 0^\circ$. The on-axis measurement is consist of 2 steps as follows. Step 1 and 2 can be swapped for each other.

- **Step 1:** First, the measuring person enters the dark room, turns on the mini bulb, attaches the mask on PMT, turns off the mini bulb, then leaves and closes the dark room. The measuring person runs the measurement script (see Appendix D) and the amount of light at entrance aperture is measured.

The measurement is subdivided into 4 times, each consisting of 500 pulses. The integral of each pulse is calculated, minus the pedestal part and filled in a graph. Then, the average of 500 pulses and its statistical error for each time are calculated from this graph as $x_{m_i} \pm \sigma_{m_i}$ ($i=0,1,2,3$ for 4 times). The average value $\bar{x}_m \pm \varepsilon_m$ of 4 times will be the final value of mask case with

$$\bar{x}_m = \frac{\sum_{i=0}^3 x_{m_i}}{4},$$

$$\varepsilon_m = \sqrt{\frac{\sum_{i=0}^3 (x_{m_i} - \bar{x}_m)^2}{4}},$$

where ε_m is known as standard deviation. The detailed calculations are described in Appendix A. Figure 3.24 shows an example of mask case results.

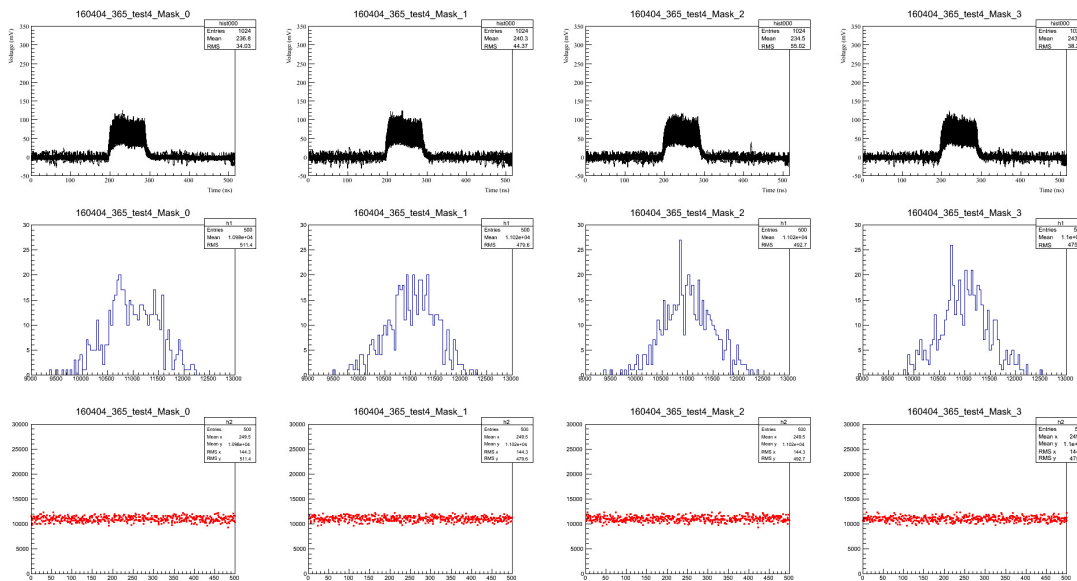


FIGURE 3.24: Top line: In each graph shows 500 signals of mask case at 365 nm. Middle line: In each graph shows the distribution of 500 signals each time. Bottom line: In each graph shows the distribution in numerical order of counts.

- **Step 2:** After that, the measuring person enters the dark room again, turns on the mini bulb, replaces mask by light concentrator, turns off the mini bulb, then leaves and closes the dark room. Finally, the measuring person runs the same measurement script and the amount of light at the exit aperture is measured as

$x_{LC_i} \pm \sigma_{LC_i}$ ($i=0,1,2,3$ for 4 times). As same as mask case, the average of 4 times is calculated as the final value of LC case as $\bar{x}_{LC} \pm \varepsilon_{LC}$ with

$$\bar{x}_{LC} = \frac{\sum_{i=0}^3 x_{LC_i}}{4},$$

$$\varepsilon_{LC} = \sqrt{\frac{\sum_{i=0}^3 (x_{LC_i} - \bar{x}_{LC})^2}{4}},$$

where ε_{LC} is known as standard deviation.

The measured values are analyzed by an analysis script based on Equation 3.4, and the RAS value is calculated as $RAS(0^\circ) \pm \varepsilon_{RAS(0^\circ)}$ with

$$RAS(0^\circ) = \frac{\bar{x}_{LC}}{\bar{x}_m} \times \frac{1}{3.7352} \times 100 \%, \quad (3.5)$$

$$\varepsilon_{RAS(0^\circ)} = RAS(0^\circ) \times \sqrt{\left(\frac{\varepsilon_{LC}}{\bar{x}_{LC}}\right)^2 + \left(\frac{\varepsilon_m}{\bar{x}_m}\right)^2},$$

where $\varepsilon_{RAS(0^\circ)}$ is known as entire standard deviation. Figure 3.25 shows an example of LC case results.

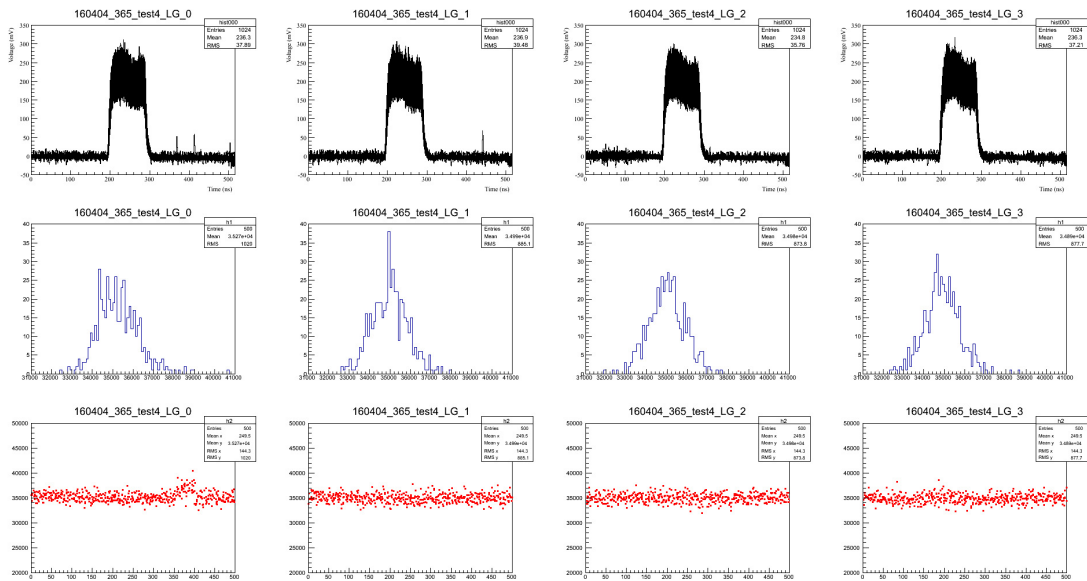


FIGURE 3.25: Top line: In each graph shows 500 signals of LC case at 365 nm. Middle line: In each graph shows the distribution of 500 signals each time. Bottom line: In each graph shows the distribution in numerical order of counts.

3.2.4.4 Rotation measurement

The rotation measurement is a procedure measuring the RAS curve of each light concentrator as a function of incident angle. The rotation measurement is consist of 2 steps as follows.

- **Step 1:** First, the measuring person enters the dark room, turns on the mini bulb, attaches the mask on PMT, turns off the mini bulb, then leaves and closes the dark room. The measuring person runs the measurement script (see Appendix D) and the amount of light at entrance aperture is measured.
- **Step 2:** After that, the measuring person enters the dark room again, turns on the mini bulb, replaced mask by light concentrator, turns off the mini bulb, then leaves and closes the dark room. Finally, the measuring person runs another measurement script for the rotation (see Appendix E). Based on this script, the system is rotated to the angle of -40° first, and then the amount of light at the exit aperture is measured by the step of 1° (0.5° in the range of $[-30^\circ, -20^\circ]$ and $[20^\circ, 30^\circ]$). Figure 3.26 shows the position of PMT at -40° , 0° and 40° . The first time the system is turned from -40° to 40° , the second time from 40° to -40° inversely, the third time from -40° to 40° and the fourth time from 40° to -40° , each time consisting of 500 pulses at each angle. The average of 4 times is calculated as the final value of light concentrator at respective incident angle. The total time for this measurement is about 1 hour and a half. The RAS value at each θ is calculated as $\text{RAS}(\theta) \pm \varepsilon_{\text{RAS}(\theta)}$ and stored in ROOT files, with

$$\text{RAS}(\theta) = \frac{\bar{x}_{LC}}{\bar{x}_m} \times \frac{1}{\cos(\theta) \times 3.7352} \times 100 \%,$$

$$\varepsilon_{\text{RAS}(\theta)} = \text{RAS}(\theta) \times \sqrt{\left(\frac{\varepsilon_{LC}}{\bar{x}_{LC}}\right)^2 + \left(\frac{\varepsilon_m}{\bar{x}_m}\right)^2},$$

where $\varepsilon_{\text{RAS}(\theta)}$ is known as entire standard deviation at θ . Figure 3.27 shows the RAS curve sample of 1 light concentrator.

Moreover, 4 rotation directions as shown in Figure 3.28 are measured for each LC. The case of $\varphi = 0^\circ$ is usually measured as the main in both on-axis and rotation measurement. Figure 3.29 shows the results of 4 rotation directions.

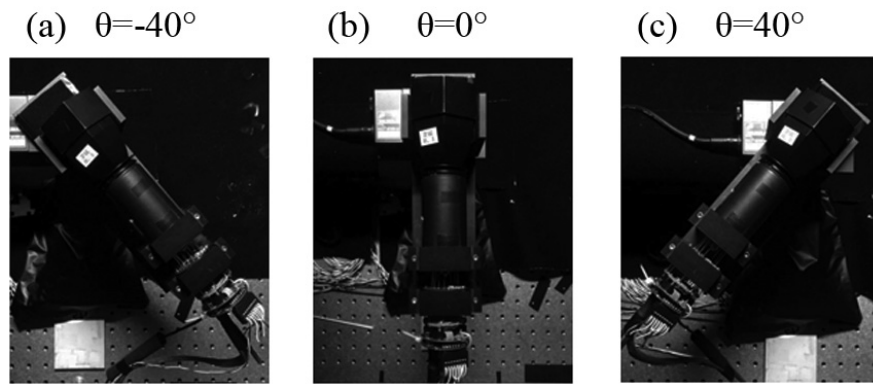


FIGURE 3.26: The position of PMT.

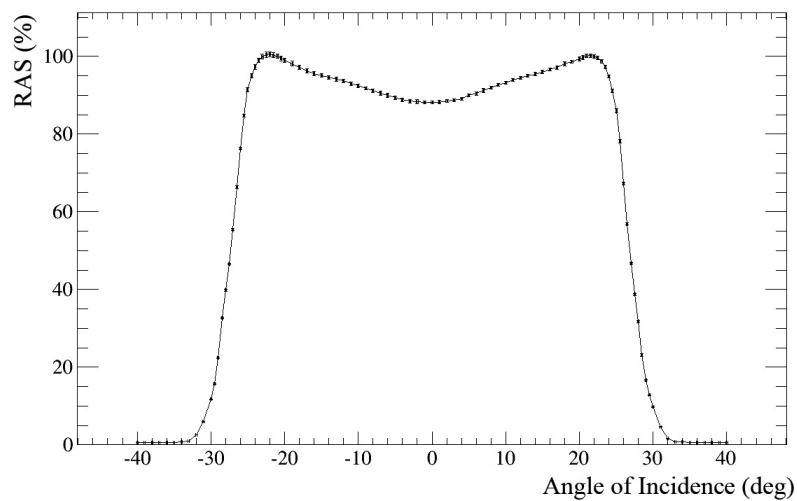
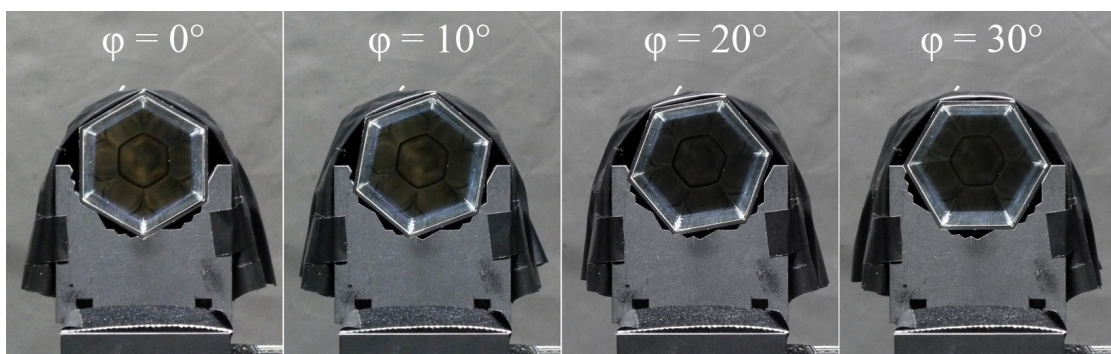
FIGURE 3.27: The RAS curve ($\varphi = 0^\circ$ case).

FIGURE 3.28: Four rotation directions.

3.2.5 Performance comparison with MST light concentrator

Professor A.Okumura brought some samples of MST light concentrator from Europe. Their reflectivity was measured, and the highest one was used to perform the rotation measurement and compared with LST light concentrator performance in three cases of 310 nm, 365 nm and 465 nm. These results are shown in Figure 3.30, 3.31 and 3.32

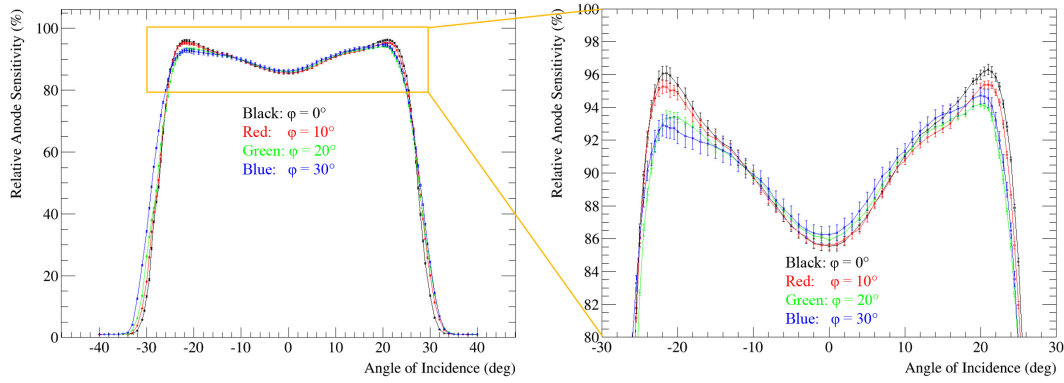


FIGURE 3.29: The results of 4 rotation directions.

respectively. The rotation measuring results of LST light concentrator No.29 in the first batch are used in this comparison.

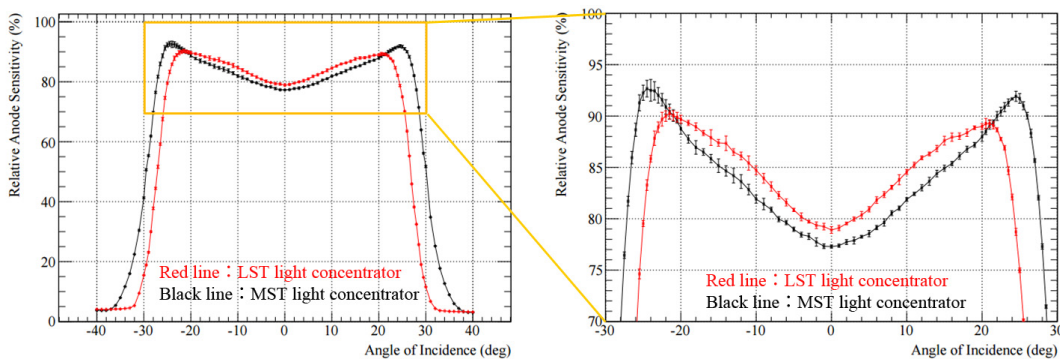


FIGURE 3.30: Comparison of LST and MST light concentrator at 310 nm.

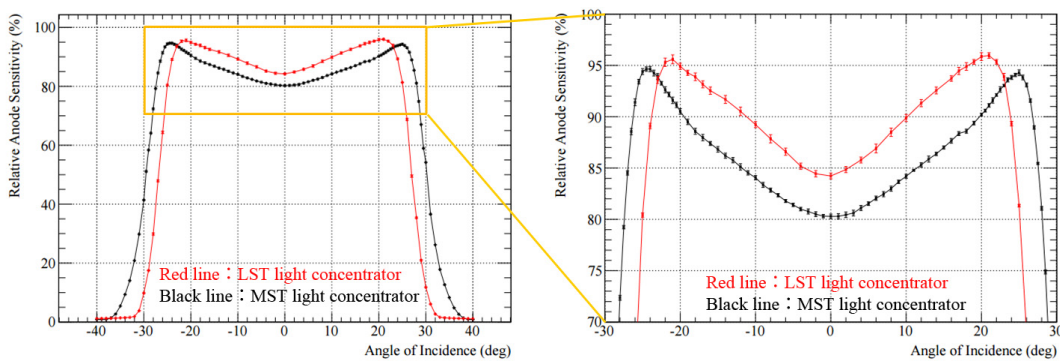


FIGURE 3.31: Comparison of LST and MST light concentrator at 365 nm.

In all three cases, the RAS values of LST light concentrator are slightly good in the range of $[-22^\circ, 22^\circ]$ comparing with the one of MST. The LST cut-off angle is smaller than MST based on the different FOV of two telescope types (4.5° versus 8° respectively).

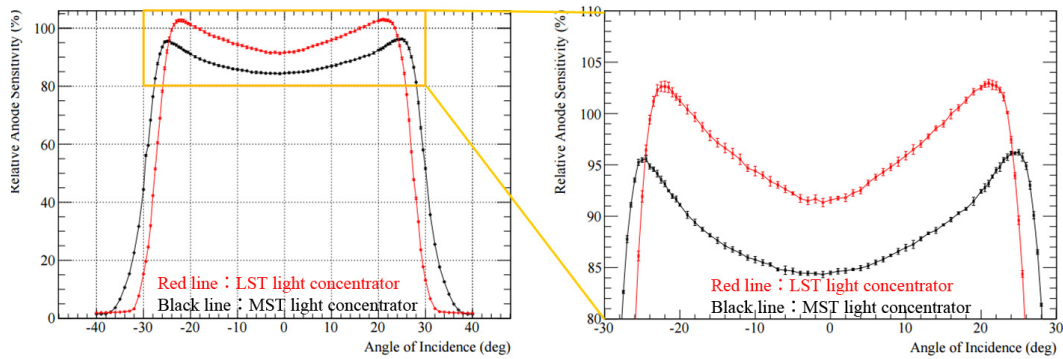


FIGURE 3.32: Comparison of LST and MST light concentrator at 465 nm.

3.3 Problems

In the current design of light concentrator, the protruding part of coated ESR warped as shown in Figure 3.33. This warpage made the ESR deformed from the ideal surface and then reduce the performance of light concentrator. The performance reduction was proved as shown in the next section. Besides, when attached in cluster, the warpage is also weak so it is pushed together by the adjacent light concentrator and deformed again or create dead space as shown in Figure 3.34.



FIGURE 3.33: The warpage can be seen near the entrance aperture of light concentrator.

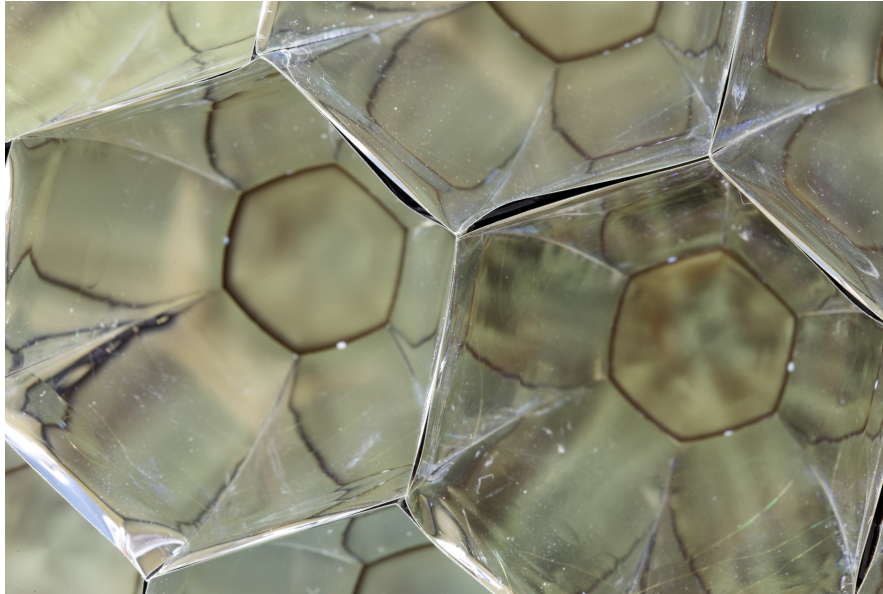


FIGURE 3.34: Influence of warpage.

3.4 Solution and discussion

3.4.1 Reinforcement of ESR by tape

- **Method:** In order to check the effect of warpage, a two-sided tape test was executed. The warpage are shown in Figure 3.36 (a-2) as a cross section, floating from the ideal surface (dashed line). First, the rotation measurement is performed. After that, 6 pieces of two-sided tapes were pasted on the back of 6 surfaces as shown in Figure 3.35. By pasting the tape directly on hexagonal frame, it was able to bring ESR film close to the ideal surface. Then, the effect of warpage was confirmed by rotation measurement once again. By comparing the results before and after taping, we can evaluate the effect of warpage. Three cases of tape whose width is 7 mm, 3 mm, and 1 mm were tested in turn.
- **Results:** The light concentrators No.264 in the second batch and No.29 were used in this tape test. Figure 3.36 (b-1), (c-1), (d-1) show the state of LC No.264 after pasting 7 mm, 3 mm, 1 mm tape respectively. Figure 3.37 shows the rotation measuring results of all 4 cases. The LC No.29 is only tested the 3 mm case for confirmation.
- **Discussion:** Adverse effects due to warpage were confirmed by rotation measurement. All cases of the test of No.264 performed better RAS values than the no-tape case in the range of $[-22^\circ, -10^\circ]$ and $[10^\circ, 22^\circ]$ (see Figure 3.37). Also in this range,

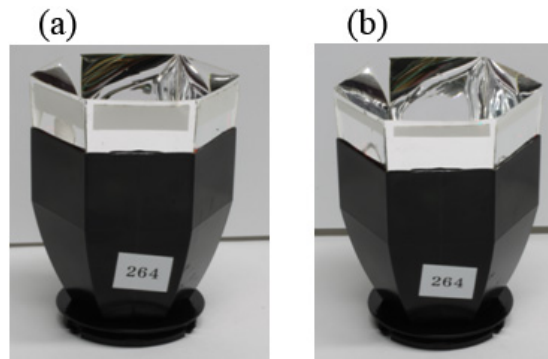


FIGURE 3.35: The state after pasting 6 pieces of two-sided tapes on the back of 6 surfaces. Left: 7 mm tape case. Right: 3 mm tape case.

the case of 3 mm tape showed the best performance, about 3% better than the case of no tape at around -22° and 22° . At large angles in the range of $[-22^\circ, -10^\circ]$ and $[10^\circ, 22^\circ]$, the RAS value is larger by 1.5% in the case of tape than none. In the range of $[-10^\circ, 10^\circ]$, the RAS of no-tape case was better, but unfortunately the number of photons reflected from primary mirror at angles in this range is small. So the RAS of this angle range is not important. For confirmation, the case of 3 mm tape was performed once again with the LC No.29. The same effect can be seen in Figure 3.38.

- **Conclusion:** The bad effects of warpage to LC performance were proved by above experiment results. Moreover, a light concentrator with the cone design covering the entire ESR was prototyped by 3D printer (see Figure 3.39). Without warpage, this new prototype also gave a better performance than current design [16]. This means that the reinforcement is necessary for current design of light concentrator.

3.4.2 Reinforcement of ESR by PET film

- **Method:** Polyethylene terephthalate (PET) is a material easy to handle. The PET film of 0.15 mm thick was used in this test for warpage reinforcement. Figure 3.40 shows the reinforcement method. First, the PET film sheet is cut into the same shape of protruding part. Next, the glue is attached to the back of warpage and spread evenly with a cotton swab. The cutting PET film is then pressed firmly attaching to the back of warpage. Leaked glue is swept with cotton swab. On the other

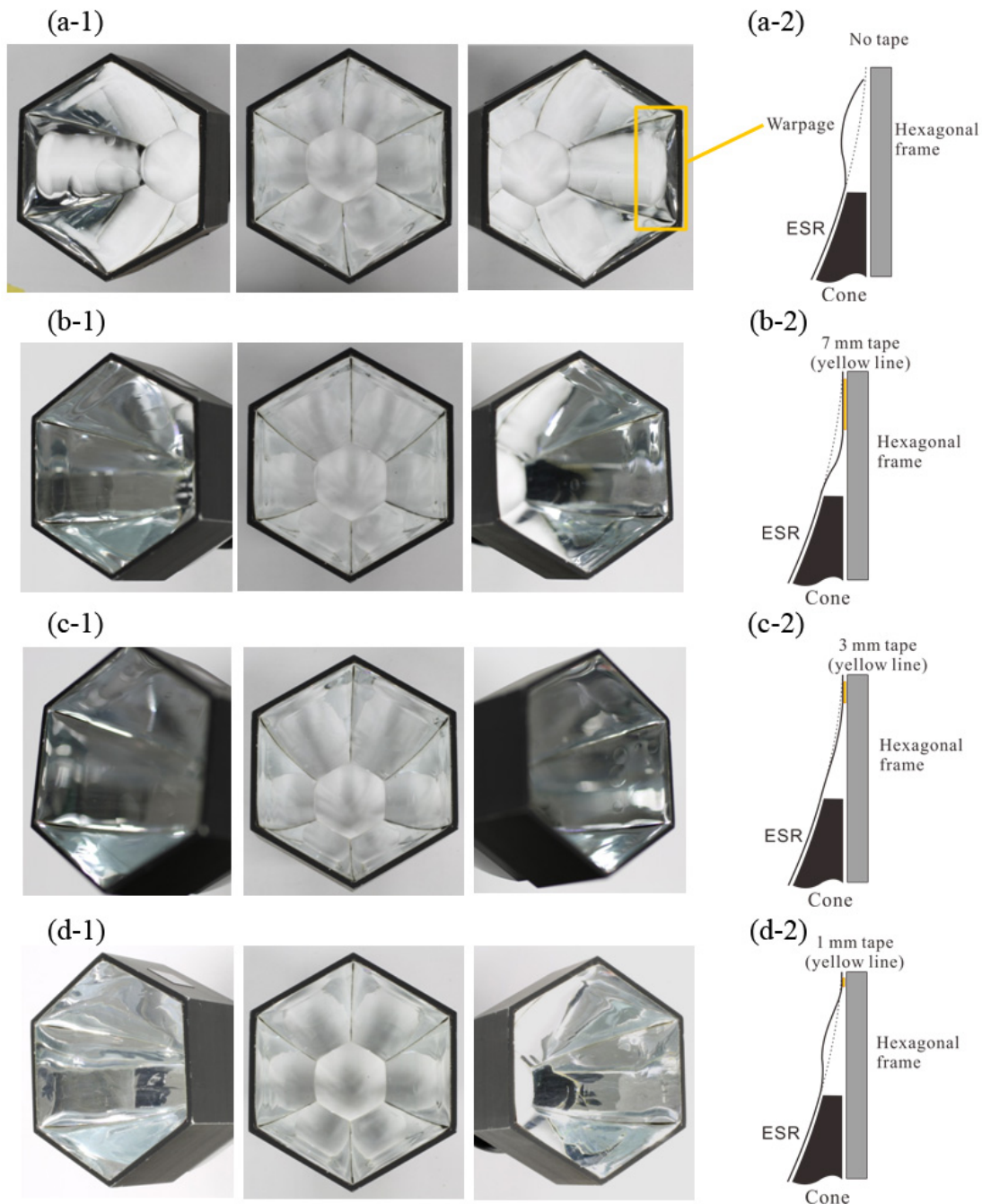


FIGURE 3.36: (a-1): The state of warpage. (a-2): The cross section of warpage floating from the ideal surface (dashed line). (b-1): The state after pasting 7 mm tape. (b-2): The cross section of 7 mm tape case. (c-1): The state after pasting 3 mm tape. (c-2): The cross section of 3 mm tape case. (d-1): The state after pasting 1 mm tape. (d-2): The cross section of 1 mm tape case.

hand, the confirmation method is the same as the case of tape. Rotation measurements are performed before and after reinforcement. The LST light concentrator No.254 and No.29 were used in this test.

- **Results:** Figure 3.41 and 3.42 show the results of No.254 and No.29 respectively.

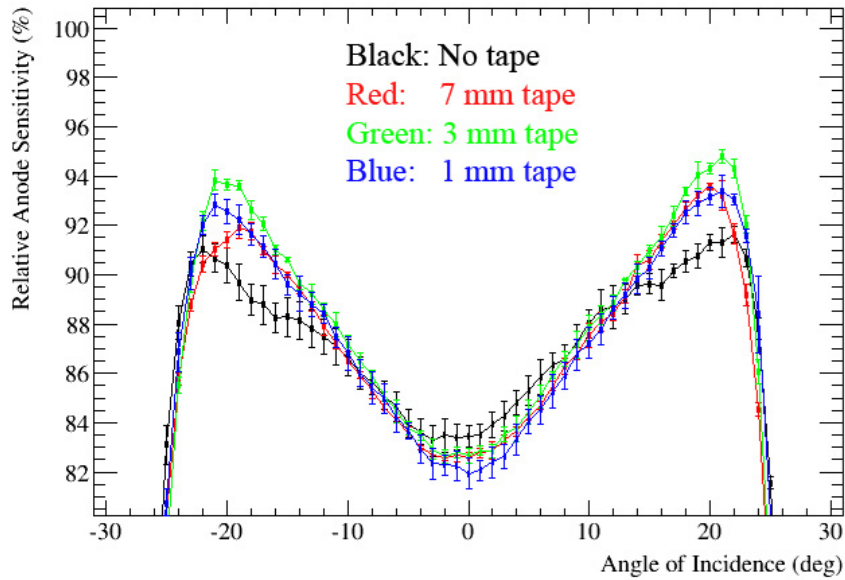


FIGURE 3.37: Rotation measuring results of LC No.264, in 4 cases of tape.

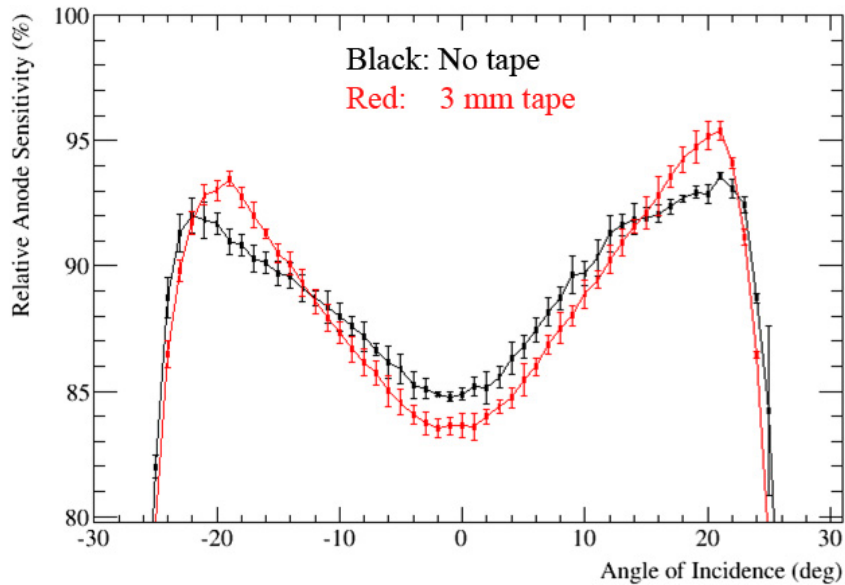


FIGURE 3.38: Rotation measuring results of LC No.29, in only 2 cases: no tape and 3 mm tape.

In the case of No.29, the past result is also included for reference. In Figure 3.43 shown the results including the tape result for comparison.

- Discussion:** The result after reinforcement gave a better RAS curve than the case of current design, in the range of $[-22^\circ, -8^\circ]$ and $[6^\circ, 22^\circ]$. Specially, the RAS values around -22° and 22° are larger by 3% comparing to the result before reinforcement. Moreover, as shown in Figure 3.43, the result after reinforcement is also better than the case of 3 mm tape over 2% around -22° and less than 1% around 22° . In the



FIGURE 3.39: Comparison of mass-produced light concentrator (left) and 3D printer prototype (right) [16].

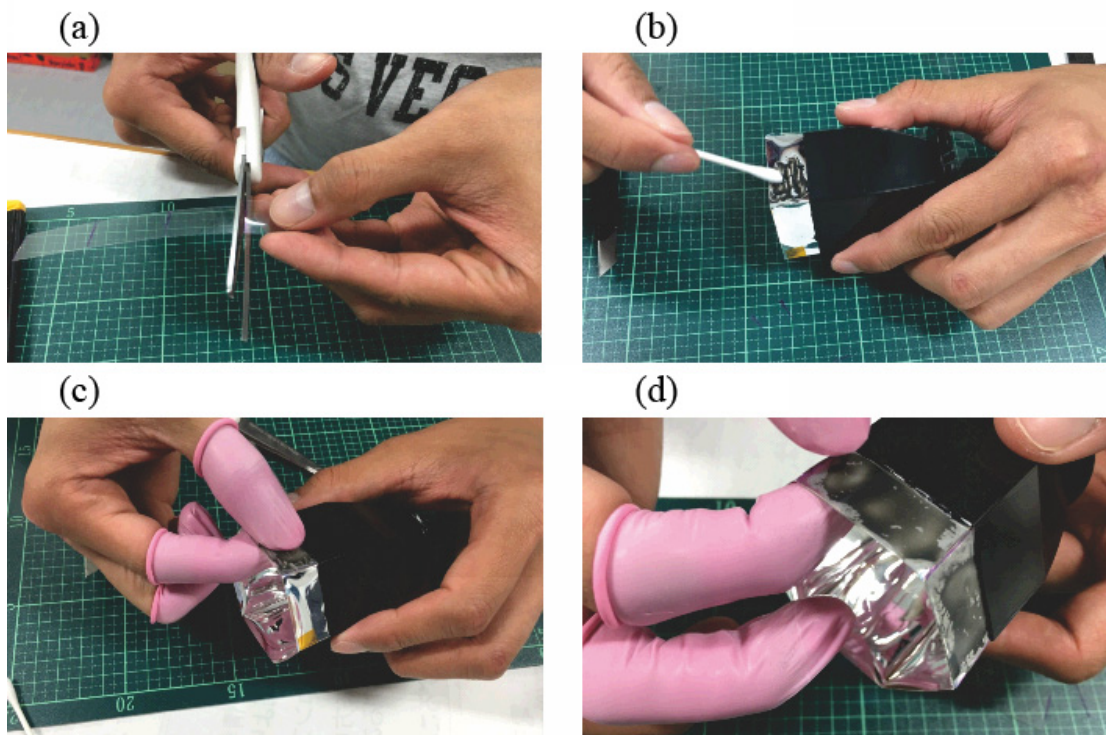


FIGURE 3.40: (a): Cutting PET film into a rectangular 14 mm x 26 mm. (b): Attaching glue to the back of warpage. (c): Pasting PET film to the back of warpage. (d): The final state after reinforcement.

range of $[-8^\circ, 6^\circ]$, the RAS values before reinforcement was better a little about 1% but it is not significant based on the optical system.

- **Conclusion:** The reinforcement by PET film was pretty good comparing to the result of reinforcement of tape. But there is still only a little warpage after reinforcement, because PET is flexible and not too hard to reinforce the warpage perfectly.

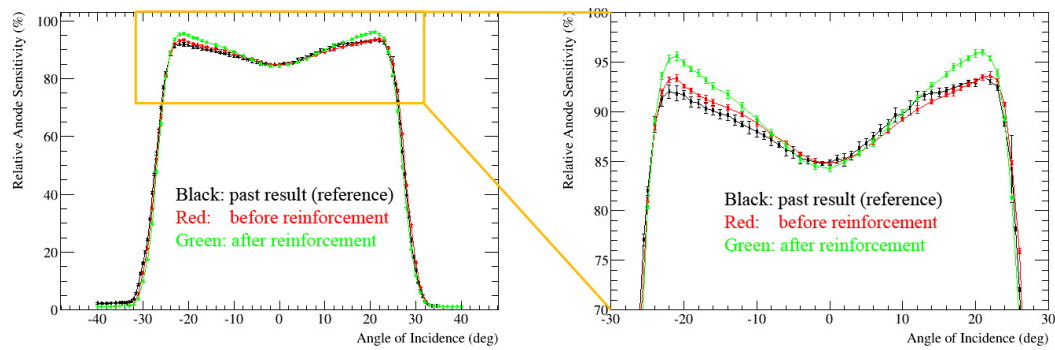


FIGURE 3.41: The results before and after the PET film reinforcement in the case of light concentrator No.29.

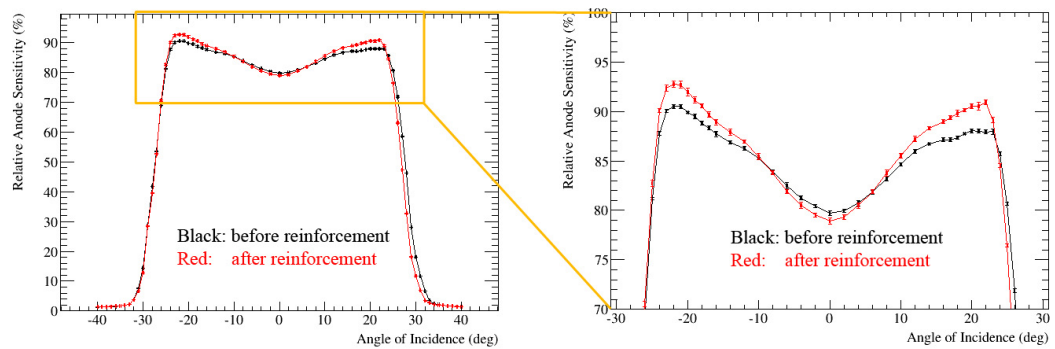


FIGURE 3.42: The results before and after the PET film reinforcement in the case of light concentrator No.254.

Besides, the size of PET film was fixed to rectangular shape of 14×26 mm, a little smaller than ESR protruding part to make a space for the glue leaks out, in order to reduce the possibility of smearing ESR surface.

3.4.3 Reinforcement of ESR by SUS film

Stainless special used steel (SUS) is the next material considered after PET. It is hard, thin and light so that can be a good candidate for the reinforcement. The samples of SUS film were ordered with rectangular shape of 13×18 mm. This smaller shape increases the space for leaked glue and reduces weight. Moreover, there were two kinds of thickness to test, as $0.1 \mu\text{m}$ and $0.05 \mu\text{m}$.

- **Method:** The reinforcement method and performance valuation are also the same as the case of PET film.
- **Results:** Figure 3.44 and Figure 3.45 show the states of film and warpage respectively after reinforcement. The appearance of SUS film looks stronger and cleaner

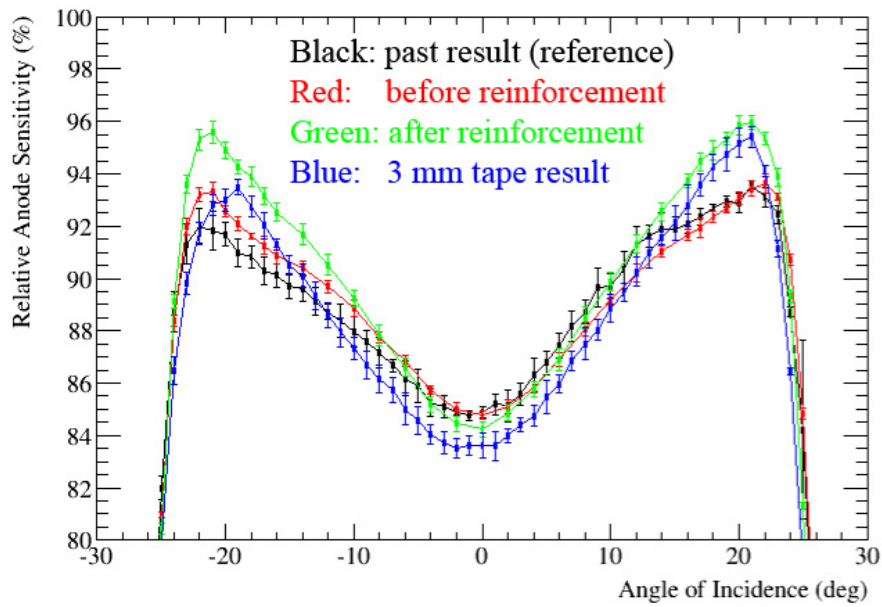


FIGURE 3.43: Performance evaluating results of PET film vs 3 mm tape .

than PET film. Figure 3.46 shows the results of 2 cases of SUS film comparing with PET film results. As shown in yellow frame, the reinforced part of warpage in both case of SUS films became flatter than the case of PET film. There are still a little warpages at 2 sides of protruding part (sky blue frames).



FIGURE 3.44: Left: the state of PET film after pasting. Right: the state of SUS film after pasting.

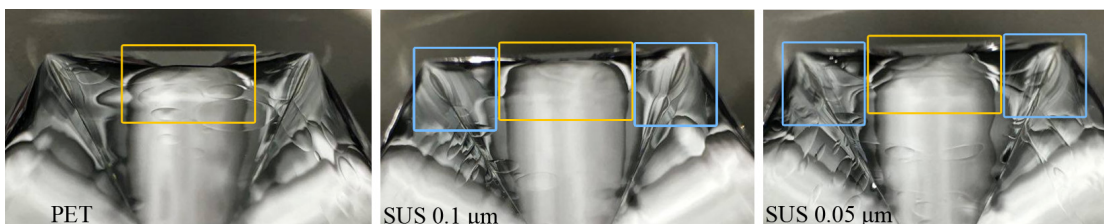


FIGURE 3.45: Left: the state of warpage after PET film reinforcement. Middle: the state of warpage after SUS 0.1 μm film reinforcement. Right: the state of warpage after SUS 0.05 μm film reinforcement.

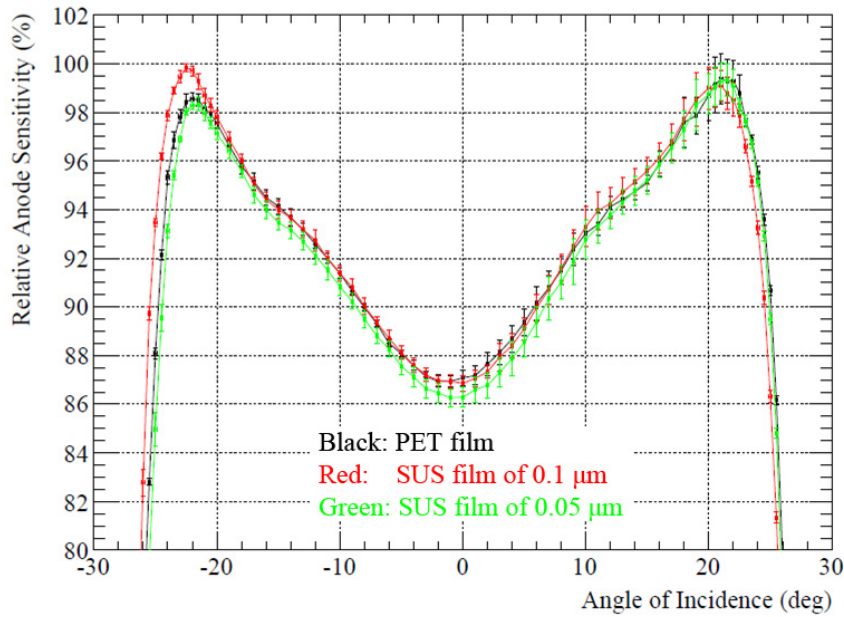


FIGURE 3.46: Performance evaluation results of PET film and 2 cases of SUS film.

- Discussion:** Three cases possess almost the same performance in the range $[-20^\circ, 22^\circ]$. Around the peak of -22° , the case of SUS $0.1 \mu\text{m}$ shows the better RAS values about under 2%. It is difficult to clear more the evaluation of 3 cases with current experiment system. The hardest SUS film of $0.1 \mu\text{m}$ has a better performance and seems to be the best choice for the reinforcement. Moreover, a deformation test was carried out in order to check the dead space created by press of adjacent light concentrator as follows.
- Deformation test:** When attached in module, LST light concentrators are pressed very strongly by PMTs from behind. Three ABS plastic hooks of each cone is not hard enough to keep the right direction. So the light concentrator is tilted a little and pushes the adjacent one, depending on the case. In this test is described the worse case when a light concentrator is pressed strongly from the adjacent one. Figure 3.47 shows the gap created when pressing 2 concentrators from 2 sides by hand, in 2 cases of SUS film and PET film. The corners of ESR protruding part bunched together with adjacent corners, and the reinforced warpages are warped again to the inside and create a gap. In the case of SUS film, a wider gap can be seen comparing with the case of PET film. Its reason is because there are still wide spaces in 2 sides of the warpage that is not reinforced (see yellow frames in Figure 3.48). These parts is weak and easy to be deformed when pushed from the side.

Besides, although PET film is softer than SUS film, it shows a good performance with narrower gap. This is due to the larger surface area of PET film.

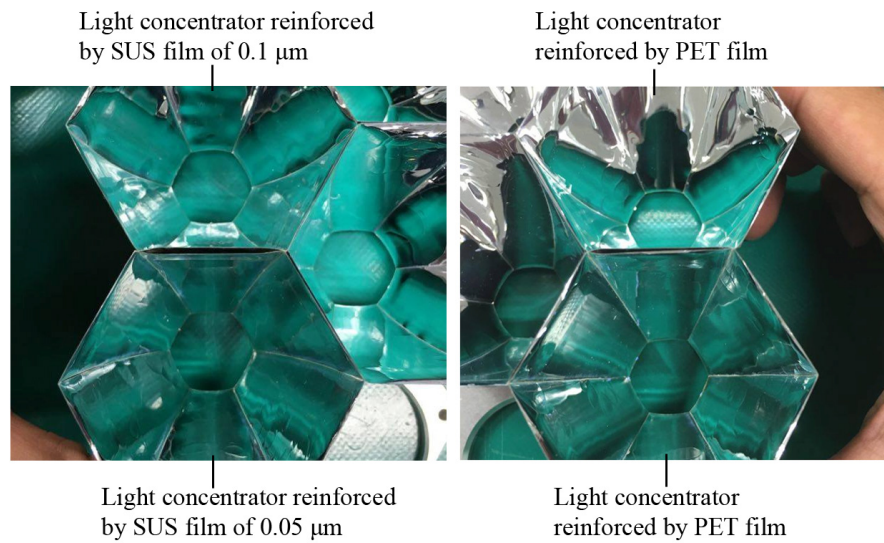


FIGURE 3.47: Left: The dead space is created by being pressed intentionally in the case that two sides are reinforced by SUS films. Right: A narrow dead space is created by being pressed intentionally in the case that two sides are reinforced by PET films.

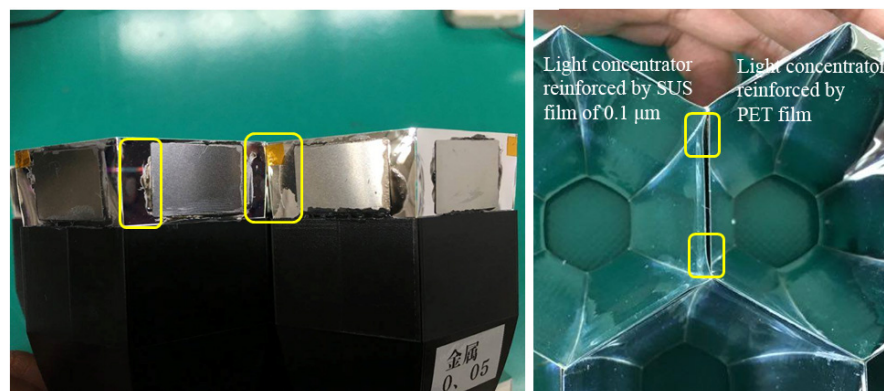


FIGURE 3.48: Yellow frame: the weak spaces which is not reinforced can be deformed easily and create the dead space.

- Conclusion:** The reinforcement by SUS film of 0.1 μm was only a little better than the result of reinforcement by PET film. But the SUS film is quite hard enough to against the warpage better than PET film. Thence it is a best choice for ESR reinforcement. Besides, based on the deformation test, the size of SUS film was fixed to 13 × 26 mm close to the size of PET film in order to reinforce the warpage better and reduce the potential to cause gap.

3.4.4 Thermostat test

A thermostat test was carried out in order to check the deformation of reinforced warpage. Two SUS film reinforced light concentrators and two PET film reinforced light concentrators were put into thermostat as the state shown in Figure 3.49 at the temperature of 69.5°C for one night (about 8 hours). After the test, there was no deformation and no glue melting in appearance. The performance before and after the test were also checked.

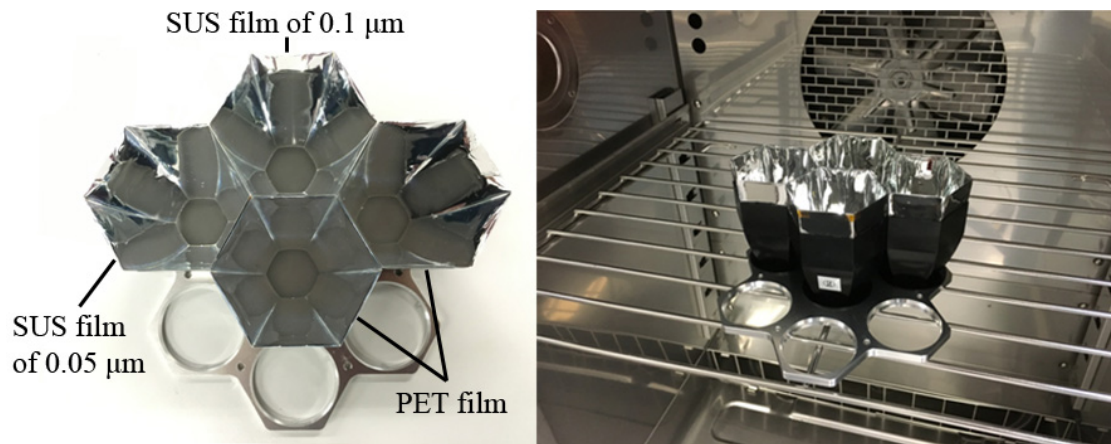


FIGURE 3.49: Thermostat test.

3.4.5 Final conclusion

By the above research, the LST light concentrator is determined to the design reinforced by SUS 0.1 μm film with rectangular shape of 13×26 mm as the final design (see Figure 3.50 and Figure 3.51). Seven new light concentrators were manufactured for performance evaluation. Figure 3.52 and 3.53 show the state when attaching into interface plate, viewed from the side and from above respectively. Performance of these LCs will be evaluated this year (2017).

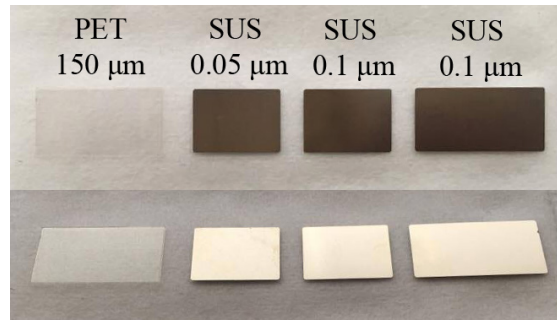


FIGURE 3.50: Above: all reinforcement films. From the left side are PET film, SUS 0.05 μm of 13×18 mm film, SUS 0.1 μm of 13×18 mm film, and the rightmost one is the final SUS 0.1 μm film with rectangular shape of 13×26 mm. SUS 0.05 μm of 13×18 mm and SUS 0.1 μm of 13×18 mm films were used in the SUS-film reinforcement test. Below: a inclined look from the side.

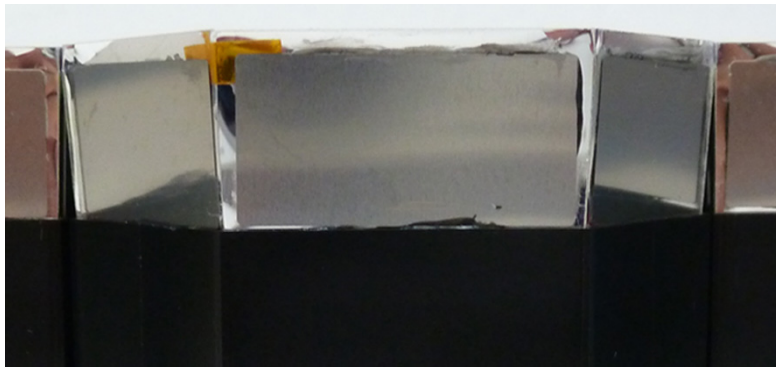


FIGURE 3.51: SUS 0.1 μm film with rectangular shape of 13×26 mm

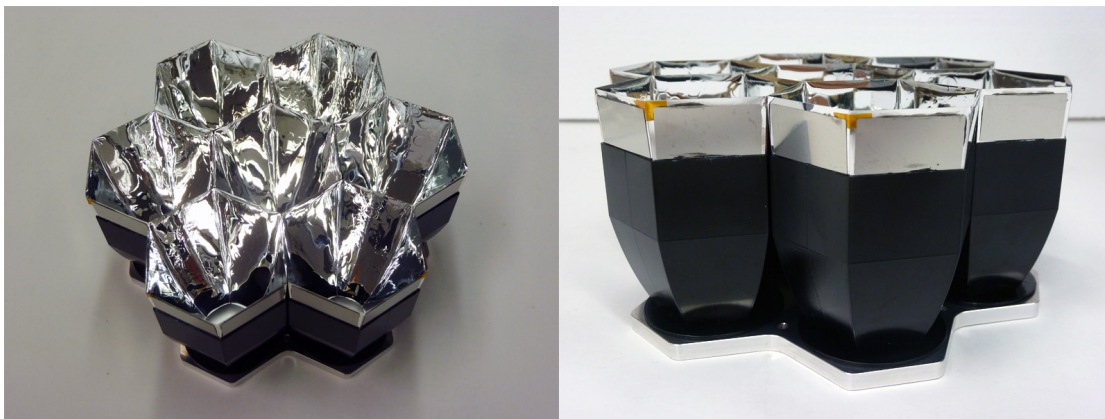


FIGURE 3.52: Cluster with 7 new light concentrators viewed from side.



FIGURE 3.53: Cluster with 7 new light concentrators viewed from above.

Chapter 4

Establishment of performance evaluation system

In parallel with the development of light concentrator, the establishment of performance evaluation system was also reviewed, repaired and renewed.

4.1 Establishment of measurement system

4.1.1 Rearrangement and cleaning

The laboratory was cleaned up after a long time of use. Unnecessary shelves and items were put out (see Figure 4.1), the high voltage appliance was rearranged below the optical table. The chair position for measuring person was also moved to close the entrance. As mentioned in sub-subsection 3.2.4.1, a black curtain was hung between LED and PMT system, only opened to approximately 17×26 cm hole in the middle for light pulses to pass through. The purpose of this curtain is to prevent light reflections from the side walls and ceilings. Some places on the side walls that look possible to reflect light were covered by black cloth too. Small torn holes on the entrance cloth were pasted with black tape in order to prevent leaked light into the dark room. The noise-preventing cloth, an aluminum foil wrapped by black electrical insulating cloth, was renewed instead of the old one.

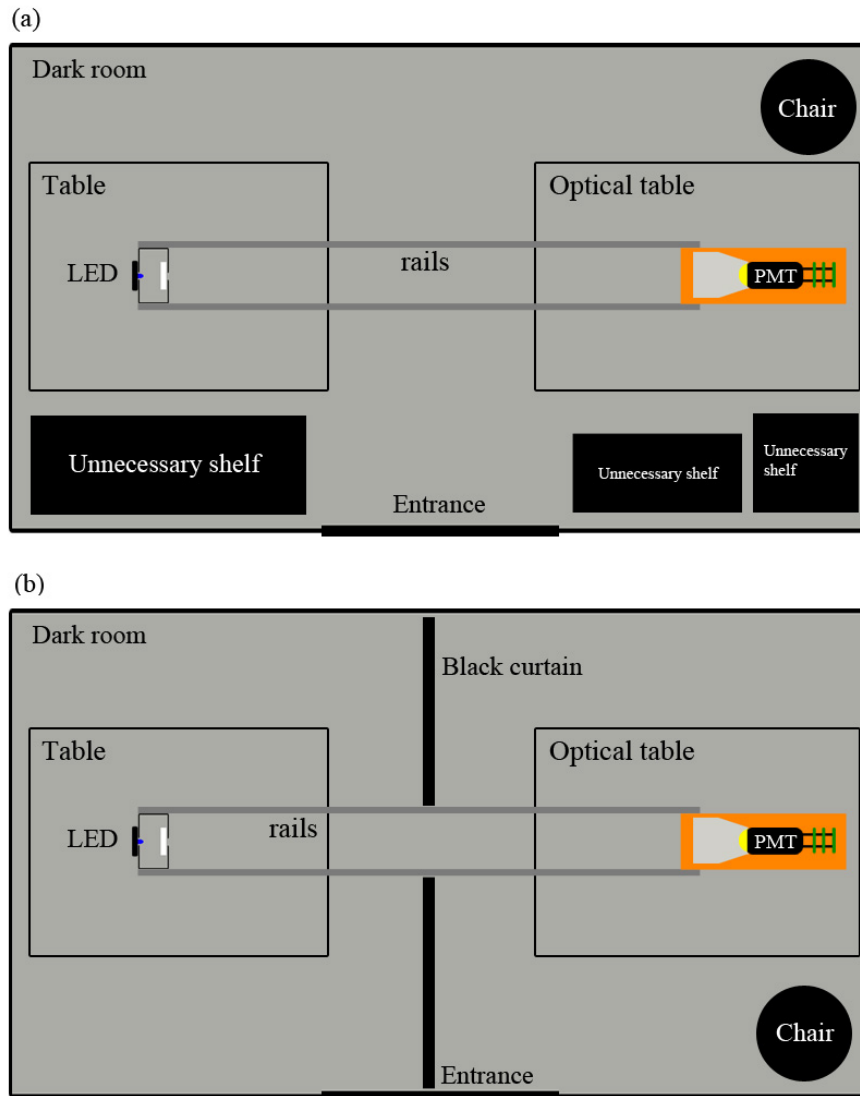


FIGURE 4.1: (a): before rearrangement. (b): after rearrangement.

4.2 Additional set-up of monitor PMT

One more PMT has been added just below the position of measuring PMT as a monitor, in order to correct the RAS value. Figure 4.2 and 4.3 show this monitor PMT and the installation state of it. Figure 4.4 shows the signals detected both PMTs in two cases of mask (left) and LC (right).

The performance of monitor PMT was evaluated and compared with measuring PMT. The content of performance test is detection of $500 \text{ signals} \times 800 \text{ times}$. One time takes about 15 seconds, thence the total time is about 3 hours 20 minutes. Figure 4.5 left shows the results of performance test. The monitor PMT values decreased gradually with time

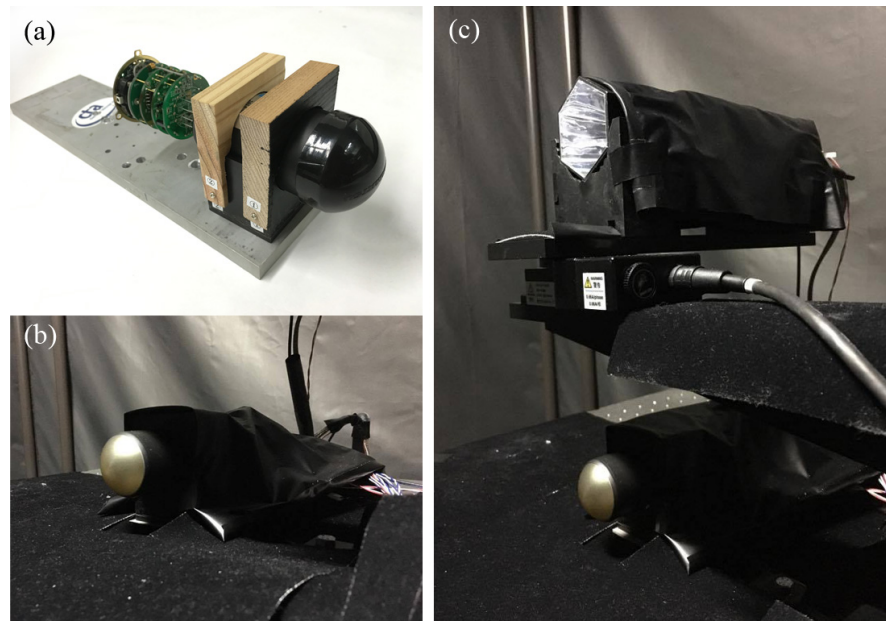


FIGURE 4.2: (a): The monitor PMT. (b): The set-up state of monitor PMT covered by the noise-preventing cloth. (c): The position of both PMTs.

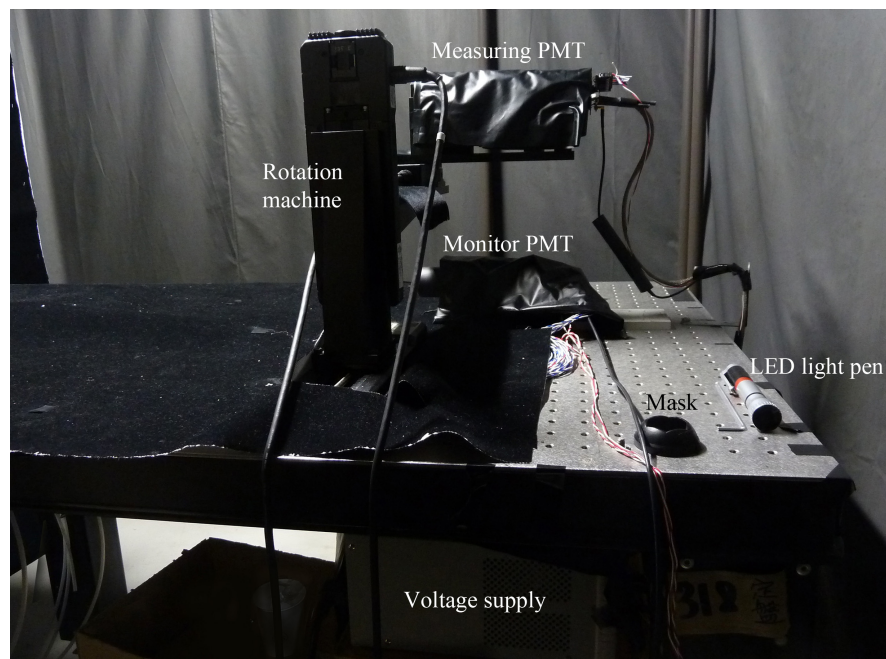


FIGURE 4.3: The experimental system after adding monitor PMT.

while the measuring PMT values were stable. After about 600 times, the monitor PMT values became equal and continued to fall lower. In order to check when the monitor PMT become stable, the LED was turned off and turned on again, after 15 minutes the second performance test was executed (in order to ensure the same initial condition). Figure 4.5 right shows the results of confirmation test. The test content was also 500 signals \times 800 times but stopped by a systematic breakdown after 700 times. The monitor PMT values

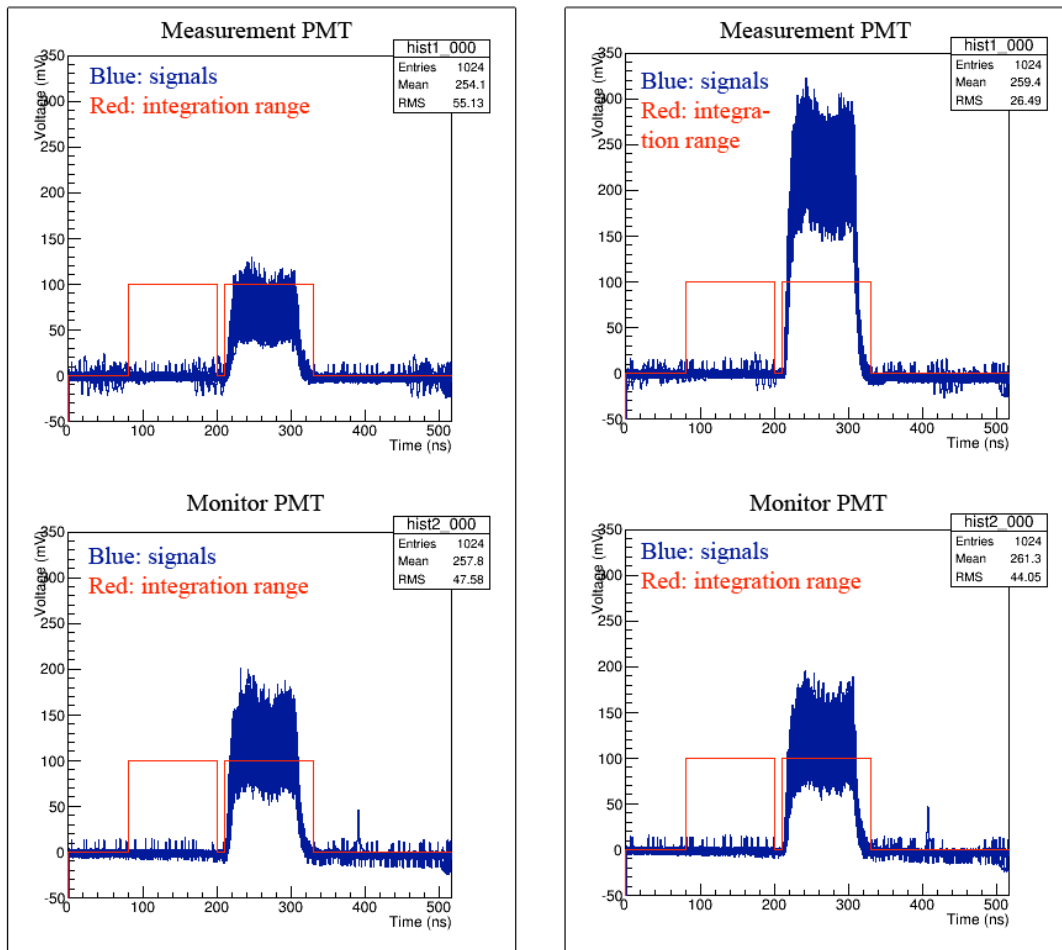


FIGURE 4.4: Left: Measurement PMT signal graph (above) and monitor PMT signal graph (below) of the mask case. Right: Measurement PMT signal graph (above) and monitor PMT signal graph (below) of the LC case.

still continued to fall lower than measurement PMT values. Because of this difference in performance, the correction of PMT by PMT seems to be difficult.

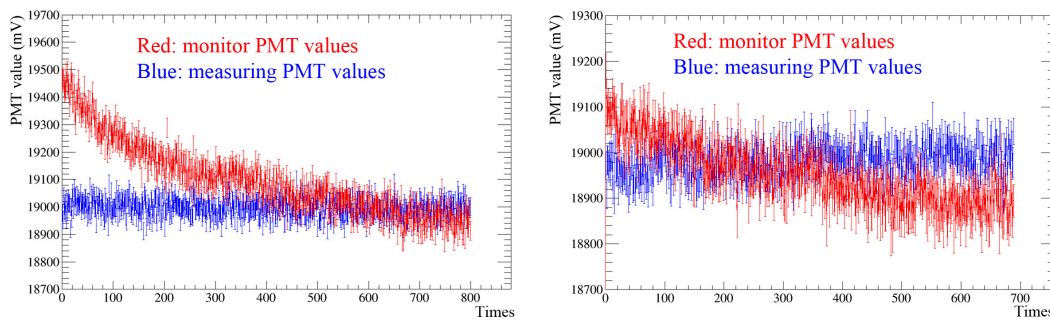


FIGURE 4.5: Left: results of the first confirmation test. Right: results of the second confirmation test.

In fact, the correction test was executed to make sure. The on-axis measurement are executed 10 consecutive times in order to get the RAS value distribution for 1 light

concentrator. The signals were detected by both monitor and measuring PMTs. The RAS value was calculated in 2 ways: the traditional one as Equation 3.5, and the new one using correction by monitor PMT gain values as follows:

$$\text{RAS}_{\text{monitor}}(0^\circ) = \frac{\bar{x}_{\text{LC}} \times \bar{y}_{\text{m}}}{\bar{x}_{\text{m}} \times \bar{y}_{\text{LC}}} \times \frac{1}{3.7352} \times 100\%, \quad (4.1)$$

where \bar{y}_{m} is the monitor PMT gain value of mask case, \bar{y}_{LC} is the monitor PMT gain value of LC case. The detailed explanation of correction analysis is mentioned in Appendix B. Figure 4.6 shows the correction results by monitor PMT. The RAS value distribution of traditional case has a sharp shape with the mean value of $86.8\% \pm 0.196\%$, while the correction case shows a flat distribution with the mean value of $86.9\% \pm 0.307\%$. Based on these unexpected results, the correction of PMT by PMT is considered impossible.

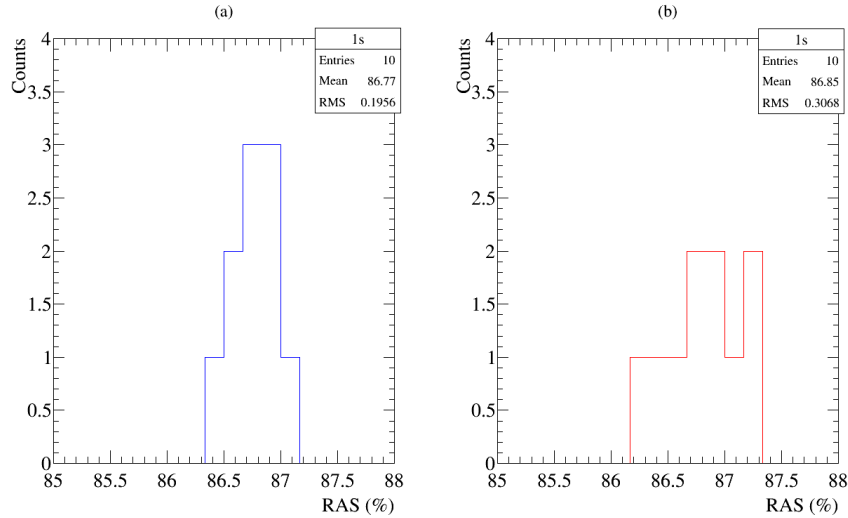


FIGURE 4.6: The results of correction test. (a): The RAS value distribution of traditional way. (b): The corrected RAS value distribution of correcting way.

4.3 Establishment of measurement scripts

The waveforms of 500 signals are drawn in the same graph, saved as 1 ROOT file. So there are 4 ROOT files for one case of mask or light concentrator. The waveforms can be seen only after finishing the measurement and this is quite inconvenient. Besides, the range of waveform and noise pedestal is defined in the sub-script connected from measurement script. So it is difficult to check whether the waveform overlaps the selected time range or not. If not, the RAS value will be calculated incorrectly. On the other hand,

the measurement script and analysis script are separate. The measured results were saved in the form of ROOT file. The analysis takes a lot of time due to the convert from raw data to ROOT file in the rotation case. Since the ROOT files can not be seen directly when opening, it is also difficult to handle a lot of data at the same time.

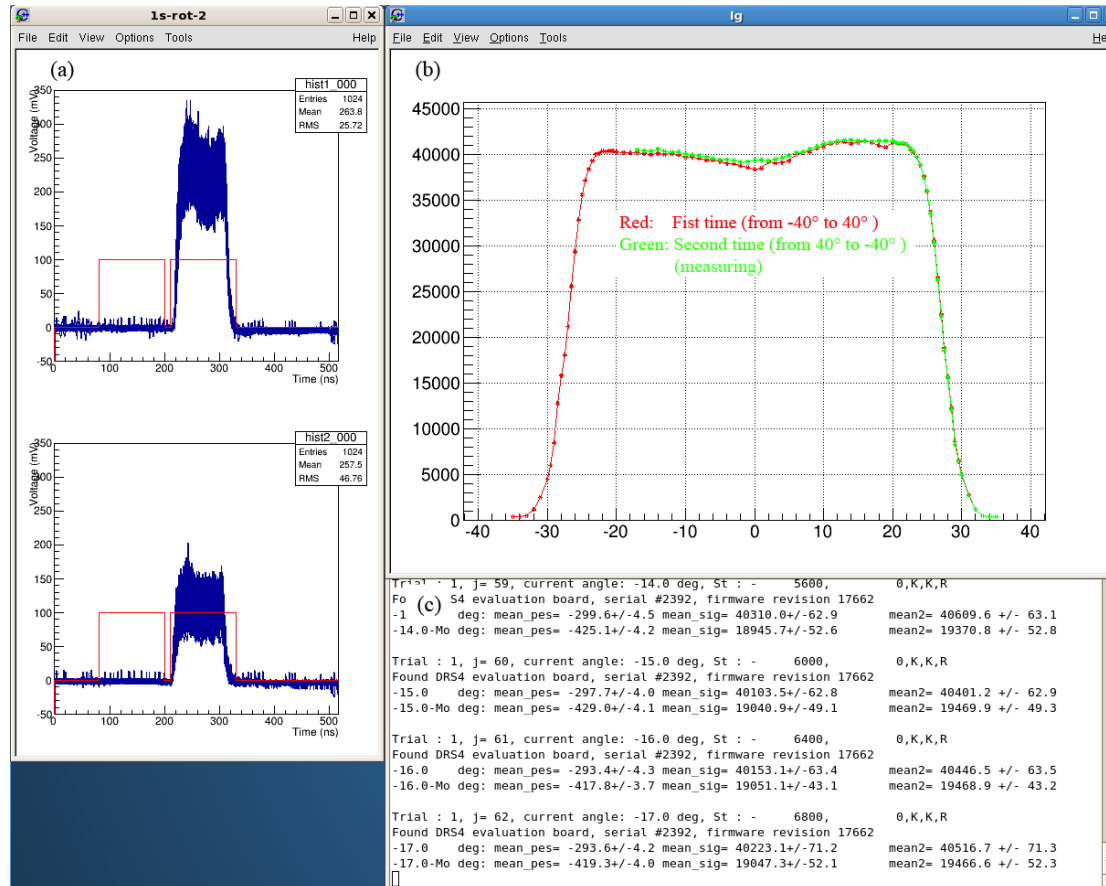


FIGURE 4.7: Screen shot when measuring the rotation case. (a): 500 pulses of each time is displayed immediately after measuring. The above graph shows waveform of 500 pulses detected by measuring PMT. The below graph shows waveform of 500 pulses detected by monitor PMT. Red line shows the time range of noise pedestal (left) and pulse (right). (b): the PMT gain value displayed when measuring so that we can check if some large systematic errors appear. (c): the gain value of pedestal, pulse and their residual were calculated (analysed) immediately after each time and displayed in detail on screen.

The measurement script and analysis script have been re-written in only 1 file for both case of mask and light concentrator. All result data (namely the PMT gain values of mask case, LC case, and the RAS value) for one performance evaluation experiment will be saved only in a text file as numerical data, in order to save time and to handle more easily. When measuring 4 times, the result of each time will be analysed immediately and displayed on the screen as both graphs and numerical data (see Figure 4.7 (a), (c)). The selected time ranges of noise pedestal and pulse are also displayed by red lines, as

shown in Figure 4.7 (a). This is very convenient for detecting whether the waveform overlap the selected range or not. Moreover, the ranges are changed automatically due to the input wavelength. After mask case and light concentrator case are both measured, RAS value is automatically calculated, displayed and written in the same result text file. In the rotation measurement, the PMT gain value of each time is also displayed one by one in the same graph, showing a curve such as a function of incident angle, in order to check current situation compared to the whole measurement results (see Figure 4.7 (b)). Moreover, the measurement will be stopped and the announcement will be displayed if measuring person makes a mistake of measuring the same case twice.

4.4 Establishment of replacement work

The replacement work is carried out between 2 measurements of mask and light concentrator, takes time about 1-2 minutes. The mini orange bulb is turned on during the replacement work (see Figure 4.8 right). Because the high voltage is not turned off, it is dangerous for measuring person when replacing by naked hand in a weak-light situation. Moreover, the light from mini bulb seems also strong for sensitive PMT and may affect the measured results after replacing.



FIGURE 4.8: Left: location of ceiling light and the experiment system. Right: the mini bulb is turned on for replacement work

In order to avoid this problem, a new solution has been thought out and tested. As shown in Figure 4.9, a red LED light pen wrapped by black tape was used when replacing

light concentrator (or mask). The light from this LED pen was reduced by black tape in order to limit the impact on PMT.

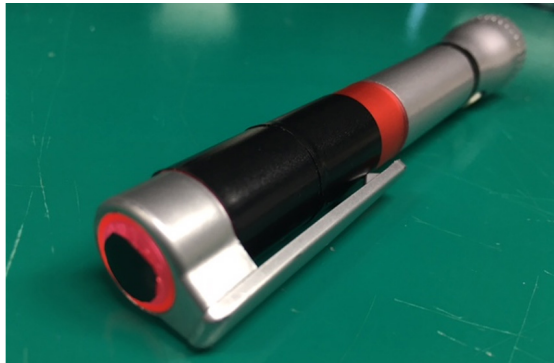


FIGURE 4.9: LED light pen wrapped in black tape to reduce light.

The confirmation test was carried out in 2 steps as follows. First, the PMT had got data of 500 signals \times 40 times (about 12 minutes) in the state of mask case. With the high voltage turned on and mini bulb turned off, the entrance window of PMT was irradiated only by red light from LED pen in 1 minute supposing in the worst case, and then the measurement was carried out again as 500 signals \times 80 times without any further action. Figure 4.10 shows the PMT gain values before and after irradiation. Although the gain decreased by about over 2% immediately after irradiation, it recovered with time, but finally was still smaller about 1% than before irradiation.

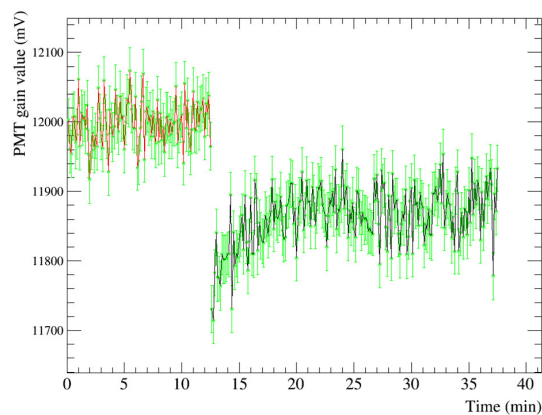


FIGURE 4.10: The measured results of LED light pen confirmation test. Red: PMT gain average value fluctuation before turning off high voltage. Black: PMT gain average value fluctuation after turning off high voltage. Green: error bars of each value.

Light from the light pen has already been reduced to minimum that be able to see with the naked eye. So the next solution is turning off the high voltage during the replacement time. The confirmation test was carried out in 2 steps as follows. First, the

PMT had got data for about 12 minutes in the state of mask case. Then the high voltage was turned off. After waiting 1 minute (as the replacement time), it was turned on again, and the PMT had got data for about 24 minutes without any further action. Figure 4.11 shows the PMT gain values before and after turning off the high voltage. The red and black lines show PMT gain average value fluctuation before and after turning off high voltage, respectively. The green line shows error bars of each value. Although the gain decreased by about over 1% immediately after high-voltage turning off, but after 2 minutes it recovered to the same fluctuation before.

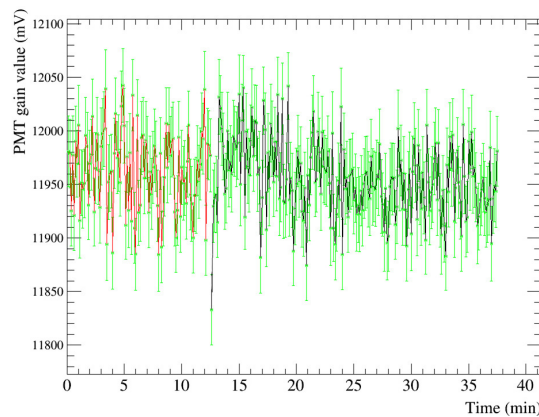


FIGURE 4.11: The measured results of confirmation test in the case turning off voltage. Red: PMT gain average value fluctuation before turning off high voltage. Black: PMT gain average value fluctuation after turning off high voltage. Green: error bars of each value.

The same PMT gain values can be got after turning on the high voltage and waiting 2 minutes. The next confirmation test is about irradiating PMT by LED pen with the high voltage turned off. The confirmation test was carried out in 2 steps as follows. First, the PMT had got data for about 12 minutes in the state of mask case. Then the high voltage was turned off. The PMT entrance window was then irradiated only by LED pen in 1 minute supposing in the worst case. After that, the high voltage was turned on again, and the PMT had got data for about 24 minutes without any further action. Figure 4.12 shows the PMT gain values before and after the test. Similar to previous measurement result, the gain decreases by about over 1% immediately, but after 2 minutes it recovers to the same fluctuation before.

Based on above measurement results, the replacement work was changed as follows to keep PMT operation stable.

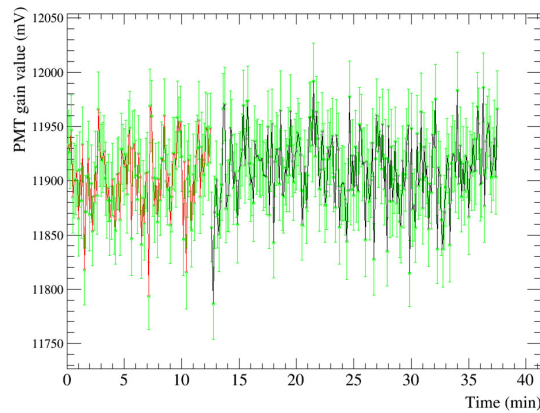


FIGURE 4.12: The measured results of confirmation test in the case turning off voltage and irradiating by the LED light pen. Red: PMT gain average value fluctuation before turning off high voltage. Black: PMT gain average value fluctuation after turning off high voltage. Green: error bars of each value.

- **Step 1:** First, the measuring person turns off the high voltage, enters the dark room, attaches the mask (or light concentrator) on PMT, leaves, and closes the dark room. The measuring person then turns on the high voltage, waits 3 minutes (in case), then runs the measurement script.
- **Step 2:** After that, the measuring person turns off the high voltage, enters the dark room again, replaces mask by light concentrator (or reversely), leaves and closes the dark room, turns on the high voltage and waits 3 minutes. Finally, the measuring person runs the measurement script.

4.5 Establishment of rotation measurement

4.5.1 Problems

Figure 4.13 show 4 times of all PMT gain values as a function of incident angle. As shown in this Figure, the first time values from -40° to 40° (red line) was lower about 1% than another times. Except the first time, all 3 times values were quite stable and overlapped together. This means that the PMT gain increase in the first time and become stable after that. After the establishment of replacement work described in the previous section, the rotation measurement was executed again to verify but the problem is still not resolved, as shown in Figure 4.13.

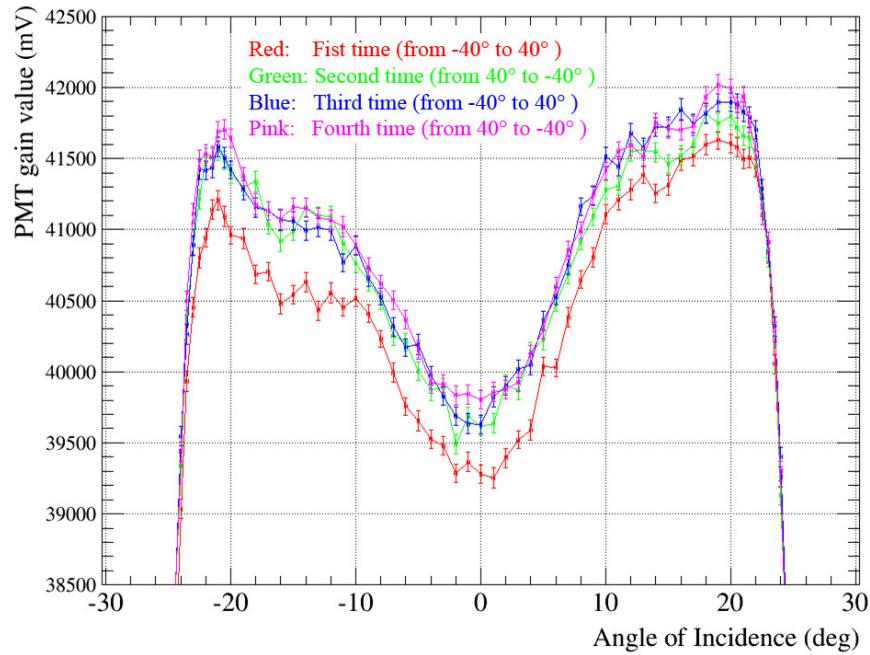


FIGURE 4.13: Measurement results of 4 times in the case of light concentrator, after the establishment of replacement work.

One round (1 time) from -40° to 40° takes about 25 minutes. So a 30 minutes waiting test was carried out in order to eliminate the increase of PMT gain in the first time. After attaching light concentrator and waiting 30 minutes, the rotation measurement was executed. The measurement results were shown in Figure 4.14. There are some jaggy places in the curve as systematic errors, but entirely the first time values is still quite low. As result, the increase of PMT gain appears when rotation measurement itself starts, regardless of waiting time.

One more detailed measurement was tested in a different day. The measurement was executed in following steps.

- Measure the mask case, get PMT gain average value \bar{x}_m (1)
- Turn off the high voltage, replace mask with light concentrator, turn on high voltage and wait for 2 minutes.
- After that, measure light concentrator case at $\theta = 0^\circ$, get PMT gain average value $\bar{x}_{LC}(2)$
- Do rotation measurement. In PMT gain values, values at $\theta = 0^\circ$ were selected for comparison as x_{LC_0} (3-0), x_{LC_1} (3-1), x_{LC_2} (3-2) and x_{LC_3} (3-3) for 4 times. The average values of 4 times are not selected.

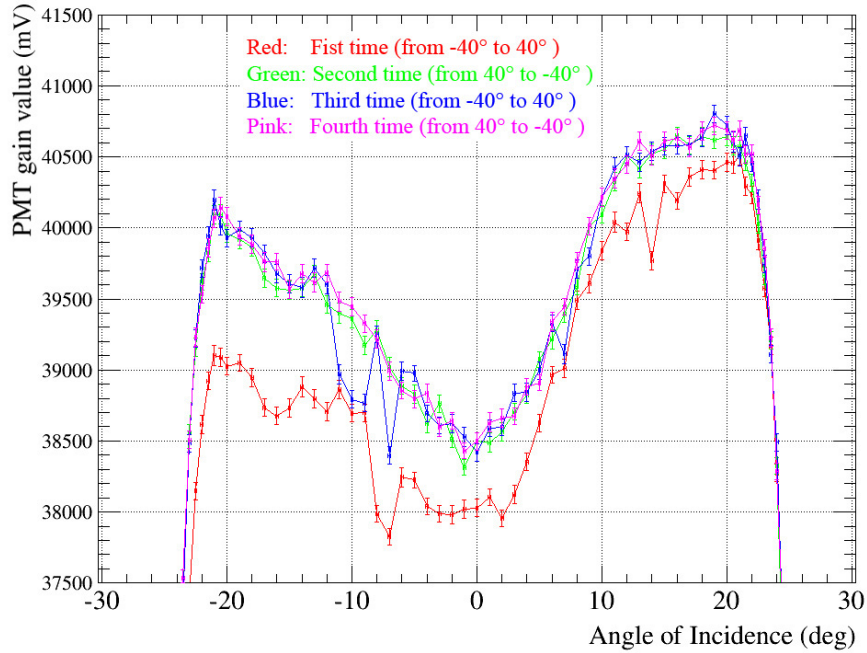


FIGURE 4.14: Measurement results of 4 times in the case of light concentrator, after waiting 30 minutes.

- Measure light concentrator case at $\theta = 0^\circ$ once again, get PMT gain average value \bar{x}_{LC} (4)
- Turn off the high voltage, replace light concentrator with mask, turn on high voltage and wait for 2 minutes.
- Measure the mask case, get PMT gain average value \bar{x}_m (5)

These above results at $\theta = 0^\circ$ are shown in Table 4.1. Based on the rotation measurement results as shown in Figure 4.15, the PMT values was still low as usual during the first time to over the half of second time.

Number	Name	PMT gain value (mV)
(1)	\bar{x}_m	12048.9
(2)	\bar{x}_{LC}	37825.1
(3-0)	x_{LC_0}	38355.1
(3-1)	x_{LC_1}	38643.3
(3-2)	x_{LC_2}	39092.9
(3-3)	x_{LC_3}	38952.2
(4)	\bar{x}_{LC}	38943.5
(5)	\bar{x}_m	12059.6

TABLE 4.1: The results of on-axis case and rotation case at $\theta = 0^\circ$.

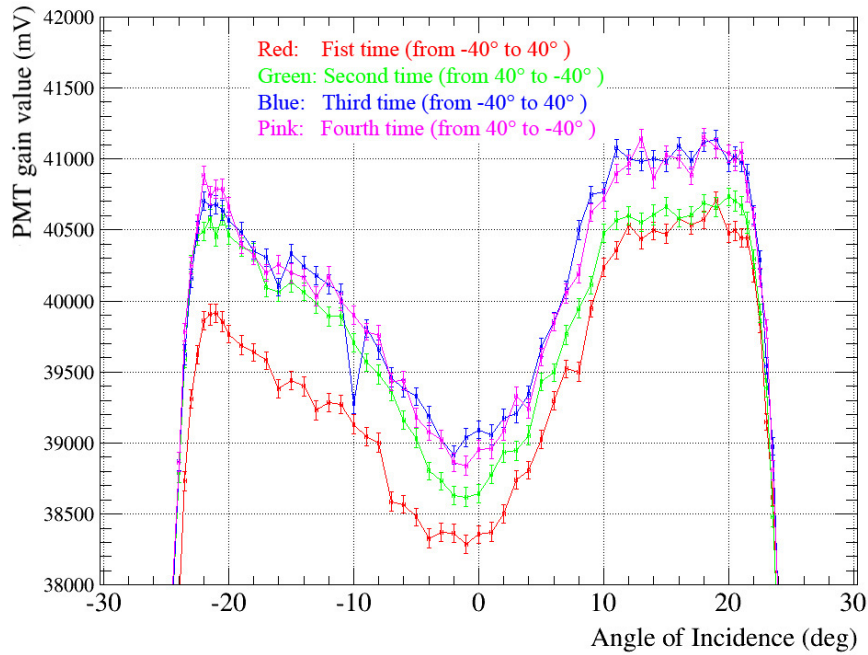


FIGURE 4.15: Rotation measurement results of 4 times in the LC case of detailed test.

PMT value of mask case does not change before and after the rotation measurement ($\bar{x}_m = 12048.9$ (1) versus $\bar{x}_m = 12059.6$ (5)). This means that the LED light is stable during the measurement. On the other hand, PMT value of LC case before rotation measurement is smaller than after rotation measurement ($\bar{x}_{LC} = 37825.1$ (2) versus $\bar{x}_{LC} = 38943.5$ (4)). Thus, there seemed to be something effected on PMT when rotating so that the PMT values increased during the rotation.

After above test, mask was replaced by light concentrator one more time, and rotation measurement was executed again (second test of LC case). Figure 4.16 left shows the results of this test. The PMT values of the first time is a little low and becomes stable quickly from around 5° .

Then the rotation measurement was carried out once again without replacement (third test of LC case). The results are shown in Figure 4.16 right. We can see that the stable state was maintained from the previous measurement due to doing nothing. There are some incorrect values in the second time (green line) from 15° to 22° . These systematic errors sometimes occur when measuring and should be remeasured.

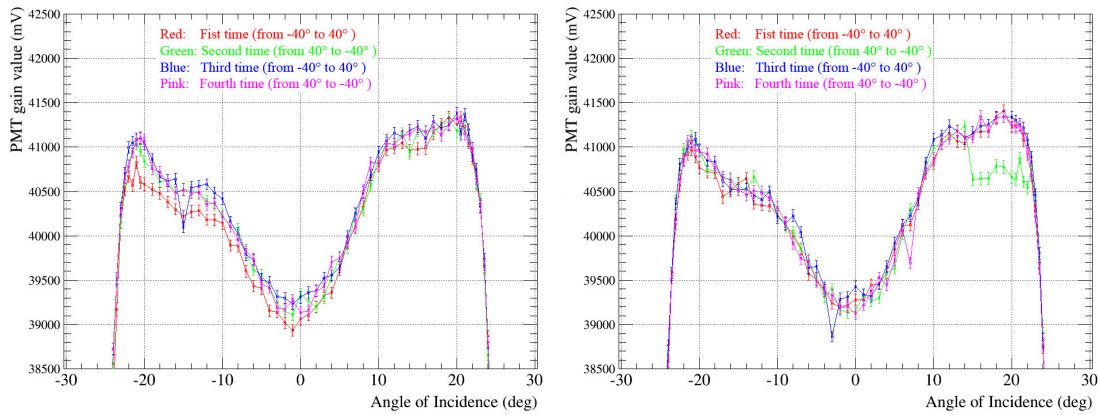


FIGURE 4.16: Left: rotation measurement results of 4 times in the second test of LC case. Right: rotation measurement results of 4 times in the third test of LC case.

4.5.2 Solution and discussion

Next the signal cable was checked as a suspicious factor. In current system, the current signal cable is short and connected with a heavy connector which hangs in the air as shown in the Figure 4.17 left. This heavy connector was guessed as the reason of the signal increase in rotation measurement. It was replaced with a new longer signal cable in order to see whether there is any effect. Figure 4.17 right shows the tidier view after changing than before. On the other hand, the static friction occurred when the cable touched the table, and the measured signal was affected when the static friction converted to dynamic friction. In order to prevent it, the signal cable and the electrical wires were divided separately as shown in Figure 4.18. This system allows wires and cable move freely up and down in the rotation experiment without touching the optical table.

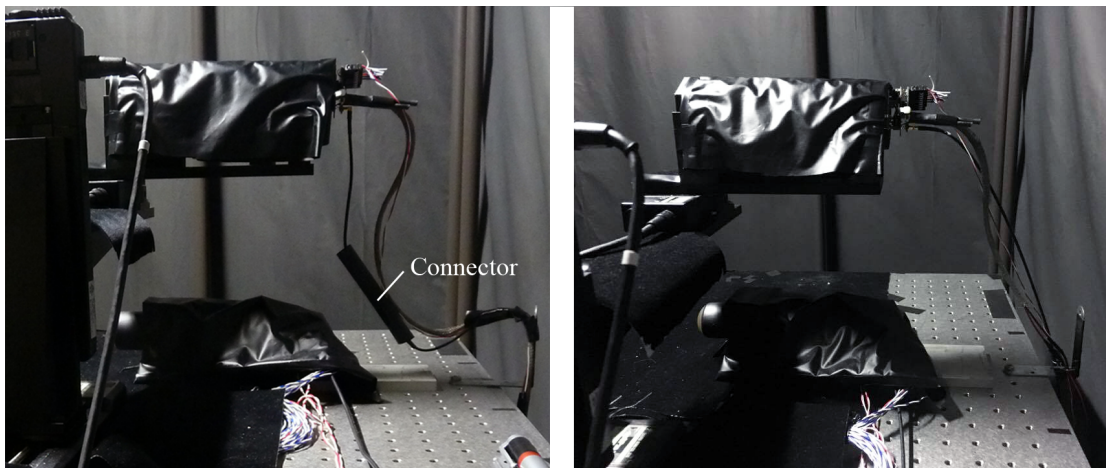


FIGURE 4.17: Left: old electrical and signal wiring before establishment, hanging a heavy connector in the air. Right: new electrical and signal wiring system.

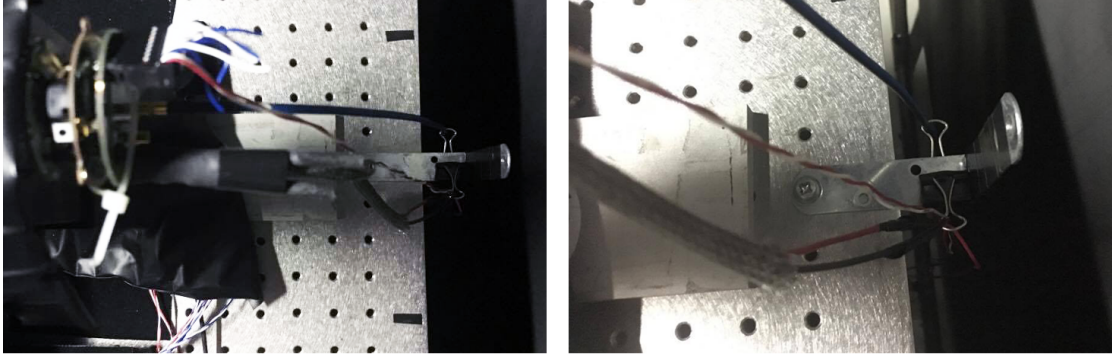


FIGURE 4.18: Left: new electrical and signal wiring viewed from above. Right: closer look.

The rotation measurement was executed once again and its results are showed in Figure 4.19. The PMT gain increasing phenomenon does not happen. There was no tendency of large changing in the PMT gain. Moreover, the RAS value at 0° was also consistent with the on-axis measurement result. Figure 4.20 shows the comparison of 2 cases before and after the entire establishment. On the left side the difference became larger, up to over 3% around $\theta = -22^\circ$, while about over 2% around $\theta = 22^\circ$ on the right side, due to the increase of PMT gain. The standard deviation became within 0.2% from the previous value of 0.4% ~ 0.6%. Besides, the result of on-axis measurement did not changed before and after the establishment of signal cable. The heavy connector seems to effect much in the rotation measurement than on-axis measurement, then caused the increase of PMT gain. By replacing with the new cable, there is no more force acting on PMT so the PMT gain values become more stable and accurate. This factor is very important to evaluate the performance of light concentrator.

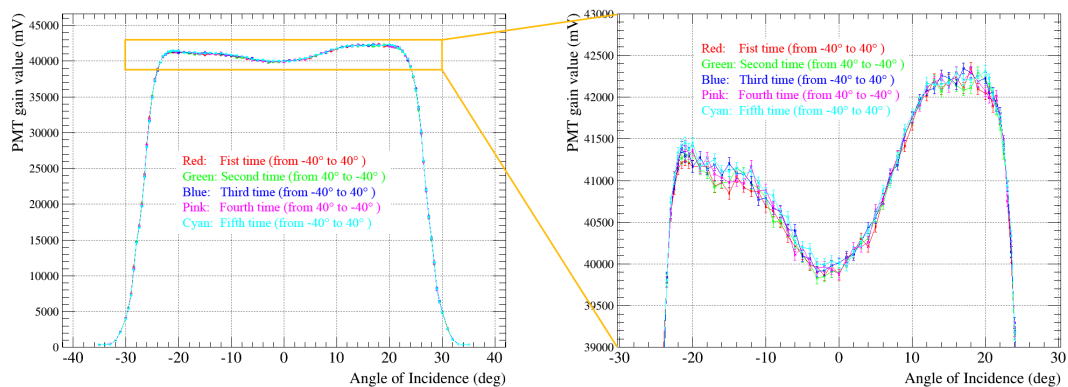


FIGURE 4.19: The measurement results after the establishment of signal cable.

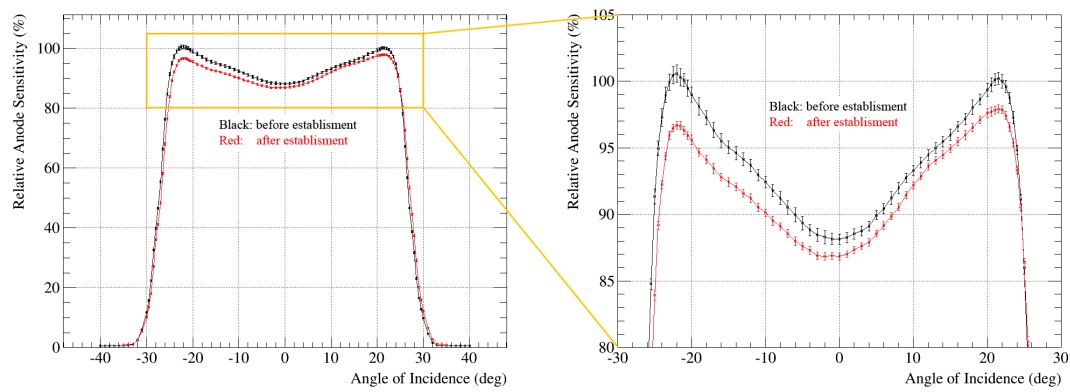


FIGURE 4.20: RAS curve comparison for 2 cases of before and after the entire establishment, as black and red line respectively.

Chapter 5

Future plan

As mentioned in Chapter 2, approximately 900 light concentrators were produced at Ibaraki University from December 2015. Besides, about 150 pieces (first batch) were measured for performance, and sent to the Institute for Cosmic Ray Research (ICRR) for mini camera test. Furthermore, 36 modules (252 LC pieces of second and third batches) were measured and sent to Spain for installation test.

However, the mass production is currently stopped because it is being discussed in the CTA Japan group whether to reinforce the remaining light guide and to use it for the first LST. Although the method of reinforcing ESR has been confirmed in this research, there are two disadvantages that it takes time by handmade production one by one, and individual difference is large. In order to solve these problems, there was a debate to change the cone material to plastic and coat Aluminum on the inner surface by vapor deposition. This work could be entrusted to a factory. It will be slightly higher in cost, but quicker in time and no worry about individual differences. Besides, there was also a discussion about whether it is better to design the cut-off angle wider to detect more photons. Because light concentrators for all 4 LSTs will be made at once, all parameters should be reviewed entirely. The light concentrator production has to be in time for the first light in November 2017, so it seems to be a difficult situation at this time.

5.1 New design

The new design of LST light concentrator is being studied at Konan University. A direct coating on current plastic cone was tested by Sanko K.K., but the reflectivity was only 40%, maybe due to the roughness of plastic surface. In the case of using current plastic cone, the surface must be polished to increase the reflectivity. Furthermore, the new design is being considered as a combination of Chrome plating and multi-layer coating to improve the ultraviolet reflectivity. Figure 5.1 shows the CAD view of new cone. It is divided to 3 parts, assembled on a jig and glued together. The method adhering the cone to the Aluminum plate by glue is also being considered too, with 1 mm Teflon sheet between cone and PMT in order to prevent the discharge. Besides, the cut-off angle should be larger than 27° as described above.

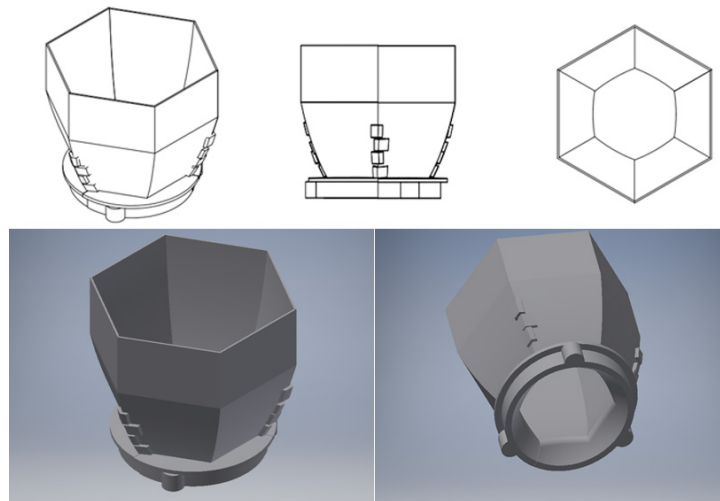


FIGURE 5.1: CAD view of new design of LST light concentrator.

All of the PMT modules will be calibrated in Tenerife, then sent to Barcelona on April 2017. The new LST light concentrators are expected to be ready on July 2017. Besides, the photon collection efficiency of the current design is very good, so a further modification should be tried. If the new design cannot be in time for the deadline of light concentrator delivery according to the construction schedule of first LST, the current design should be used. In addition, the current design has been finally confirmed and evaluated performance as a finished product, and we are proceeding to publish paper. At least the mass-produced light concentrators were used for mini camera test at ICRR and installation test in La Palma well. Whether the current design will be used in CTA depends on the current research and development of the new one.

Chapter 6

Summary

In this study, we confirmed the warpage problem in current design of CTA LST light concentrator and studied the reinforcement with two-side tapes, PET films, and SUS films. Based on rotation measurement results at 365 nm as shown in chapter 3, the LST light concentrator is determined to the design reinforced by SUS 0.1 μm film with rectangular shape of 13×26 mm as the final design. Seven new light concentrators were manufactured and being measured to evaluate the performance at 310 nm, 365 nm, and 465 nm.



FIGURE 6.1: All light concentrators. From the left side are LC without reinforcement, PET reinforced LC, SUS 0.05 μm LC, SUS 0.1 μm LC, final design LC (1s) and 3D printer LC.

On the other hand, the performance evaluation system has been established overall. The inside of dark room was rearranged and cleaned. The measurement and analysis scripts are checked, fixed and re-written in order to confirm clearly the result during measurement, reduce mistakes and handle the result data more flexibly. One monitor PMT was added and checked but the correction could not be executed, due to the difference in time dependence of the gain of 2 PMTs. The replacement work from mask to LC between

measurements of mask case and LC case (or inversely) was reviewed and the high voltage is decided to be turned off during the replacement work. The signal cable connecting PMT to DRS4 was changed by a new long one. Without the impact of heavy connector on PMT, the signals could be transmitted stable with less systematic errors. Based on these establishments, the rotation measurement result at 0° were matched with on-axis measurement result. The increase of PMT gain values which caused the systematic error of 1.6% difference at $\theta = 0^\circ$ was solved.

Besides, about 900 light guides had been completed in February 2016 as mass production. 150 pieces of finished products were sent to ICRR for mini camera test. 252 pieces (36 clusters) of finished light concentrators have been evaluated with LED 365 nm and sent to ICRR in 2 batches, and then sent to Spain for attachment test. The average value of RAS of first and second batch was $84.5\% \pm 1.66\%$ and $85.1\% \pm 1.55\%$ respectively (see Figure 3.15 and 3.16 left). However, the mass production has been stopped from March 2016 until now because of the internal discussion in Japan group about current design of LST light concentrator. Now, the new design of it and interface plate are being studied at Konan University. The prototype of new design will be completed soon and compared performance with the current one in order to have a best choice for LST light concentrator.

Appendix A

RAS value and standard deviation

This Appendix describes in detail how to calculate the RAS value in details. Figure A.1 shows the signal graphs of both mask case and LC case.

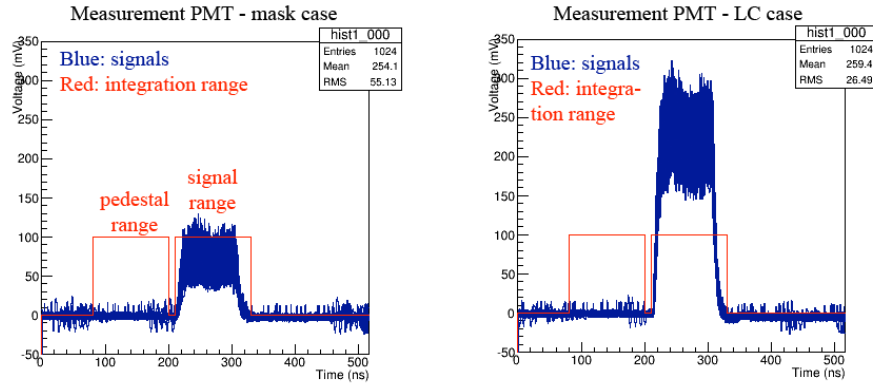


FIGURE A.1: Left: the signal graph of mask case. Right: the signal graph of LC case.

- **Pedestal, signal and residual:** The measurement is subdivided into 4 times ($N_{\text{trial}} = 4$), each consisting of 500 pulses ($N = 500$). In each time of mask case (or LC case), the integral of each signal and its noise pedestal is calculated as $s_{m_i} \pm \sigma_{s_i}$ and $p_{m_i} \pm \sigma_{p_i}$ ($i=0,1,2,3$ for 4 times) respectively, with

$$s_{m_i} = \frac{\sum_{k=1}^N s_{m_k}}{N}, \sigma_{s_i} = \sqrt{\frac{\sum_{k=1}^N (s_{m_k} - s_{m_i})^2}{N \times N}},$$

$$p_{m_i} = \frac{\sum_{k=1}^N p_{m_k}}{N}, \sigma_{p_i} = \sqrt{\frac{\sum_{k=1}^N (p_{m_k} - p_{m_i})^2}{N \times N}}.$$

where $k = 0,1,2,\dots,N$, σ_{s_i} and σ_{p_i} are the statistical errors calculated by ROOT command of "GetMeanError()". Then, the average of 500 pulses and its statistical error for each trial are calculated as $x_{m_i} \pm \sigma_{m_i}$ with

$$x_{m_k} = s_{m_k} - p_{m_k},$$

$$x_{m_i} = \frac{\sum_{k=1}^N x_{m_k}}{N}, \sigma_{m_i} = \sqrt{\sigma_{s_i}^2 + \sigma_{p_i}^2},$$

where σ_{m_i} is the statistical error of average value x_{m_i} , calculated by formula of error propagation. These calculation is written in the measurement script as follows.

```

# total sum of pedestal
P_1 = h1.Integral(p_start,p_end)
pes1.Fill(P_1)

# total sum of signal
S_1 = h1.Integral(t_start, t_end)
sig1.Fill(S_1)

# total sum of residual
s_p_1 = S_1 - P_1
charge1.Fill(s_p_1)

(bowdlerise)

# calculate LG (or Mask) value:
mean_pes_1 = pes1.GetMean()
err_pes_1 = pes1.GetMeanError()
mean_sig_1 = sig1.GetMean()
err_sig_1 = sig1.GetMeanError()
mean_1 = charge1.GetMean()
err_all1 = math.sqrt(pow(err_sig_1,2)+pow(err_pes_1,2))
print "%.1f deg: mean_pes= %.1f+/-%.1f mean_sig= %.1f+/-%.1f
↪ mean2= %.1f +/- %.1f" % (current_angle,mean_pes_1, err_pes_1, mean_sig_1,
↪ err_sig_1, mean_1, err_all1)

```

- **Average value of 4 times:** In mask case, the average value $\bar{x}_m \pm \varepsilon_m$ of 4 times (Ntrial = 4) will be the final value of mask case with

$$\bar{x}_m = \frac{\sum_{i=0}^3 x_{m_i}}{4}, \varepsilon_m = \sqrt{\frac{\sum_{i=0}^3 (x_{m_i} - \bar{x}_m)^2}{4}},$$

where ε_m is known as standard deviation. In LC case, the same calculation is also executed to find the average value $\bar{x}_{LC} \pm \varepsilon_{LC}$ with

$$\bar{x}_{LC} = \frac{\sum_{i=0}^3 x_{LC-i}}{4}, \varepsilon_{LC} = \sqrt{\frac{\sum_{i=0}^3 (x_{LC-i} - \bar{x}_{LC})^2}{4}},$$

where ε_{LC} is known as standard deviation. These calculation is written in the measurement script as follows.

```

mean_all_1 = sum_all_1/Ntrial
sum_pow_1 = 0
if Ntrial == 1:
    RMS_1 = err_all_1
else:
    for i in range(Ntrial):
        sum_pow_1 += pow ( (li_me_1[i]-mean_all_1) ,2)
    RMS_1 = math.sqrt(sum_pow_1/Ntrial)
txtfile.write("%s %.1f %f %f\n" % ( keyword, current_angle ,
- mean_all_1, RMS_1) )
print 'Mean_all = %.1f +/- %.1f' % ( mean_all_1, RMS_1)

```

- **RAS value:** The RAS value at each θ is calculated as $RAS(\theta) \pm \varepsilon_{RAS(\theta)}$ with

$$RAS(\theta) = \frac{\bar{x}_{LC}}{\bar{x}_m} \times \frac{1}{\cos\theta \times 3.7352} \times 100 \%,$$

$$\varepsilon_{RAS(\theta)} = RAS(\theta) \times \sqrt{\left(\frac{\varepsilon_{LC}}{\bar{x}_{LC}}\right)^2 + \left(\frac{\varepsilon_m}{\bar{x}_m}\right)^2},$$

where $\varepsilon_{RAS(\theta)}$ is known as entire standard deviation at θ , calculated by the error propagation formula. The RAS value calculation is written in the measurement script as follows.

```

ras = lg[i] /(m * math.cos(angle[i]/180*math.pi) *3.7352) *100
ras_err = ras * math.sqrt( pow( m_err/m ,2) + pow( lg_err[i]/lg[i] ,2) )
print '%.1f RAS    = %.1f +/- %.1f' % (angle[i], ras, ras_err)
f.write("RAS %.1f %f %f\n" % ( angle[i], ras, ras_err))

```


Appendix B

RAS value correction by monitor PMT

This Appendix describes in detail how to compensate the RAS value by monitor PMT gain values. The analysis of monitor PMT gain values are also executed as the same as measurement PMT gain values (see Appendix A. After measuring the mask case, we get 2 average values of measurement PMT and monitor PMT as $\bar{x}_m \pm \varepsilon_m$ and $\bar{y}_m \pm \eta_m$ with

$$\bar{x}_m = \frac{\sum_{i=0}^3 x_{m_i}}{4}, \varepsilon_m = \sqrt{\frac{\sum_{i=0}^3 (x_{m_i} - \bar{x}_m)^2}{4}},$$
$$\bar{y}_m = \frac{\sum_{i=0}^3 y_{m_i}}{4}, \eta_m = \sqrt{\frac{\sum_{i=0}^3 (y_{m_i} - \bar{y}_m)^2}{4}}.$$

After measuring the LC case, we get 2 average values of measurement PMT and monitor PMT as $\bar{x}_{LC} \pm \varepsilon_{LC}$ and $\bar{y}_{LC} \pm \eta_{LC}$ with

$$\bar{x}_{LC} = \frac{\sum_{i=0}^3 x_{LC_i}}{4}, \varepsilon_{LC} = \sqrt{\frac{\sum_{i=0}^3 (x_{LC_i} - \bar{x}_{LC})^2}{4}},$$
$$\bar{y}_{LC} = \frac{\sum_{i=0}^3 y_{LC_i}}{4}, \eta_{LC} = \sqrt{\frac{\sum_{i=0}^3 (y_{LC_i} - \bar{y}_{LC})^2}{4}}.$$

The compensated RAS value at each θ is calculated as $\text{RAS}_{\text{mo}}(\theta) \pm \varepsilon_{\text{mo}}$ with

$$\text{RAS}_{\text{mo}}(\theta) = \frac{\bar{x}_{\text{LC}}}{\bar{x}_{\text{m}}} \times \frac{\bar{y}_{\text{m}}}{\bar{y}_{\text{LC}}} \times \frac{1}{\cos\theta \times 3.7352} \times 100 \%,$$

$$\varepsilon_{\text{mo}} = \text{RAS}_{\text{mo}}(\theta) \times \sqrt{\left(\frac{\varepsilon_{\text{LC}}}{\bar{x}_{\text{LC}}}\right)^2 + \left(\frac{\varepsilon_{\text{m}}}{\bar{x}_{\text{m}}}\right)^2 + \left(\frac{\eta_{\text{LC}}}{\bar{y}_{\text{LC}}}\right)^2 + \left(\frac{\eta_{\text{m}}}{\bar{y}_{\text{m}}}\right)^2},$$

where ε_{mo} is known as entire standard deviation, calculated by the error propagation formula. The RAS value calculation is written in the measurement script as follows.

```

ras_mo = lg[i] * m_mo / (m * lg_mo[i] *math.cos(angle[i]/180*math.pi) * 3.7352)
← *100
ras_mo_err = ras_mo * math.sqrt( pow( m_err/m ,2) + pow( m_mo_err/m_mo ,2) +pow(
← lg_err[i]/lg[i] ,2) + pow( lg_mo_err[i]/lg_mo[i] ,2))
#print 'LG = %.1f +/- %.1f ; Mask = %.1f +/- %.1f' % (lg,lg_err, m, m_err)
print ' RAS-Mo = %.1f +/- %.1f' % ( ras_mo, ras_mo_err)
f.write("RAS-Mo %.1f %f %f\n" % ( angle[i] , ras_mo, ras_mo_err))

```

Appendix C

RAS tables of the second and third batch

This Appendix lists all the RAS value measured by me, divided into 2 table of second and third batch.

TABLE C.1: The RAS value table of second batch. The ESR of No.156 was used for test. The LCs of No.167, 178, 187, 194, 237, and 254 were left at Ibaraki University. The rest (126 pieces - 18 clusters) was sent to Spain for attachment test.

LC No.	RAS value	LC No.	RAS value	LC No.	RAS value
147	84.4	192	82.5	<u>237</u>	84.5
148	83.6	193	85.4	238	85.8
149	82.5	<u>194</u>	80.7	239	86.0
150	85.1	195	82.4	240	88.2
151	82.8	196	83.7	241	85.9
152	85.4	197	84.6	242	85.7
153	84.0	198	82.4	243	84.9
154	86.9	199	82.2	244	85.4
155	81.7	200	81.3	245	85.1
156	None	201	84.2	246	85.0
157	85.7	202	83.1	247	87.5
158	86.0	203	84.3	248	89.1
159	85.5	204	82.4	249	84.0
160	85.6	205	84.1	250	84.9

161	85.6	206	83.5	251	86.4
162	82.7	207	84.8	252	85.3
163	85.5	208	82.8	253	84.5
164	83.7	209	84.1	<u>254</u>	81.5
165	86.0	210	82.7	255	85.1
166	84.9	211	83.4	256	87.5
<u>167</u>	81.0	212	84.1	257	83.0
168	81.8	213	84.6	258	84.6
169	82.7	214	84.2	259	84.4
170	82.7	215	81.0	260	84.8
171	83.7	216	85.2	261	87.5
172	81.1	217	84.7	262	84.9
173	85.7	218	84.1	263	83.3
174	84.2	219	83.5	264	83.0
175	84.9	220	84.1	265	83.4
176	82.5	221	82.9	266	81.9
177	86.6	222	83.6	267	82.3
<u>178</u>	84.4	223	85.8	268	82.8
179	83.2	224	84.0	269	81.5
180	83.6	225	84.0	270	83.5
181	85.9	226	84.1	271	85.3
182	85.0	227	83.8	272	85.6
183	88.0	228	83.6	273	83.9
184	89.1	229	86.8	274	83.4
185	86.3	230	85.2	275	83.0
186	88.0	231	83.6	276	85.4
<u>187</u>	88.8	232	85.9	277	85.5
188	88.9	233	85.0	278	85.1
189	85.5	234	85.5	279	84.1
190	83.5	235	86.5	Average	84.5
191	85.7	236	85.3		

TABLE C.2: The RAS value table of third batch. The LCs of No.349, 350, 351, 352, and 353 were left at Ibaraki University. The rest (126 pieces - 18 clusters) was sent to Spain for attachment test.

LC No.	RAS value	LC No.	RAS value	LC No.	RAS value
280	82.7	324	84.9	368	85.7
281	86.4	325	84.6	369	85.0
282	88.5	326	84.6	370	83.6
283	87.2	327	85.4	371	85.0
284	87.0	328	84.9	372	85.0
285	83.9	329	86.5	373	83.9
286	85.4	330	84.1	374	85.1
287	83.8	331	84.4	375	84.7
288	83.1	332	85.9	376	85.6
289	86.1	333	86.7	377	86.6
290	84.6	334	85.7	378	84.2
291	86.6	335	82.7	379	86.4
292	84.9	336	81.3	380	84.9
293	83.1	337	84.9	381	86.0
294	82.8	338	86.0	382	85.0
295	84.3	339	83.1	383	86.2
296	85.1	340	84.3	384	85.7
297	85.2	341	86.0	385	85.3
298	85.7	342	86.7	386	86.9
299	84.3	343	85.0	387	85.7
300	86.1	344	84.6	388	87.2
301	85.8	345	85.4	389	87.6
302	85.8	346	85.8	390	84.3
303	85.3	347	85.0	391	87.0
304	85.1	348	84.2	392	84.3
305	84.1	<u>349</u>	86.6	393	85.2
306	86.2	<u>350</u>	59.9	394	88.1
307	85.1	<u>351</u>	67.5	395	86.3
308	82.9	<u>352</u>	68.9	396	86.8
309	84.5	<u>353</u>	73.0	397	86.2

310	85.0	354	82.7	398	84.8
311	84.1	355	83.1	399	85.6
312	84.0	356	85.4	400	86.6
313	83.6	357	82.4	401	86.4
314	87.2	358	85.8	402	86.6
315	83.0	359	85.2	403	87.2
316	83.3	360	87.4	404	85.9
317	85.4	361	86.8	405	87.5
318	86.2	362	83.3	406	85.2
319	83.0	363	79.2	407	88.6
320	84.8	364	82.9	408	84.9
321	81.6	365	85.3	409	88.0
322	84.2	366	84.9	410	86.8
323	84.6	367	86.4	Average	85.3

Appendix D

On-axis measurement script

The re-written on-axis measurement script is recorded as follows. This script is used for LC case of on-axis measurement, and mask case of both on-axis and rotation measurement.

```
1  #!/bin/sh
2  #!/usr/bin/env python
3
4  import ROOT
5  import gpd3303s
6  import sigma_koki
7  import sys
8  import os
9  import time
10 import subprocess
11 import math
12
13 argv = sys.argv
14 argc = len(argv)
15 values = {}
16 if argc != 8:
17     print 'Usage:'
18     #print 'rotation_byTan.py DRS4_Events_Number Rotation_Angle1 STEP1
19     ↪ Rotation_Angle2 STEP2 Rotaion_Angle3 STEP3 Trial_Number'
20     print 'rotation_byTan_withMo.py DRS4_Events_Number Trial_Number Number LG(or
21     ↪ Mask)')
22     sys.exit()
23
24 DRS_EXE="/home/cta/tanaka/work/11100301_simple_drs4_daq2/drs-4.0.0/drs_simple_ch1-2"
25 THD=0.5
26 DEG = 400 # 400 is equal to 1 degree
27 #####
28 NEVE=int(argv[1]) #
```

```

27 Ntrial=int(argv[2]) #
28 length=int(argv[3]) # wave length: 365, 465 or 310
29 month=argv[4] #
30 day=argv[5]
31 number=argv[7]
32 keyword=argv[6]
33 if keyword == "M":
34     keyword = "Mask"
35 DIR="/home/cta/work/LightGuide/17%s%s_\\d_\\s/with%s" \% (month, day, length,
    ↪ number, keyword)
36 fin_dir = "/home/cta/work/LightGuide/17%s%s_\\d_\\s/" \% (month, day, length,
    ↪ number) # for text file
37 vfile = open("%s/voltage.txt" \% DIR, "w")
38 #####
39 gpd = gpd3303s.GPD3303S()
40 gpd.open("/dev/ttyUSB0")
41
42 gsc02 = sigma_koki.GSC02()
43 gsc02.open('/dev/ttyUSB1', 2)
44 status = gsc02.getStatus()
45 print "Initial Status", status
46 current_pos = int(status.split(",")[0])
47
48 print "current_pos =", current_pos
49 if current_pos!=0:
50     gsc02.move(-current_pos, 0) # reset position
51     time.sleep(5) # 5
52
53 for i in range(1): # 10
54     #time.sleep(1)
55     status = gsc02.getStatus()
56     print "Current Status", status
57     if status == '    \\d,    \\d,K,K,R' \% (current_pos , current_pos): # oldver
    ↪ is 40000
58         break
59
60 current_angle = float(status.split(",")[0])/400
61
62 trial = 0
63 sum_all_1, sum_all_2 = 0.0, 0.0
64 li_me_1 = [] # li_me = list means,
65 li_me_2 = []
66
67 dt = (1./2.) # ns
68
69 if length == 310:
70     ns = 0 # chousei you
71     tstart = 240. # Signal start
72     tend = tstart + ns+100. # Signal end
73     pend = tstart - 10 # Pedestal start
74     pstart = pend - ns-100. # Pedestal end
75     p_start = int(pstart/dt); # pedestal start cell

```

```

76  p_end   = int(pend/dt);   # pedestal end cell
77  t_start = int(tstart/dt); # signal start cell
78  t_end   = int(tend/dt);   # signal end cell
79
80  tstart_mo = tstart- 0.   # Signal start - monitor
81  tend_mo   = tend  - 0.   # Signal end - monitor
82  pend_mo   = pend  - 0.   # Pedestal start - monitor
83  pstart_mo = pstart- 0.   # Pedestal end - monitor
84  p_start_mo = int((pstart_mo)/dt); # pedestal start cell - monitor
85  p_end_mo   = int((pend_mo)/dt);   # pedestal end cell - monitor
86  t_start_mo = int((tstart_mo)/dt); # signal start cell - monitor
87  t_end_mo   = int((tend_mo)/dt);   # signal end cell - monitor
88
89  elif length == 365:
90      pstart   = 80.           # Pedestal start
91      pend     = pstart + 120. # Pedestal end
92      tstart   = 210.          # Signal start
93      tend     = tstart + 120. # Signal end
94      p_start = int(pstart/dt); # pedestal start cell
95      p_end   = int(pend/dt);   # pedestal end cell
96      t_start = int(tstart/dt); # signal start cell
97      t_end   = int(tend/dt);   # signal end cell
98
99      sa = 0.
100     tstart_mo = tstart- sa # Signal start - monitor
101     tend_mo   = tend  - sa # Signal end - monitor
102     pend_mo   = pend  - sa # Pedestal start - monitor
103     pstart_mo = pstart- sa # Pedestal end - monitor
104     p_start_mo = int((pstart_mo)/dt); # pedestal start cell - monitor
105     p_end_mo   = int((pend_mo)/dt);   # pedestal end cell - monitor
106     t_start_mo = int((tstart_mo)/dt); # signal start cell - monitor
107     t_end_mo   = int((tend_mo)/dt);   # signal end cell - monitor
108
109     elif length == 465:
110         ns     = 35
111         tstart = 210.          # Signal start
112         tend   = tstart + ns+20. # Signal end
113         pend   = tstart - 10     # Pedestal start
114         pstart = pend  - ns-20. # Pedestal end
115         p_start = int(pstart/dt); # pedestal start cell
116         p_end   = int(pend/dt);   # pedestal end cell
117         t_start = int(tstart/dt); # signal start cell
118         t_end   = int(tend/dt);   # signal end cell
119
120         tstart_mo = tstart- 5.   # Signal start - monitor
121         tend_mo   = tend  - 5.   # Signal end - monitor
122         pend_mo   = pend  - 5.   # Pedestal start - monitor
123         pstart_mo = pstart- 5.   # Pedestal end - monitor
124         p_start_mo = int((pstart_mo)/dt); # pedestal start cell - monitor
125         p_end_mo   = int((pend_mo)/dt);   # pedestal end cell - monitor
126         t_start_mo = int((tstart_mo)/dt); # signal start cell - monitor
127         t_end_mo   = int((tend_mo)/dt);   # signal end cell - monitor

```

```

128 else :
129     print 'Need to change the pedestal and signal range with wavelength.'
130
131 #li_err = [] # li_me = list means, li_err = list errors
132 txtfile = open("%strial_all.txt" % ( fin_dir),"a") #
133 f = open("%strial_all.txt" % ( fin_dir),"r+b")
134 i = 0
135 lines = f.readlines()
136 for i,line in enumerate(lines):
137     #type_, average= line.split(" ")
138     type_ = line.split("-")[0]
139     if type_ == keyword:
140         print "%s has already done" % keyword
141         f.close()
142         sys.exit()
143 f.close()
144
145 # pedestal & signal range's graph
146 h_range = ROOT.TH1D("test", "test",560,-30.,530)
147 h_range.SetAxisRange(-50,350,"Y")
148 ma,z = int(0), int(0)
149 for ma in range (100):
150     for z in range (int(pstart),int(pend+1)):
151         h_range.Fill(z)
152     for z in range (int(tstart),int(tend+1)):
153         h_range.Fill(z)
154
155 # pedestal & signal range's graph - monitor
156 h_range_mo = ROOT.TH1D("test2", "test2",560,-30.,530)
157 h_range_mo.SetAxisRange(-50,350,"Y")
158 ma,z = int(0), int(0)
159 for ma in range (100):
160     for z in range (int(pstart_mo),int(pend_mo+1)):
161         h_range_mo.Fill(z)
162     for z in range (int(tstart_mo),int(tend_mo+1)):
163         h_range_mo.Fill(z)
164
165 c1 = ROOT.TCanvas(number, number, 0,0,400,800)
166 c1.Divide(1,2)
167 #c1.cd(1)
168
169
170 i=0
171 for trial in range(Ntrial):
172     #for j in range(SumNS): #
173         #print "Trial : %d, current angle : %.1f deg, St : %s" %
174         ← (trial,current_angle, gsc02.getStatus())
175         #time.sleep(0.5)
176         c1.cd(1)
177         fname = "%s/trial%04d_%.1fdeg.dat" % (DIR, trial, current_angle)
178         fout_name = "%s/trial%04d_%.1fdeg.root" % (DIR, trial, current_angle)
179         os.system("%s %f %d %s true 2." % (DRS_EXE, THD, NEVE, fname))

```

```

179         vfile.write("%d %s %f %s\n" % (time.time(), fname,
↳ gpd.getVoltageOutput(1), gsc02.getStatus()))
180         vfile.flush()
181         #print "j : %d " % j
182
183         # save to ROOT file
184         f = open(fname)
185         lines = f.readlines()
186         nlines = len(lines)
187         t1 = -1e10
188         for i, line in enumerate(lines):
189             t, v1, v2 = line.split(" ")
190             t = float(t)
191             if i == 0:
192                 tstart = t
193             if t1 > t:
194                 tend = t1
195                 f.close()
196                 break
197             else:
198                 t1 = t
199
200         nsamples = i
201         nevents = nlines/nsamples
202         f = open(fname)
203         lines = f.readlines()
204         fout = ROOT.TFile(fout_name, "create")
205         for i, line in enumerate(lines):
206             if i\%nsamples == 0:
207                 if NEVE <1000:
208                     hist1 = ROOT.TH1D("hist1_\\%03d" % (i/nsamples), ";Time (ns);Voltage
↳ (mV)", nsamples, tstart - (tend - tstart)/(nsamples - 1)/2., tend + (tend -
↳ tstart)/(nsamples - 1)/2.)
209                     hist2 = ROOT.TH1D("hist2_\\%03d" % (i/nsamples), ";Time (ns);Voltage
↳ (mV)", nsamples, tstart - (tend - tstart)/(nsamples - 1)/2., tend + (tend -
↳ tstart)/(nsamples - 1)/2.)
210                 else:
211                     hist1 = ROOT.TH1D("hist1_\\%04d" % (i/nsamples), ";Time (ns);Voltage
↳ (mV)", nsamples, tstart - (tend - tstart)/(nsamples - 1)/2., tend + (tend -
↳ tstart)/(nsamples - 1)/2.)
212                     hist2 = ROOT.TH1D("hist2_\\%04d" % (i/nsamples), ";Time (ns);Voltage
↳ (mV)", nsamples, tstart - (tend - tstart)/(nsamples - 1)/2., tend + (tend -
↳ tstart)/(nsamples - 1)/2.)
213                     t, v1,v2 = line.split(" ")
214                     t = float(t)
215                     v1 = float(v1)
216                     v2 = float(v2)
217                     hist1.Fill(t, v1)
218                     hist2.Fill(t, v2)
219
220                 if i\%nsamples == nsamples - 1:
221                     hist1.Write()

```

```
222         hist2.Write()
223
224     # calculate signal of LC or Mask
225     sig1,sig2 = ROOT.TH1D("", "", 100, 0, 0),ROOT.TH1D("", "", 100, 0, 0)
226     charge1, charge2 = ROOT.TH1D("", "", 100, 0, 0),ROOT.TH1D("", "", 100, 0, 0)
227     pes1,pes2     = ROOT.TH1D("", "", 100, 0, 0),ROOT.TH1D("", "", 100, 0, 0)
228     #c1.cd(trial+1)
229     #c1.Update()
230     for i in range(NEVE):
231         if NEVE <1000:
232             h1 = fout.Get("hist1_\\%03d" \\% i)
233         else:
234             h1 = fout.Get("hist1_\\%04d" \\% i)
235         if not h1:
236             break
237         # draw all signals to 1 graph
238         if (i ==0):
239             h1.SetAxisRange(-50,350, "Y")
240             h1.Draw()
241         else:
242             h1.Draw("SAME")
243         # total sum of pedestal
244         P_1 = h1.Integral(p_start,p_end)
245         pes1.Fill(P_1)
246
247         # total sum of signal
248         S_1 = h1.Integral(t_start, t_end)
249         sig1.Fill(S_1)
250
251         s_p_1 = S_1 - P_1
252         charge1.Fill(s_p_1)
253     h_range.SetLineColor(2)
254     h_range.Draw("SAME")
255     c1.Update()
256
257     # calculate signal of Monitor
258     c1.cd(2)
259     for i in range(NEVE):
260         if NEVE <1000:
261             h2 = fout.Get("hist2_\\%03d" \\% i)
262         else:
263             h2 = fout.Get("hist2_\\%04d" \\% i)
264
265         if not h2:
266             break
267         # draw all Monitor's signals to 1 graph
268         if (i ==0):
269             h2.SetAxisRange(-50,350, "Y")
270             h2.Draw()
271         else:
272             h2.Draw("SAME")
273         # total sum of pedestal
```

```

274         P_2 = h2.Integral(p_start_mo,p_end_mo)
275         pes2.Fill(P_2)
276
277         # total sum of signal
278         S_2 = h2.Integral(t_start_mo, t_end_mo)
279         sig2.Fill(S_2)
280
281         s_p_2 = S_2 - P_2
282         charge2.Fill(s_p_2)
283         h_range_mo.SetLineColor(2)
284         h_range_mo.Draw("SAME")
285         c1.Update()
286
287         # calculate LG (or Mask) value:
288         mean_pes_1 = pes1.GetMean()
289         err_pes_1 = pes1.GetMeanError()
290         mean_sig_1 = sig1.GetMean()
291         err_sig_1 = sig1.GetMeanError()
292         mean_1 = charge1.GetMean()
293         err_1 = charge1.GetMeanError()
294         err_all_1 = math.sqrt(pow(err_sig_1,2)+pow(err_pes_1,2)) # total error
295         mean_1 = mean_sig_1 - mean_pes_1
296         print "%.1f deg: mean_pes= %.1f+/-%.1f mean_sig= %.1f+/-%.1f
↳ mean2= %.1f +/- %.1f" \% (current_angle,mean_pes_1, err_pes_1, mean_sig_1,
↳ err_sig_1, mean_1, err_all_1)
297         #print "%.1f deg: mean= %.1f +/- %.1f" \% (current_angle, mean, err)
298
299         li_me_1.append(mean_1)
300         sum_all_1 += li_me_1[trial]
301         if Ntrial >1:
302             txtfile.write("%s-%d %.1f %f %f\n" \% ( keyword, trial, current_angle
↳ , mean_1, err_all_1))
303
304         # calculate Monitor's value:
305         mean_pes_2 = pes2.GetMean()
306         err_pes_2 = pes2.GetMeanError()
307         mean_sig_2 = sig2.GetMean()
308         err_sig_2 = sig2.GetMeanError()
309         mean_2 = charge2.GetMean()
310         err_2 = charge2.GetMeanError()
311         err_all_2 = math.sqrt(pow(err_sig_2,2)+pow(err_pes_2,2)) # total error
312         mean_2 = mean_sig_2 - mean_pes_2
313         print "%.1f-Mo deg: mean_pes= %.1f+/-%.1f mean_sig= %.1f+/-%.1f
↳ mean2= %.1f +/- %.1f" \% (current_angle,mean_pes_2, err_pes_2, mean_sig_2,
↳ err_sig_2, mean_2, err_all_2)
314         #print "%.1f deg: mean= %.1f +/- %.1f" \% (current_angle, mean, err)
315
316         li_me_2.append(mean_2)
317         sum_all_2 += li_me_2[trial]
318         if Ntrial >1:
319             txtfile.write("%s-Mo-%d %.1f %f %f\n" \% ( keyword,trial,
↳ current_angle , mean_2, err_all_2))

```

```

320
321     fout.Close()
322     f.close()
323     # finish saving to ROOT file
324
325     if trial == Ntrial-1:
326         print 'The Measurement has just finished.'
327
328         mean_all_1 = sum_all_1/Ntrial
329         sum_pow_1 = 0
330         if Ntrial == 1:
331             RMS_1 = err_all_1
332         else:
333             for i in range(Ntrial):
334                 sum_pow_1 += pow ( (li_me_1[i]-mean_all_1) ,2)
335             RMS_1 = math.sqrt(sum_pow_1/Ntrial)
336             txtfile.write("\%s \%.1f \%.1f \%.1f\n" \% ( keyword, current_angle ,
↵ mean_all_1, RMS_1) )
337             print 'Mean_all = \%.1f +/-\%.1f' \% ( mean_all_1, RMS_1)
338
339             mean_all_2 = sum_all_2/Ntrial
340             sum_pow_2 = 0
341             if Ntrial == 1:
342                 RMS_2 = err_all_2
343             else:
344                 for i in range(Ntrial):
345                     sum_pow_2 += pow ( (li_me_2[i]-mean_all_2) ,2)
346                 RMS_2 = math.sqrt(sum_pow_2/Ntrial)
347                 txtfile.write("\%s-Mo \%.1f \%.1f \%.1f\n" \% ( keyword, current_angle ,
↵ mean_all_2, RMS_2) )
348                 print 'Mean_Monitor = \%.1f +/-\%.1f\n' \% ( mean_all_2, RMS_2)
349
350             #sys.exit()
351 txtfile.close()
352
353 # calculate RAS
354 f = open("\%strial_all.txt" \% ( fin_dir),"r+w" ) #
355 i = 0
356 lines = f.readlines()
357 count = 0
358 for i,line in enumerate(lines):
359     type_ = line.split(" ")[0]
360     if type_ == "LG":
361         current_angle = float(line.split(" ")[1])
362         lg = float(line.split(" ")[2]) # LG
363         lg_err = float(line.split(" ")[3]) # LG's error
364         count += 1
365     elif type_ == "LG-Mo":
366         lg_mo = float(line.split(" ")[2]) # LG's monitor
367         lg_mo_err = float(line.split(" ")[3]) # LG's monitor error
368         count += 1
369     elif type_ == "Mask":

```

```

370     m = float(line.split(" ")[2])      # mask
371     m_err = float(line.split(" ")[3])  # mask's error
372     count += 1
373     elif type_ == "Mask-Mo":
374         m_mo = float(line.split(" ")[2]) # mask's monitor
375         m_mo_err = float(line.split(" ")[3]) # mask's monitor error
376         count += 1
377
378 if count == 2 :
379     print 'No LG or M'
380 elif count == 4:
381     ras = lg/(m*math.cos(current_angle/180*math.pi)*3.7352) *100
382     ras_err = ras * math.sqrt( pow( m_err/m ,2) + pow( lg_err/lg ,2) )
383     print 'LG = %.1f +/- %.1f ; LG-Mo = %.1f +/- %.1f' \% (lg,lg_err, lg_mo,
← lg_mo_err)
384     print 'Mask = %.1f +/- %.1f ; Mask-Mo = %.1f +/- %.1f' \% ( m,m_err, m_mo,
← m_mo_err)
385     print 'RAS = %.1f +/- %.1f' \% ( ras, ras_err)
386     f.write("RAS %.1f \%f \%f\n" \% ( current_angle, ras, ras_err))
387
388     ras_mo = lg * m_mo / (m *math.cos(current_angle/180*math.pi)* lg_mo * 3.7352) *100
389     ras_mo_err = ras_mo * math.sqrt( pow( m_err/m ,2) + pow( m_mo_err/m_mo ,2) +pow(
← lg_err/lg ,2) + pow( lg_mo_err/lg_mo ,2))
390     #print 'LG = %.1f +/- %.1f ; Mask = %.1f +/- %.1f' \% (lg,lg_err, m, m_err)
391     print 'RAS-Mo = %.1f +/- %.1f' \% ( ras_mo, ras_mo_err)
392     f.write("RAS-Mo %.1f \%f \%f\n" \% ( current_angle , ras_mo, ras_mo_err))
393 else:
394     print "count = \%d :Sthing's wrong!" \% (count)
395 f.close()
396 time.sleep(3)
397
398 sys.exit()

```


Appendix E

Rotation measurement script

The re-written rotation measurement script is recorded as follows. This script is only used for LC case of rotation measurement.

```
1  #!/bin/sh
2  #!/usr/bin/env python
3
4  import ROOT
5  import gpd3303s
6  import sigma_koki
7  import sys
8  import os
9  import time
10 import subprocess
11 import math
12
13 argv = sys.argv
14 argc = len(argv)
15 # date ; python rotation_byTan_withMo.py 500 20 1 30 0.5 40 1 4 1011 365 3s-rot-3 ;
16 ↪ python hvoff.py 0
17
18 if argc != 12:
19     print 'Usage:'
20     print 'rotation_editbyTanaka.py DRS4_Events_Number Rotation_Angle1 STEP1
21     ↪ Rotation_Angle2 STEP2 Rotaion_Angle3 STEP3 Trial_Number'
22     sys.exit()
23
24 day = argv[9]
25 number =argv[11]
26 length = int (argv[10])
27
28 DIR="/home/cta/work/LightGuide/17%s_%d_%s/withLG" % (day,length, number)
29 fin_dir = "/home/cta/work/LightGuide/17%s_%d_%s/" % ( day, length, number) # for text
30 ↪ file
31 vfile = open("%s/voltage.txt" % DIR, "w")
```

```

28
29 #time.sleep(60*90)
30
31 DRS_EXE="/home/cta/tanaka/work/11100301_simple_drs4_daq2/drs-4.0.0/drs_simple_ch1-2"
32 THD=0.5
33 EX=0.1
34 #NEVE=500 # ~10 sec
35 DEG = 400 # 400 is equal to 1 degree
36 #####
37 NEVE=int(argv[1]) #
38 Rotdeg1=int(argv[2]) # Rotation Angle (deg)
39 STEP1=float(argv[3]) #
40 Rotdeg2=int(argv[4])
41 STEP2=float(argv[5])
42 Rotdeg3=int(argv[6])
43 STEP3=float(argv[7])
44 Ntrial=int(argv[8])
45
46 #####
47 gpd = gpd3303s.GPD3303S()
48 gpd.open("/dev/ttyUSB0")
49
50 gsc02 = sigma_koki.GSC02()
51 gsc02.open('/dev/ttyUSB2', 2)
52 status = gsc02.getStatus()
53 current_angle = -Rotdeg3
54 NSTEP1 = int(Rotdeg1/STEP1)+1 #
55 NSTEP2 = int((Rotdeg2-Rotdeg1)/STEP2)-1
56 NSTEP3 = int((Rotdeg3-Rotdeg2)/STEP3)+1
57 SumNS = int((NSTEP1+NSTEP2+NSTEP3)*2-1)
58 print "NSTEP1 = %d , NSTEP2 = %d , NSTEP3 = %d , SumNS = %d" % ( NSTEP1 , NSTEP2 ,
↳ NSTEP3 , SumNS)
59 angle = []
60
61 sa=200
62 print "Initial Status", status
63 current_pos = int(status.split(",")[0])
64 if current_pos != 0:
65     gsc02.move(-current_pos, 0) # reset position
66     time.sleep(7) # 15
67
68 gsc02.move(-Rotdeg3*DEG, 0) # go to -Rotdeg3 degree
69 for i in range(8): # 10
70     time.sleep(1)
71     status = gsc02.getStatus()
72     print "Current Status", status
73     if status == ' %d, %d,K,K,R' % (-Rotdeg3*DEG , -Rotdeg3*DEG): # oldver is
↳ 40000
74         break
75
76 # edited by Tan
77 sum_all_1, sum_all_2 = [], []

```

```

78 mean_all_1, mean_all_2 = [], []
79 err_all_1, err_all_2 = [], []
80 RMS_1, RMS_2 = [], []
81
82 li_me_1 = [] # li_me = list means,
83 li_me_2 = []
84
85 dt      = (1./2.) # ns
86
87 # wavelength's
88 if length == 310:
89     ns      = 0          # chousei you
90     tstart  = 240.       # Signal start
91     tend    = tstart + ns+100. # Signal end
92     pend    = tstart - 10 # Pedestal start
93     pstart  = pend - ns-100. # Pedestal end
94     p_start = int(pstart/dt); # pedestal start cell
95     p_end   = int(pend/dt); # pedestal end cell
96     t_start = int(tstart/dt); # signal start cell
97     t_end   = int(tend/dt); # signal end cell
98
99     tstart_mo = tstart- 0. # Signal start - monitor
100    tend_mo   = tend - 0. # Signal end - monitor
101    pend_mo    = pend - 0. # Pedestal start - monitor
102    pstart_mo  = pstart- 0. # Pedestal end - monitor
103    p_start_mo = int((pstart_mo)/dt); # pedestal start cell - monitor
104    p_end_mo   = int((pend_mo)/dt); # pedestal end cell - monitor
105    t_start_mo = int((tstart_mo)/dt); # signal start cell - monitor
106    t_end_mo   = int((tend_mo)/dt); # signal end cell - monitor
107
108 elif length == 365:
109     pstart = 80. # Pedestal start
110     pend   = pstart + 120. # Pedestal end
111     tstart = 210. # Signal start
112     tend   = tstart + 120. # Signal end
113     p_start = int(pstart/dt); # pedestal start cell
114     p_end   = int(pend/dt); # pedestal end cell
115     t_start = int(tstart/dt); # signal start cell
116     t_end   = int(tend/dt); # signal end cell
117
118     tstart_mo = tstart # Signal start - monitor
119     tend_mo   = tend # Signal end - monitor
120     pend_mo    = pend # Pedestal start - monitor
121     pstart_mo  = pstart # Pedestal end - monitor
122     p_start_mo = int((pstart_mo)/dt); # pedestal start cell - monitor
123     p_end_mo   = int((pend_mo)/dt); # pedestal end cell - monitor
124     t_start_mo = int((tstart_mo)/dt); # signal start cell - monitor
125     t_end_mo   = int((tend_mo)/dt); # signal end cell - monitor
126
127 elif length == 465:
128     ns      = 35
129     tstart  = 210. # Signal start

```

```

130     tend    = tstart + ns+20. # Signal end
131     pend    = tstart - 10     # Pedestal start
132     pstart  = pend - ns-20.  # Pedestal end
133     p_start = int(pstart/dt); # pedestal start cell
134     p_end   = int(pend/dt);  # pedestal end cell
135     t_start = int(tstart/dt); # signal start cell
136     t_end   = int(tend/dt);  # signal end cell
137
138     tstart_mo = tstart- 5.    # Signal start - monitor
139     tend_mo   = tend - 5.     # Signal end - monitor
140     pend_mo   = pend - 5.     # Pedestal start - monitor
141     pstart_mo = pstart- 5.    # Pedestal end - monitor
142     p_start_mo = int((pstart_mo)/dt); # pedestal start cell - monitor
143     p_end_mo   = int((pend_mo)/dt);  # pedestal end cell - monitor
144     t_start_mo = int((tstart_mo)/dt); # signal start cell - monitor
145     t_end_mo   = int((tend_mo)/dt);  # signal end cell - monitor
146
147     else :
148         print 'Need to change the pedestal and signal range with wavelength.'
149         print length
150
151
152     #li_err = [] # li_me = list means, li_err = list errors
153     txtfile = open("%strial_all.txt" % ( fin_dir),"a") #
154     f = open("%strial_all.txt" % ( fin_dir),"r+b")
155     i = 0
156     lines = f.readlines()
157     for i,line in enumerate(lines):
158         #type_, average= line.split(" ")
159         type_ = line.split("-")[0]
160         typ   = line.split(" ")[0]
161         if type_ == "LG":
162             print "Measurement has already done"
163             sys.exit()
164         if typ == "Mask-Mo":
165             mmo = float(line.split(" ")[2])
166             print "Mask-Mo:", mmo
167
168     f.close()
169
170     # lg gain graph
171     h_lg0 = ROOT.TGraphErrors()
172     h_lg0.SetName("ras")
173     h_lg1 = ROOT.TGraphErrors()
174     h_lg2 = ROOT.TGraphErrors()
175     h_lg3 = ROOT.TGraphErrors()
176
177     # pedestal & signal range's graph
178     h_range = ROOT.TH1D("test", "test", 560, -30., 530)
179     h_range.SetAxisRange(-50, 350, "Y")
180     ma, z = int(0), int(0)
181     for ma in range (100):

```

```

182     for z in range (int(pstart),int(pend+1)):
183         h_range.Fill(z)
184     for z in range (int(tstart),int(tend+1)):
185         h_range.Fill(z)
186
187     # pedestal & signal range's graph - monitor
188     h_range_mo = ROOT.TH1D("test2", "test2",560,-30.,530)
189     h_range_mo.SetAxisRange(-50,350,"Y")
190     ma,z = int(0), int(0)
191     for ma in range (100):
192         for z in range (int(pstart_mo),int(pend_mo+1)):
193             h_range_mo.Fill(z)
194         for z in range (int(tstart_mo),int(tend_mo+1)):
195             h_range_mo.Fill(z)
196
197     c1 = ROOT.TCanvas(number, number, 0,0,400,800)
198     c1.Divide(1,2)
199     c2 = ROOT.TCanvas("lg", "lg", 0,0,800,600)
200     #c1.cd(1)
201
202     #ROOT.TH1D *h[4]
203     #h[Ntrial] = ROOT.TH1D("hist_%01d" % (Ntrial),"hist_%01d" % (Ntrial),560,-30.,530)
204
205     i=0
206     # end
207     brk=0
208     trial = 0
209     a = 1 # ratio 1 (for +side) or -1 (for -side)
210
211     for trial in range(Ntrial):
212         j=0
213         while (j < SumNS):
214             #for j in range(SumNS): # (+)side . example: from -40 -> 40
215                 time.sleep(2.5)
216                 c1.cd(1)
217                 print "\nTrial : %d, j= %d, current angle: %.1f deg, St : %s" %
↳ (trial,j,current_angle, gsc02.getStatus())
218                 time.sleep(0.5)
219                 fname="%s/trial%04d_%.1fdeg.dat" % (DIR, trial, current_angle)
220                 fout_name = "%s/trial%04d_%.1fdeg.root" % (DIR, trial, current_angle)
221                 os.system("%s %f %d %s true 2." % (DRS_EXE, THD, NEVE, fname))
222                 vfile.write("%d %s %f %s\n" % (time.time(), fname, gpd.getVoltageOutput(1),
↳ gsc02.getStatus()))
223                 vfile.flush()
224
225
226                 # save to ROOT file
227                 f = open(fname)
228                 lines = f.readlines()
229                 nlines = len(lines)
230                 t1 = -1e10
231                 for i, line in enumerate(lines):

```

```

232         t, v1, v2 = line.split(" ")
233         t = float(t)
234         if i == 0:
235             tstart = t
236         if t1 > t:
237             tend = t1
238             f.close()
239             break
240         else:
241             t1 = t
242
243     nsamples = i
244     nevents = nlines/nsamples
245     f = open(fname)
246     lines = f.readlines()
247     fout = ROOT.TFile(fout_name, "create")
248     for i, line in enumerate(lines):
249         if i%nsamples == 0:
250             if NEVE <1000:
251                 hist1 = ROOT.TH1D("hist1_%03d" % (i/nsamples), ";Time (ns);Voltage
↳ (mV)", nsamples, tstart - (tend - tstart)/(nsamples - 1)/2., tend + (tend -
↳ tstart)/(nsamples - 1)/2.)
252                 hist2 = ROOT.TH1D("hist2_%03d" % (i/nsamples), ";Time (ns);Voltage
↳ (mV)", nsamples, tstart - (tend - tstart)/(nsamples - 1)/2., tend + (tend -
↳ tstart)/(nsamples - 1)/2.)
253             else:
254                 hist1 = ROOT.TH1D("hist1_%04d" % (i/nsamples), ";Time (ns);Voltage
↳ (mV)", nsamples, tstart - (tend - tstart)/(nsamples - 1)/2., tend + (tend -
↳ tstart)/(nsamples - 1)/2.)
255                 hist2 = ROOT.TH1D("hist2_%04d" % (i/nsamples), ";Time (ns);Voltage
↳ (mV)", nsamples, tstart - (tend - tstart)/(nsamples - 1)/2., tend + (tend -
↳ tstart)/(nsamples - 1)/2.)
256
257         t, v1,v2 = line.split(" ")
258         t = float(t)
259         v1 = float(v1)
260         v2 = float(v2)
261         hist1.Fill(t, v1)
262         hist2.Fill(t, v2)
263
264         if i%nsamples == nsamples - 1:
265             hist1.Write()
266             hist2.Write()
267
268         # calculate
269         sig1,sig2 = ROOT.TH1D("", "", 100, 0, 0),ROOT.TH1D("", "", 100, 0, 0)
270         charge1, charge2 = ROOT.TH1D("", "", 100, 0, 0),ROOT.TH1D("", "", 100, 0, 0)
271         pes1,pes2 = ROOT.TH1D("", "", 100, 0, 0),ROOT.TH1D("", "", 100, 0, 0)
272         #c1.cd(trial+1)
273         for i in range(NEVE):
274             if NEVE <1000:
275                 h1 = fout.Get("hist1_%03d" % i)

```

```
276         else:
277             h1 = fout.Get("hist1_%04d" % i)
278         if not h1:
279             break
280         # draw all signals to 1 graph
281         if (i ==0):
282             h1.SetAxisRange(-50,350,"Y")
283             h1.Draw()
284         else:
285             h1.Draw("SAME")
286         # total sum of pedestal from 80 to 180
287         P_1 = h1.Integral(p_start,p_end)
288         pes1.Fill(P_1)
289
290         # total sum of signal from 200 to 300
291         S_1 = h1.Integral(t_start, t_end)
292         sig1.Fill(S_1)
293
294         s_p_1 = S_1 - P_1
295         charge1.Fill(s_p_1)
296         h_range.SetLineColor(2)
297         h_range.Draw("SAME")
298         c1.Update()
299
300         # calculate signal of Monitor
301         c1.cd(2)
302         for i in range(NEVE):
303             if NEVE <1000:
304                 h2 = fout.Get("hist2_%03d" % i)
305             else:
306                 h2 = fout.Get("hist2_%04d" % i)
307             if not h2:
308                 break
309             # draw all Monitor's signals to 1 graph
310             if (i ==0):
311                 h2.SetAxisRange(-50,350,"Y")
312                 h2.Draw()
313             else:
314                 h2.Draw("SAME")
315             # total sum of pedestal from 80 to 180
316             P_2 = h2.Integral(p_start_mo,p_end_mo)
317             pes2.Fill(P_2)
318
319             # total sum of signal from 200 to 300
320             S_2 = h2.Integral(t_start_mo, t_end_mo)
321             sig2.Fill(S_2)
322
323             s_p_2 = S_2 - P_2
324             charge2.Fill(s_p_2)
325             h_range_mo.SetLineColor(2)
326             h_range_mo.Draw("SAME")
327             c1.Update()
```

```

328
329     # calculate LG (or Mask) value:
330     mean_pes_1 = pes1.GetMean()
331     err_pes_1  = pes1.GetMeanError()
332     mean_sig_1 = sig1.GetMean()
333     err_sig_1  = sig1.GetMeanError()
334     mean_1     = charge1.GetMean()
335     err_1      = charge1.GetMeanError()
336     err_all1 = math.sqrt(pow(err_sig_1,2)+pow(err_pes_1,2)) # total error
337
338     mean_1 = mean_sig_1 - mean_pes_1
339     print "%.1f    deg: mean_pes= %.1f+/-%.1f mean_sig= %.1f+/-%.1f    mean2=
↳  "%.1f +/- %.1f" % (current_angle,mean_pes_1, err_pes_1, mean_sig_1, err_sig_1,
↳  mean_1, err_all1)
340     #print "%.1f deg:    mean= %.1f +/- %.1f" % (current_angle, mean, err)
341     if (current_angle== -22.5) and (trial ==0) :
342         ras_now= mean_1
343     if (abs(current_angle)<= 22) and (abs(ras_now - mean_1) >sa ) :
344         os.remove(fname)
345         os.remove(fout_name)
346         brk =brk+1
347         if brk == 1:
348             sa = sa*2
349         if brk == 2:
350             sa = sa*2
351         if brk == 3:
352             sa = sa*2
353         if brk == 4:
354             sa = sa*2
355         continue
356     brk=0
357     sa=200
358     err_all_1.append(err_all1)
359     ras_now= mean_1
360     li_me_1.append(mean_1)
361     if trial == 0 and Ntrial == 4:
362         sum_all_1.append(mean_1)
363     elif trial == 0 and Ntrial == 5:
364         sum_all_1.append(0)
365     elif trial ==2 or trial ==4:
366         sum_all_1[j]= sum_all_1[j]+ mean_1
367     elif trial == 1 or trial ==3:
368         sum_all_1[SumNS-1-j]= sum_all_1[SumNS-1-j]+ mean_1
369     if Ntrial!= 1:
370         txtfile.write("LG_%d %.1f %f %f\n" % ( trial, current_angle , mean_1,
↳  err_all1))
371
372     #draw LG gain
373     if trial==0:
374         h_lg0.SetPoint(j , current_angle , mean_1)
375         h_lg0.SetPointError(j,EX, err_all1)
376         h_lg0.SetLineColor(trial+1)

```

```

377         c2.cd()
378         if j == 0:
379             h_lg0.Draw("AP")
380         else :
381             h_lg0.Draw("SAME")
382     elif trial==1:
383         h_lg1.SetPoint(j , current_angle , mean_1)
384         h_lg1.SetPointError(j,EX, err_all1)
385         h_lg1.SetLineColor(trial+1)
386         c2.cd()
387         h_lg1.Draw("SAME")
388     elif trial==2:
389         h_lg2.SetPoint(j , current_angle , mean_1)
390         h_lg2.SetPointError(j,EX, err_all1)
391         h_lg2.SetLineColor(trial+1)
392         c2.cd()
393         h_lg2.Draw("SAME")
394     elif trial==3:
395         h_lg3.SetPoint(j , current_angle , mean_1)
396         h_lg3.SetPointError(j,EX, err_all1)
397         h_lg3.SetLineColor(trial+1)
398         c2.cd()
399         h_lg3.Draw("SAME")
400     else:
401         print "debug_draw"
402     c2.Update()
403
404     # calculate Monitor's value:
405     mean_pes_2 = pes2.GetMean()
406     err_pes_2  = pes2.GetMeanError()
407     mean_sig_2 = sig2.GetMean()
408     err_sig_2  = sig2.GetMeanError()
409     mean_2     = charge2.GetMean()
410     err_2      = charge2.GetMeanError()
411     err_all2 = math.sqrt(pow(err_sig_2,2)+pow(err_pes_2,2)) # total error
412     err_all_2.append(err_all2)
413     mean_2 = mean_sig_2 - mean_pes_2
414     print "%.1f-Mo deg: mean_pes= %.1f+/-%.1f mean_sig= %.1f+/-%.1f      mean2=
↳ %.1f +/- %.1f" % (current_angle,mean_pes_2, err_pes_2, mean_sig_2, err_sig_2,
↳ mean_2, err_all2)
415     #print "%.1f deg:      mean= %.1f +/- %.1f" % (current_angle, mean, err)
416
417     li_me_2.append(mean_2)
418     if trial == 0:
419         sum_all_2.append(mean_2)
420     elif trial ==2:
421         sum_all_2[j]= sum_all_2[j]+ mean_2
422     elif trial == 1 or trial ==3:
423         sum_all_2[SumNS-1-j]= sum_all_2[SumNS-1-j]+ mean_2
424
425     if Ntrial != 1:

```

```
426         txtfile.write("LG-Mo_%d %.1f %f %f\n" % (trial, current_angle , mean_2,
↳ err_all_2[j]))
427         angle.append(current_angle)
428         fout.Close()
429         f.close()
430         # finish saving to ROOT file
431
432
433
434     if j == SumNS-1:
435         print 'break the loop.'
436         a *=-1
437         break
438     if a == 1:
439         if -Rotdeg3 <= current_angle < 0 :
440             if -Rotdeg3 <= current_angle < -Rotdeg2 :
441                 gsc02.move(STEP3*DEG, 0) # increase by STEP3 deg
442                 current_angle += STEP3
443                 #time.sleep(0.5)
444             elif -Rotdeg2 <= current_angle < -Rotdeg1 :
445                 gsc02.move(STEP2*DEG, 0) # increase by STEP2 deg
446                 current_angle += STEP2
447                 #time.sleep(0.5)
448             elif -Rotdeg1 <= current_angle < 0 :
449                 gsc02.move(STEP1*DEG, 0) # increase by STEP1 deg
450                 current_angle += STEP1
451                 #time.sleep(0.5)
452             else :
453                 print "debug1"
454                 sys.exit()
455             time.sleep(0.5)
456
457         elif 0 <= current_angle <= Rotdeg3 :
458             if 0 <= current_angle < Rotdeg1 :
459                 gsc02.move(STEP1*DEG, 0) # increase by STEP1 deg
460                 current_angle += STEP1
461                 #time.sleep(0.5)
462             elif Rotdeg1 <= current_angle < Rotdeg2 :
463                 gsc02.move(STEP2*DEG, 0) # increase by STEP2 deg
464                 current_angle += STEP2
465                 #time.sleep(0.5)
466             elif Rotdeg2 <= current_angle <= Rotdeg3 :
467                 gsc02.move(STEP3*DEG, 0) # increase by STEP3 deg
468                 current_angle += STEP3
469                 #time.sleep(0.5)
470             else :
471                 print "debug2"
472                 sys.exit()
473             time.sleep(0.5)
474         else :
475             print "debug3"
476             sys.exit()
```

```
477     if a == -1:
478         if 0 < current_angle <= Rotdeg3 :
479             #if -Rotdeg3 <= current_angle < 0 :
480                 if Rotdeg2 < current_angle <= Rotdeg3 :
481                     gsc02.move(-STEP3*DEG, 0) # decrease by STEP3 deg
482                     current_angle -= STEP3
483                     #time.sleep(0.5)
484                 elif Rotdeg1 < current_angle <= Rotdeg2 :
485                     gsc02.move(-STEP2*DEG, 0) # decrease by STEP2 deg
486                     current_angle -= STEP2
487                     #time.sleep(0.5)
488                 elif 0 < current_angle <= Rotdeg1 :
489                     gsc02.move(-STEP1*DEG, 0) # decrease by STEP1 deg
490                     current_angle -= STEP1
491                     #time.sleep(0.5)
492                 else :
493                     print "debug4"
494                     sys.exit()
495                 time.sleep(0.5)
496
497             elif -Rotdeg3 <= current_angle <= 0 :
498                 if -Rotdeg1 < current_angle <= 0 :
499                     gsc02.move(-STEP1*DEG, 0) # decrease by STEP1 deg
500                     current_angle -= STEP1
501                     #time.sleep(0.5)
502                 elif -Rotdeg2 < current_angle <= -Rotdeg1 :
503                     gsc02.move(-STEP2*DEG, 0) # decrease by STEP2 deg
504                     current_angle -= STEP2
505                     #time.sleep(0.5)
506                 elif -Rotdeg3 <= current_angle <= -Rotdeg2 :
507                     gsc02.move(-STEP3*DEG, 0) # decrease by STEP3 deg
508                     current_angle -= STEP3
509                     #time.sleep(0.5)
510                 else :
511                     print "debug5"
512                     sys.exit()
513                 time.sleep(0.5)
514             else :
515                 print "debug6"
516                 sys.exit()
517         j=j+1
518
519
520     if trial == Ntrial-1:
521         print 'The Measurement has just finished.'
522         k=0
523         for k in range(SumNS):
524             if Ntrial == 4:
525                 mean_all_1.append(sum_all_1[k]/Ntrial)
526             if Ntrial == 5: # error for 1 run
527                 mean_all_1.append(sum_all_1[k]/4)
528         sum_pow_1 = 0
```

```

529     if Ntrial == 1: # error for 1 run
530         RMS1 = err_all_1[k]
531     elif Ntrial == 5:
532         for i in range(1,Ntrial):
533             if i== 2 or i ==4:
534                 z = k + SumNS*i
535             if i == 1:
536                 z = SumNS*2 -1 - k
537             if i == 3:
538                 z = SumNS*4 -1 - k
539             #print li_me_1[z], mean_all_1[k]
540             sum_pow_1 += pow ( (li_me_1[z]-mean_all_1[k]) ,2)
541         RMS1 =math.sqrt(sum_pow_1/4)
542
543     else: # error for 4 runs
544         for i in range(Ntrial):
545             if i ==0 or i== 2:
546                 z = k + SumNS*i
547             if i == 1:
548                 z = SumNS*2 -1 - k
549             if i == 3:
550                 z = SumNS*4 -1 - k
551             #print li_me_1[z], mean_all_1[k]
552             sum_pow_1 += pow ( (li_me_1[z]-mean_all_1[k]) ,2)
553         RMS1 =math.sqrt(sum_pow_1/Ntrial)
554     RMS_1.append(RMS1)
555     txtfile.write("LG %.1f %f %f\n" % ( angle[k] , mean_all_1[k], RMS_1[k]) )
556     print '%.1f deg: Mean_all = %.1f +/-%.1f' % (angle[k], mean_all_1[k],
↳ RMS_1[k])
557
558     mean_all_2.append(sum_all_2[k]/Ntrial)
559     sum_pow_2 = 0
560     if Ntrial == 1:
561         RMS2 = err_all_2[k]
562     else:
563         for i in range(Ntrial):
564             if i ==0 or i== 2:
565                 z = k + SumNS*i
566             if i == 1:
567                 z = SumNS*2 -1 - k
568             if i == 3:
569                 z = SumNS*4 -1 - k
570             #print li_me_2[z], mean_all_2[k]
571             sum_pow_2 += pow ( (li_me_2[z]-mean_all_2[k]) ,2)
572         RMS2 = math.sqrt(sum_pow_2/Ntrial)
573     RMS_2.append(RMS2)
574     txtfile.write("LG-Mo %.1f %f %f\n" % ( angle[k] , mean_all_2[k], RMS_2[k])
↳ )
575     print '%.1f deg: Mean_Monitor = %.1f +/-%.1f\n' % (angle[k],
↳ mean_all_2[k], RMS_2[k])
576
577     #sys.exit()

```

```

578
579 txtfile.close()
580 current_pos = int(status.split(",")[0])
581 #print current_pos, current_angle
582 if current_angle != 0:
583     gsc02.move(-current_angle*400, 0) # reset position
584
585
586 # calculate RAS
587 f = open("%strial_all.txt" % ( fin_dir),"r+w") #
588 i = 0
589 lines = f.readlines()
590 count = 0
591 lg, lg_err,angle = [], [], []
592 lg_mo, lg_mo_err = [], []
593 for i,line in enumerate(lines):
594     type_ = line.split(" ")[0]
595     deg = line.split(" ")[1]
596     if type_ == "Mask":
597         m = float(line.split(" ")[2]) # mask
598         m_err = float(line.split(" ")[3]) # mask's error
599         count += 1
600     elif type_ == "Mask-Mo":
601         m_mo = float(line.split(" ")[2]) # mask's monitor
602         m_mo_err = float(line.split(" ")[3]) # mask's monitor error
603         count += 1
604     elif type_ == "LG":
605         #print line
606         angle.append( float(line.split(" ")[1]))
607         lg.append( float(line.split(" ")[2]))
608         lg_err.append(float(line.split(" ")[3])) # deg, LG , LG's error
609         count += 1
610     elif type_ == "LG-Mo":
611         #print line
612         lg_mo.append( float(line.split(" ")[2]))
613         lg_mo_err.append(float(line.split(" ")[3])) # deg, LG's monitor , LG's
614         ← monitor error
615         count += 1
616     elif type_ == "RAS" or type_ == "RAS-Mo":
617         del lines[i-1]
618 #print lg_mo
619 #print lg_mo_err
620 if count == 2 :
621     print 'No LG'
622 elif count == (2 + SumNS*2):
623     for i in range (SumNS):
624         ras = lg[i] / (m * math.cos(angle[i]/180*math.pi) *3.7352) *100
625         ras_err = ras * math.sqrt( pow( m_err/m ,2) + pow( lg_err[i]/lg[i] ,2) )
626         #print '%.1f : ' % (angle[i])
627         #print ' LG = %.1f +/- %.1f ; LG-Mo = %.1f +/- %.1f' % (lg[i],lg_err[i],
628         ← lg_mo[i], lg_mo_err[i])

```

```
627     #print '    Mask = %.1f +/- %.1f ; Mask-Mo = %.1f +/- %.1f' % ( m,m_err, m_mo,
↳ m_mo_err)
628     print '%.1f RAS    = %.1f +/- %.1f' % (angle[i], ras, ras_err)
629     f.write("RAS %.1f %f %f\n" % ( angle[i], ras, ras_err))
630
631     ras_mo = lg[i] * m_mo / (m * lg_mo[i] *math.cos(angle[i]/180*math.pi) * 3.7352)
↳ *100
632     ras_mo_err = ras_mo * math.sqrt( pow( m_err/m ,2) + pow( m_mo_err/m_mo ,2) +pow(
↳ lg_err[i]/lg[i] ,2) + pow( lg_mo_err[i]/lg_mo[i] ,2))
633     #print 'LG = %.1f +/- %.1f ; Mask = %.1f +/- %.1f' % (lg,lg_err, m, m_err)
634     print '    RAS-Mo = %.1f +/- %.1f' % ( ras_mo, ras_mo_err)
635     f.write("RAS-Mo %.1f %f %f\n" % ( angle[i] , ras_mo, ras_mo_err))
636 #elif count == 0:
637 else:
638     print "count = %d :Sthing's wrong!" % (count)
639 f.close()
640 #txtfile.close()
641
642 # reset position
643 current_pos = int(status.split(",")[0])
644 if current_pos != 0:
645     gsc02.move(-current_pos, 0) # reset position
646 sys.exit()
```

Bibliography

- [1] M. Nagano and A. A. Watson. Observations and implications of the ultrahigh-energy cosmic rays. 1 July 2000. URL <http://journals.aps.org/rmp/pdf/10.1103/RevModPhys.72.689>.
- [2] T. Weekes. *Very high energy gamma-ray astronomy*. Institute of Physics Publishing, 2003.
- [3] K. Yoshida. Observation of supernova remnant HB3 by Fermi satellite. Master thesis. 2014. URL http://golf.sci.ibaraki.ac.jp/pukiwiki/index.php?plugin=attach&refer=%B3%D8%B0%CC%CF%CO%CA%B8&openfile=2014_yoshida_syuron.pdf.
- [4] Fermi homepage. 2017. URL <http://fermi.gsfc.nasa.gov/>.
- [5] H.E.S.S. homepage. . URL <https://www.mpi-hd.mpg.de/hfm/HESS/>.
- [6] VERITAS homepage. . URL <http://veritas.sao.arizona.edu/>.
- [7] MAGIC homepage, picture gallery. 2009. URL <https://magicold.mpp.mpg.de/gallery/pictures/>.
- [8] R. Marcus Wagner. Measurement of very high energy gamma-ray emission from four blazars using the magic telescope and a comparative blazar study. PhD thesis. 2006.
- [9] S. Tanaka. Basic development for mass production of light concentrator for large-sized telescope in the next generation gamma-ray observatory cta. Master thesis. 2013. URL http://www.cta-observatory.jp/Publications/Theses/Master/Mth_2013_Tanaka.pdf.
- [10] D. Tesaro. TeV γ -ray observations of nearby Active Galactic Nuclei with the MAGIC telescope: exploring the high energy region of the multiwavelength picture. 2010.

-
- [11] F. Aharonian, J. Buckley, T. Kifune, and G. Sinnis. High energy astrophysics with ground-based gamma ray detectors. 2008.
- [12] C. Fruck. A new LIDOR system for the MAGIC telescopes and site search instrumentation for CTA. 2011.
- [13] CTA-Japan. 2017. URL <http://cta.scphys.kyoto-u.ac.jp>.
- [14] I. Ishio. Development of a High-Speed Data Acquisition System for the Large-Sized Telescopes of CTA. Master thesis. 2015. URL http://www.cta-observatory.jp/Publications/Theses/Master/Mth_2014_Ishio.pdf.
- [15] Hamamatsu Photonics K.K. Photocathode technology. URL <https://www.hamamatsu.com/us/en/technology/innovation/photocathode/index.html>.
- [16] S. Ono. Mass production and performance evaluation of light concentrators for the first large-sized telescope of the next generation gamma-ray observatory cta. Master thesis. 2015. URL http://www.cta-observatory.jp/Publications/Theses/Master/Mth_2015_Ono.pdf.
- [17] Hamamatsu Photonics K.K. CTA-FPI: PMT update from Hamamatsu. 2011.
- [18] A. Okumura, S. Ono, S. Tanaka, M. Hayashida, H. Katagiri, and T. Yoshida for the CTA Consortium. Prototyping of Hexagonal Light Concentrators for the Large-Sized Telescopes of the Cherenkov Telescope Array. arXiv:1508.07776. Proceedings of the 34th International Cosmic Ray Conference (ICRC2015). URL <https://arxiv.org/pdf/1508.07776v1.pdf>.
- [19] A Okumura. Optimization of the collection efficiency of a hexagonal light collector using quadratic and cubic bézier curves. arXiv:1205.3968. URL <https://arxiv.org/pdf/1205.3968.pdf>.